U.S. Department
of Transportation
**National Highway
Traffic Safety
Administration**

NHTSA
www.nhtsa.gov

DOT HS 811 860

December 2013

Sensitivity Analysis of The Response of a 6-Year-Old Child in Automotive Crashes

Suggested APA Format Citation

Van Rooij, Broos, J., & van Nunen, E.. (2013, December). Sensitivity analysis on the response of a 6-year-old child in automotive crashes. (Report No. DOT HS 811 860). Washington, DC: National Highway Traffic Safety Administration

Technical Report Documentation Page

1. Report No. DOT HS 811 860	**2. Government Accession No.**	**3. Recipient's Catalog No.**
4. Title and Subject Sensitivity Analysis on the Response of a 6-Year-Old Child in Automotive Crashes		**5. Report Date** December 2013 **6. Performing Organization Code**
7. Authors Lex van Rooij, Jeroen Broos, Ellen van Nunen		**8. Performing Organization Report No.**
9. Performing Organization Name and Address TASS/TNO North America 38701 7 Mile Road, Suite 260 Livonia, MI 48152		**10. Work Unit No. (TRAIS)** **11. Contract or Grant No.** DTNH22-07-H-00086
12. Sponsoring Agency Name and Address National Highway Traffic Safety Administration Human Injury Research Division, NVS-323 U.S. Department of Transportation 1200 New Jersey Avenue SE. Washington, DC 20590		**13. Type of Report and Period Covered** NHTSA Technical Report **14. Sponsoring Agency Code** NHTSA, NVS-323

15. Supplementary Notes

16. Abstract

Prior studies have shown that child anthropometric test devices (ATDs) could benefit from improved biofidelity. Defining child ATD biofidelity based on traditional biomechanical testing methods can be ethically and technically (e.g., scaling) difficult. Therefore, this project explored a modeling approach for defining biofidelity test conditions/responses that could be applied towards new frontal child ATD development. This project used new knowledge from child-focused biomechanical and anthropometry studies as input in efforts to update, parameterize, and optimize a Hybrid III 6-year-old-based numerical model that was then applied in defining new biofidelity targets for a 6-year-old frontal ATD.

The first phase of the study involved parameterizing and updating a Hybrid III-based 6-year-old model to include improved pelvis, abdomen, and shoulder anthropometry and an additional joint in the thoracic spine.The updated and parameterized 6-year-old model was then used to complete a parameter sensitivity analysis. Twelve setups were implemented, all representing biomechanical test conditions. These conditions included four belt load tests on the abdomen and thorax, pendulum and cardiopulmonary resuscitation tests on the thorax, neck flexion/extension and tension tests, and three whole-body conditions. Almost all stiffness and damping parameters were found to be sensitive.

The model was then optimized for various responses (e.g., force-displacement, head excursion) and various criteria (e.g., peak value, curve fit). The same 12 setups from the parameter sensitivity analysis were used together with a few additional conditions. In general, the optimization process improved the response of the model. However, the final optimized model did not achieve biofidelic head excursions in whole body sled conditions. This may be attributed to parameter limits implemented in the spine (tensile and flexion properties). Shoulder flexibility may also have contributed. While the shoulder was updated, shoulder flexibility was not parameterized.

The final task involved using the updated and optimized model to develop biofidelity targets for a frontal 6-year-old ATD. The conditions largely represented those from existing standards or from biomechanical studies used in the sensitivity and optimization tasks. Proposed conditions and biofidelity targets are presented.

17. Key Words Anthropometric test device; child; sensitivity; optimization; biofidelity; model	**18. Distribution Statement** Document is available to the public from the National Technical Information Service www.ntis.gov

19. Security Classif. (of this report) Unclassified	**20. Security Classif. (of this page)** Unclassified	**21. No. of Pages** 107	**22. Price**

Form DOT F 1700.7 (8-72) **Reproduction of completed page authorized**

Summary

Previous studies have shown that child anthropometric test devices (ATD) could benefit from improved biofidelity. While traditional methods, based on biomechanical testing, are ethically difficult, in this project a hybrid approach was adopted. Research partners in the project performed detailed biomechanical studies for specific conditions or body regions. This data was used as input to this project, which focused on updating, parameterizing and optimizing a numerical model of a Hybrid III 6-year-old such that a more biofidelic model was the end result. An additional objective was the creation of biofidelity test setups and responses that could be performed for future ATD biofidelity certification.

First, the baseline MADYMO Hybrid III 6-year-old model was updated to represent higher degrees of biofidelity. University of Michigan Transportation Research Institute (UMTRI) provided a more realistic pelvis and abdomen geometry. Based on a study from University of Virginia, thoracic spine stiffness was added. Duke University provided insight in the properties of the neck; however, the neck model was not altered. Finally, UMTRI provided anthropometrical locations of shoulder landmarks based upon which a more human-like shoulder model was implemented.
With the updated Hybrid III 6-year-old model, after parameterizing it, a sensitivity analysis was performed. Parameters with accompanying ranges of variation were chosen in abdomen, thorax, head, neck and spine. The sensitivity analysis consisted of variations of single parameters in three increments and their effects on responses were quantified in terms of sensitivity ratios. In total, 12 setups were developed, all representing biomechanical tests, including four belt load tests on abdomen and thorax, pendulum and cardiopulmonary resuscitation test on the thorax, neck flexion and tension tests and three whole body sled test setups. It was shown that almost all stiffness and damping characteristics, as well as all geometrical parameters, had a sensitivity enabling them to be tuned towards more biofidelic responses. From this analysis, the parameters were chosen that were used in order to optimize the model.

In the optimization study, a gradient descent algorithm was used with an objective function that minimizes the weighted errors in various test setups for various responses (e.g. force-time, force-displacement and trajectory) and for various criteria (peak height, peak time and curve fit). As a basis, the same 12 setups from the sensitivity analysis were used; however, a few were added or altered. Based on the optimization and some manual adjustment, a set of final scaling factors for the updated and parameterized Hybrid III 6-year-old model were determined. Typically, stiffness parameters were reduced while damping factors were adjusted to meet rate sensitivity requirements. The optimization of the response in whole body sled setups did not result in achieving a biofidelic level of upper torso and head excursion, which was attributed to limited flexibility in the spine and possible differences in the implementation of the test setups.

Finally, the optimized model was used to develop biofidelity test setups, which can be implemented in ATD certification environments. Thorax, neck and head pendulum tests,

thorax and abdomen belt load tests and a whole body sled setup tests were developed, including possible criteria and threshold values.

Contents

Summary iii

1 Introduction 1

2 Dummy Model Design Updates 3
2.1 Pelvis and abdomen update 3
2.2 Thoracic spine update 5
2.3 Neck update 6
2.4 Shoulder update 7

3 Sensitivity Analysis for Assessment of Biomechanical Parameters 11
3.1 Crash scenarios and test setups 11
3.2 Parameter choice and ranges 24
3.3 Design of sensitivity study 26
3.4 Sensitivity analysis results 29
3.5 Conclusion 37

4 Optimization Study for Response Requirements for Future ATDs 39
4.1 Crash scenarios and test setups 39
4.2 Parameter choice and limits 44
4.3 Design of optimization study 46
4.4 Results 49
4.5 Discussion 60
4.6 Conclusion 61

5 Biofidelity Test Corridor Development 63
5.1 Introduction 63
5.2 Selection of biofidelity tests 63
5.3 Results 66
5.4 Conclusion 74

6 Conclusions and Recommendations 76
6.1 Dummy Model Design Updates 76
6.2 Sensitivity Analysis for Assessment of Biomechanical Parameters 76
6.3 Optimization Study for Response Requirements for Future ATDs 77
6.4 Biofidelity Test Corridor Development 78
6.5 Recommendations 79

7 References 80

8 Signature 83

9 Appendix A: Abdomen parameter optimization 84

10 Appendix B: Ford Taurus rear bench, booster and 3-point belt setup validation 86

11 Appendix C: CHOP sled setup validation 89
11.1 Model setup 89
11.2 Results 89

1 Introduction

Currently, vehicle safety for children is assessed using anthropometric test devices (ATD). Various child ATD designs are accepted throughout the world for various functions. For example, the Hybrid III 3- and 6-year-old dummies (U.S.) and the P3- and P6-year-old dummies (Europe) are used for regulatory testing. The Q3- and Q6-year-old dummies, and derivations thereof, are currently being proposed for regulatory testing.

As new initiatives in child ATDs development are taken, it is important to fully understand the child biomechanical parameters that affect kinematics and injury during impacts, such that existing ATDs can be improved and new ATDs can be developed with improved biofidelity.

Historically, understanding impact biomechanics has been achieved through experimental studies using post mortem human subjects (PMHS). The results of these studies have shown to have a direct influence on reducing injuries and saving lives (King, 1995) through the development of improved safety systems. However, when considering child safety, one is faced with far more complicated ethical issues when attempting to conduct child post mortem human subject tests. As a result, researchers turn towards numerical techniques in an effort to better understand child injuries and improve safety as presented in this study.

Numerical studies however possess additional challenges associated with the lack of known biomechanical properties for children. These are often overcome by implementing advanced scaling techniques to translate adult human properties into children, accounting for anthropometric and mass differences (Ivarsson, 2004a, 2004b). However, the fundamental knowledge of child biomechanical properties, and their relation to adult properties, remains limited. Within the scope of the 6-year-old child biofidelity project at the National Highway Traffic Safety Administration, various partners have assessed biomechanical properties of children based on child volunteer and surrogate testing and numerical simulation. This data gradually came available for the purpose of the current study.

In the report *Development of child human body models and simulated testing environments for the improvement of child safety* (Forbes, 2007), the first phase of this project was reported. The following tasks were performed:

- Update and validation of MADYMO Q6 ellipsoid dummy model and MADYMO 6-year-old facet child human body model;
- Parameterization of MADYMO Hybrid III 6-year-old ellipsoid dummy model, MADYMO Q6 ellipsoid dummy model, and MADYMO 6-year-old facet child human body model;
- Simulated test environment development of Kallieris child PMHS sled tests and dummy reconstructions thereof; and
- Simulations with MADYMO facet child human body models of Kallieris child PMHS sled tests.

In the previous study it was recommended that the parameterized Hybrid III 6-year-old and the parameterized 6-year-old facet child human body model be used for future sensitivity and optimization studies. The parameterized Q6 ellipsoid dummy model showed low correlation to the physical Q6 dummy, hence it was withdrawn from future recommendations.

In the definition of the Statement of Work for the current project, the parameterized Hybrid III 6-year-old ellipsoid dummy model in MADYMO was chosen as the human surrogate model to perform the current project with. The parameterized Hybrid III 6-year-old ellipsoid dummy model has the advantage over a human model that its level of detail and degrees of freedom is more similar to that of a potential future dummy design, allowing rapid translation of model parameters to physical dummy parameters. The parameterized 6-year-old facet child human body model would have had the advantage over the Hybrid III that its level of detail and degrees of freedom is more similar to that of an actual child, making it more likely to better meet the biomechanical responses used as input.

The objective of this study is to develop a numerical ATD model that can serve as a design brief for a future 6-year-old ATD. It should be noted that this study is limited to frontal impact scenarios only.

Based on the previous study and in order to meet the objective, in the current study the following tasks were performed:

- Task 4: Dummy model design updates;
- Task 1: Sensitivity Analysis for Assessment of Biomechanical Parameters;
- Task 2: Optimization Study for Response Requirements for Future ATDs;
- Task 5: Biofidelity Test Corridor Development; and
- Task 3: Modeling support to partners.

These tasks are listed in a logical and chronological order, while their task numbers are not, purely for contractual reasons.

In Task 4, the parameterized Hybrid III 6-year-old ellipsoid dummy model was updated to represent more realistic human characteristics, based on input from partners. In Task 1 a sensitivity analysis was performed with the updated model to assess which parameters are of what influence on which response. Subsequently, in Task 2 optimization of the Hybrid III 6-year-old ellipsoid dummy model was performed to best represent the biomechanical response data. With the optimized model, in Task 5 biofidelity tests were developed that could be performed by dummy manufacturers in laboratory setups on a future 6-year-old ATD. As a continuous task, modeling support to partners was provided on the use of the delivered models. All tasks will be reported in the following chapters in the logical and chronological order presented above.

2 Dummy Model Design Updates

2.1 Pelvis and abdomen update

For 6-year-old children undergoing frontal impact in a vehicle good engagement of the lap portion of the 3-point belt is often critical (Arbogast, 2004). It was shown that children 4 to 8 years old were at the highest risk of abdominal injury: They were 24.5 times and 2.6 times more likely to sustain an abdominal injury coded as AIS2+[1] than those children 3 and younger old and 9- to 15 years old, respectively. Also, the abdominal injury risk was virtually eliminated in 4- to 8-year-olds with the use of child restraint or belt positioning booster seats: Children 4- to 8 year olds in vehicle belts were 34 times as likely to sustain an AIS2+ abdominal organ injury as those in child restraints or booster seats. The 6-year-old Hybrid III dummy contains a rigid pelvis geometry as well as softer foams representing soft tissues. However, the geometry of the pelvis is not representative of the current 6-year-old population (Reed, Sochor, Rupp, Klinich, , & Manary, 2009). As such, UMTRI has developed an anthropometrically correct pelvis geometry. In the original Hybrid III 6-year-old ellipsoid model, interaction between dummy and seat belts is simulated by a contact algorithm between belt and the ellipsoid describing the outer surface. As such, this model does not accurately simulate the engagement of the lap belt on the pelvis. The UMTRI pelvis geometry and an accompanying outer surface were implemented in the parameterized ellipsoid 6-year-old Hybrid III. This section details the approach followed.

2.1.1 UMTRI pelvis and abdomen geometry

At UMTRI, an updated pelvis geometry was developed, which is shown in Figure 2-1 (Reed, Sochor, Rupp, Klinich, , & Manary, 2009). This represents a shape that is more representative of a 6-year-old child, especially where lap belt interaction is involved due to the lowered anterior-superior iliac spines (ASIS). Besides alterations in dimensions, the major modification consists of a chamfering of the dorsal-anterior part of the iliac crest. An Initial Graphics Exchange Specification (IGES) geometry file of the pelvis and surrounding soft tissue representing parts was supplied as well.

[1] AIS2+: Abbreviated Injury Scale (AIS) where 2+ indicates an injury that is at moderate or more severe

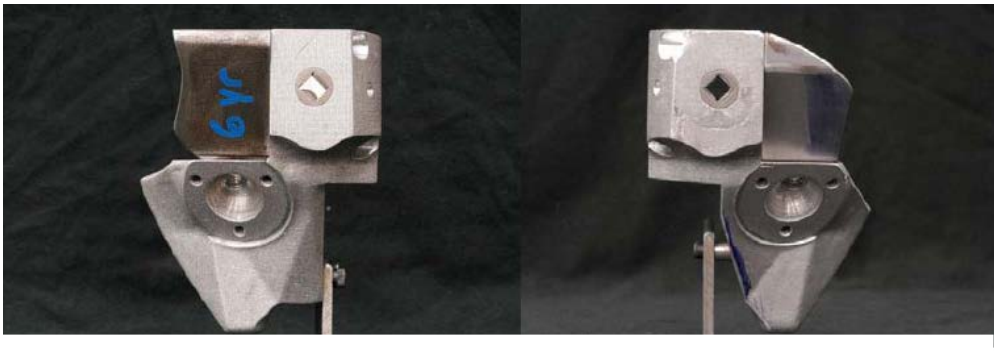

Left view, original 6YO pelvis.

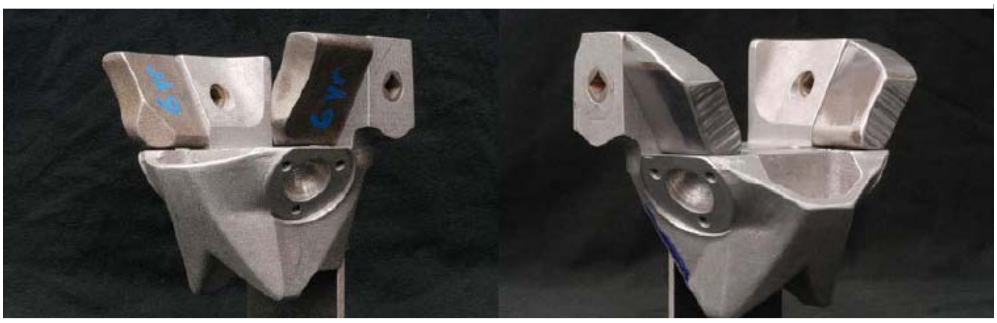

Left oblique view, original 6YO pelvis. Right oblique

Figure 2-1. Original Hybrid III 6-year-old pelvis (left) versus modified pelvis geometry as used in updated ellipsoid Hybrid III 6-year-old model (right), courtesy of UMTRI.

2.1.2 *Implementation into parameterized ellipsoid Hybrid III 6-year-old model*

The geometry of both the soft tissues as well as the pelvis geometry were implemented in the model. In Figure 2-2 the new soft tissues geometry is shown in comparison to the original model. In Figure 2-3 the updated pelvis geometry is shown in a typical sled test setup with a 3-point belt.

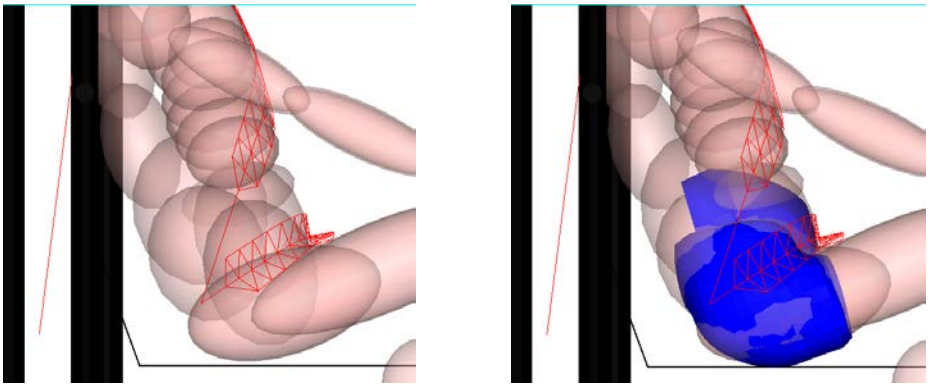

Figure 2-2. Original ellipsoid Hybrid III 6-year-old model (left) and UMTRI pelvis and abdominal area implemented in parameterized ellipsoid Hybrid III 6-year-old model (right).

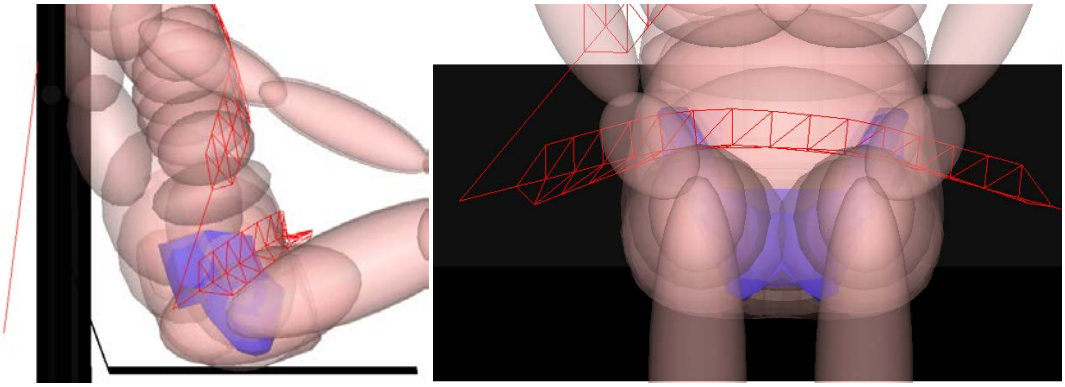

Figure 2-3. UMTRI pelvis geometry implemented in parameterized ellipsoid Hybrid III 6-year-old model in lateral view (left) and frontal view (right).

The pelvis was positioned relative to the multi-body model by UMTRI (Hu, 2011), ensuring a realistic location of the pelvis in relation to the joint locations and outer geometry. The contact stiffness function for the outer geometry was adopted from the original model, while the pelvis geometry received rigid properties, hence requiring a penalty-based contact. Hu (2011) implemented different belt to abdomen contact stiffness properties compared to the original model. Figure 2-4 shows that UMTRI's contact stiffness is lower than that implemented in the original MADYMO model. This causes the validation that UMTRI performed on their model to not be applicable to TNO's model. Therefore the results of the UMTRI validation study are omitted from this report.

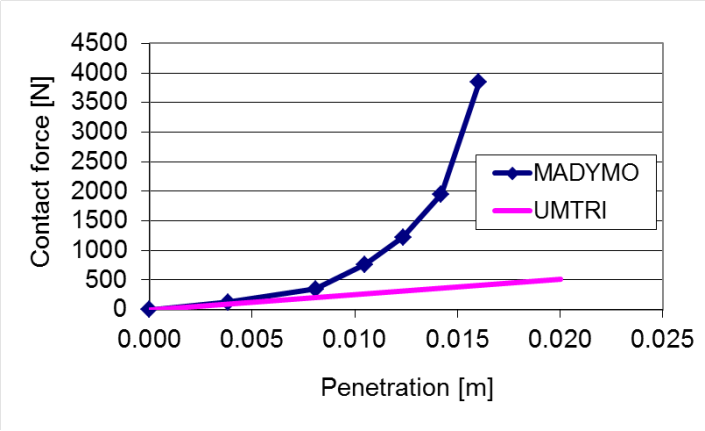

Figure 2-4. Contact stiffness characteristics as implemented in original MADYMO ellipsoids Hybrid III 6-year-old model and as implemented in UMTRI model (Hu, 2011).

2.2 Thoracic spine update

In a study focusing on neck injury assessment with the Hybrid III 6-year-old dummy, it was concluded that the rigid thoracic spine of the dummy causes a non-biofidelic neck response (Sherwood, 2003). In a numerical study, an additional hinge joint was added halfway between lumbar spine degree of freedom and the first neck degree of freedom,

allowing flexion-extension of the thoracic spine. This joint was given a stiffness value intended to represent the combined flexion stiffness of the entire thoracic spine (106.5 Nm/rad), and was chosen such that the kinematics of the dummy were similar to those of the cadaver analyzed in this study. This resulted in a large reduction in neck injury values. The flexible thoracic spine decreased the upper neck injury predictor N_{ij} from 1.32 to 0.65. The upper neck tensile load decreased from 2910 N to 1393 N. The most dramatic change in the lower neck was the reduction of the flexion moment from 264 Nm to 84 Nm.

2.2.1 Implementation into parameterized ellipsoid Hybrid III 6-year-old model

In the current model, this exact joint definition was copied, as is shown in Figure 2-5. No validation was performed on this joint implementation, due to the lack of experimental validation data.

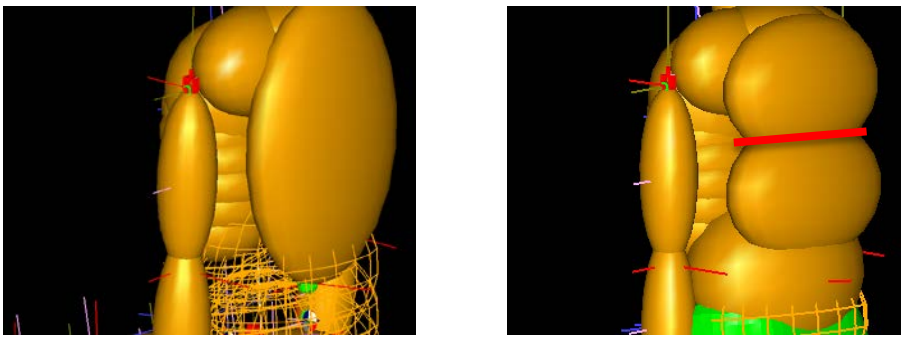

Figure 2-5. Original ellipsoid Hybrid III 6-year-old model with rigid thoracic spine (left) and updated thoracic joint implemented in parameterized ellipsoid Hybrid III 6-year-old model (right).

2.3 Neck update

In the cooperative agreement it was defined that an update to the neck was to be made based on the construction of the THOR neck. In THOR, in addition to the neck segments, steel cables are implemented representing neck musculature. While this implementation is more realistic due to the inclusion of two load paths, i.e. cervical spine and neck musculature, it was chosen in agreement with the partners not to represent this in the modified ellipsoid Hybrid III 6-year-old model. Since the focus of this project is whole body kinematic response and since biomechanical data would be delivered assessing whole neck response, it was chosen to maintain a single load path in the modified dummy model. This single load path was deemed sufficient for sensitivity analysis and optimization, helped by the fact that the original Hybrid III 6-year-old model contains a three pivot neck.

2.3.1 Implementation into parameterized ellipsoid Hybrid III 6-year-old model

The neck joint structure of original and hence also modified model is shown in Figure 2-6. The lower neck joint allows three degrees of freedom, for flexion-extension, lateral bending and yaw motion. The middle neck joints allows flexion-extension and neck tension. The upper neck joint allows three degrees of freedom, identical to the lower neck, for flexion-extension, lateral bending, and yaw motion.

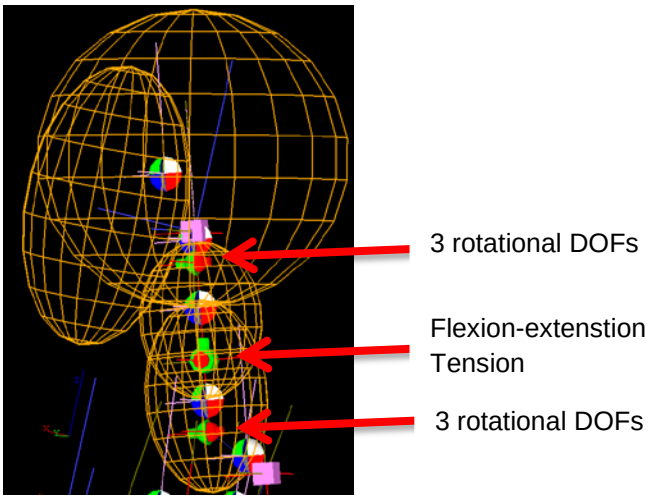

Figure 2-6. Original (and modified) ellipsoid Hybrid III 6-year-old model neck with three kinematic joints: lower for 3 rotations, middle for flexion-extension and tension and upper for 3 rotations.

While pediatric neck properties were determined (Dibb, 2010), these could not be implemented in the modified model since properties were determined for separate structures, i.e. cervical spine and neck musculature. As a result the mechanical properties in the modified model were adopted from the original ellipsoid Hybrid III model. Validation of the neck model of the original dummy was performed against neck biofidelity tests (Madymo, 2011).

2.4 Shoulder update

The shoulder geometry in the Hybrid III 6-year-old is simplified with respect to that of a child. The gleno-humeral joint connects the humerus to the rigid thoracic spine only via the clavicle. The clavicle in its turn is connected to the thoracic spine. In reality the humerus is connected to the thoracic spine via a double load path. One path connects the gleno-humeral joint to the clavicle, which is articulated to the sternum. The sternum is connected to the spine through the ribcage. The other load patch connects the gleno-humeral joint to the scapula, which is connected to the thoracic spine through musculature. These two load paths and its articulations allow for relative motion of the gleno-humeral joint with respect to the thoracic spine. The Hybrid III 6-year-old dummy cannot replicate this motion. In addition, for seat belt engagement, a more realistic engagement with the clavicle is required.

2.4.1 UMTRI shoulder geometry

UMTRI performed a study in which target contour and skeletal landmarks in the shoulder were scanned based on 5 boys and 6 girls in the age range from 5 to 10 years old (Reed, 2009). Based on skeletal landmarks the joint locations were estimated. The results were scaled to the current Hybrid III 6-year-old based on its erect seated height. An image of the target contour and skeletal landmarks is shown in Figure 2-7. The locations of the landmarks with respect to the suprasternal are shown in Table 2-1.

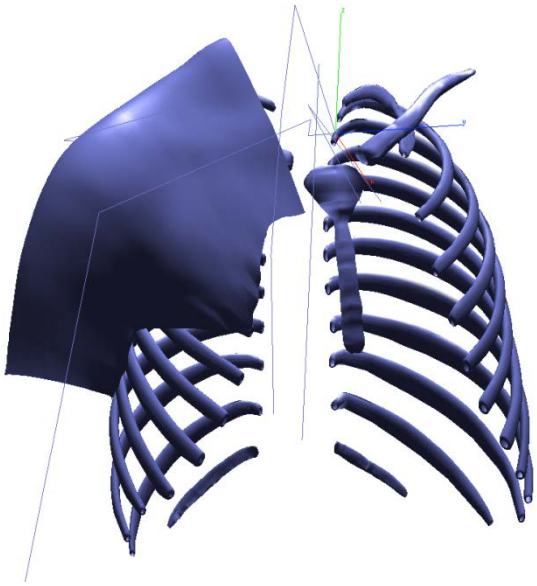

Figure 2-7. Target contour and skeletal landmarks for a 6-year-old based on UMTRI study, courtesy of UMTRI.

Table 2-1. Target landmarks and estimated joint locations for the right shoulder, courtesy of UMTRI.

Target Landmark and Joint Locations (mm)

Landmark	X	Y	Z
Suprasternale	0	0	0
C7	-76	0	31
T4	-86	-1	-26
T8	-86	-3	-96
T12	-75	-2	-170
Medial Clavicle	2	-13	1
Humeral Head Center*	-16	-105	-38
Lateral Humeral Epicondyle	60	-175	-190
Medial Humeral Epicondyle	45	-134	-223
Elbow Joint*	53	-155	-207
T12/L1*	-33	0	-165
C7/T1*	-33	0	20
Sternoclavicular Joint*	-10	-9	3
Lateral Clavicle	-32	-99	1
Acromion (Ant. Sup.)	-19	-107	-5
Medial Spine Scapula	-91	-56	-24
Lateral Spine Scapula	-33	-118	-9

* Estimated internal joint locations.

2.4.2 *Implementation into parameterized ellipsoid Hybrid III 6-year-old model*

Since the ellipsoid Hybrid III 6-year-old model represents the shoulder geometry of the hardware dummy, which was deemed too simplified, an update to the model was required. The update consisted of an implementation of the double load path shoulder

geometry, of locating the joint locations based on the UMTRI study and of an implementation of a clavicle for good belt engagement.

The double load path implementation was based on the 6-year old child human model in MADYMO (MADYMO, 2011). In this model, a more realistic load path was implemented. The implementation is shown in the schematic in Figure 2-8 for the left shoulder. The humerus is connected to the sternum through the clavicle in one load path via two kinematic joints. The sternum itself is connected to the thoracic spine through the ribcage model. The humerus is connected to the thoracic spine through the scapula via one kinematic joint and a spring-damper.

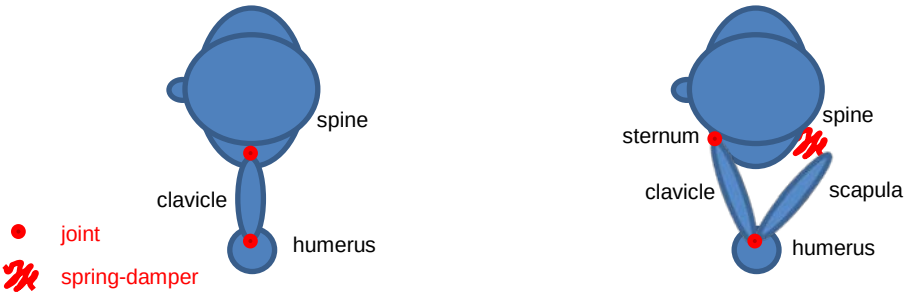

Figure 2-8. Schematic of original shoulder implementation (left) and modified shoulder implementation (right), top view.

The partial implementation in the modified ellipsoid Hybrid III 6-year-old model is shown in Figure 2-9. For display purposes, this figure shows the implementation for the right shoulder only. The modified model obviously contains the implementation for both shoulders.

A procedure was followed for the implementation of the correct joint locations:

- The humeral head center was used to position the landmarks provided by UMTRI (Table 2-1);
- The sterno-clavicular joint was positioned;
- The average of the medial clavicle and lateral clavicle was used to position the clavicle body;
- The joint between clavicle and scapula was based on the position of the acromion;
- The average of the medial spine scapula and lateral spine scapula was used to position the scapula body; and
- The joint between humerus and scapula was maintained on the original location.

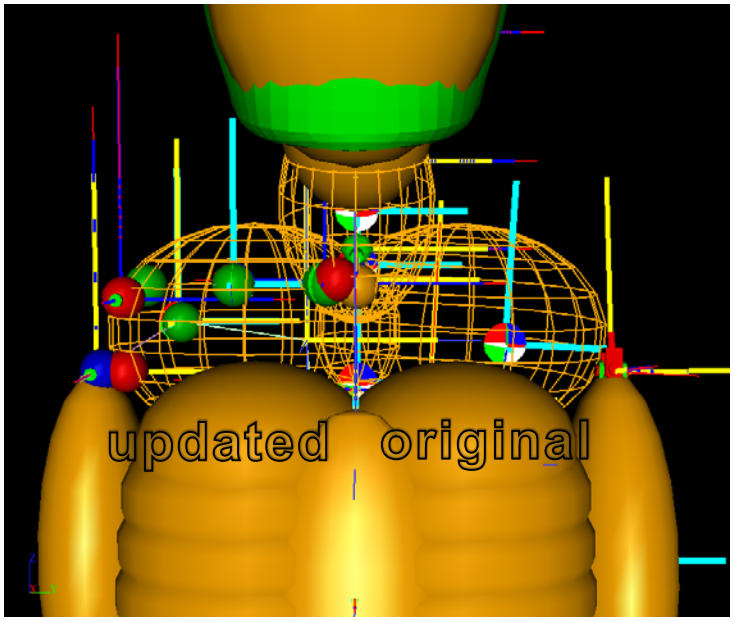

Figure 2-9. Original (left shoulder, right view) and modified (right shoulder, left view) shoulder implemented in parameterized ellipsoid Hybrid III 6-year-old model.

A clavicle shape was implemented in the model, based on an available adult geometry, which was scaled to represent a 6-year-old. The shape was positioned relative to the kinematic joints and external contour based on a comparison between the dummy model and UMTRI data. The location of the clavicle in the shoulder of the ellipsoid Hybrid III model is shown in Figure 2-10.

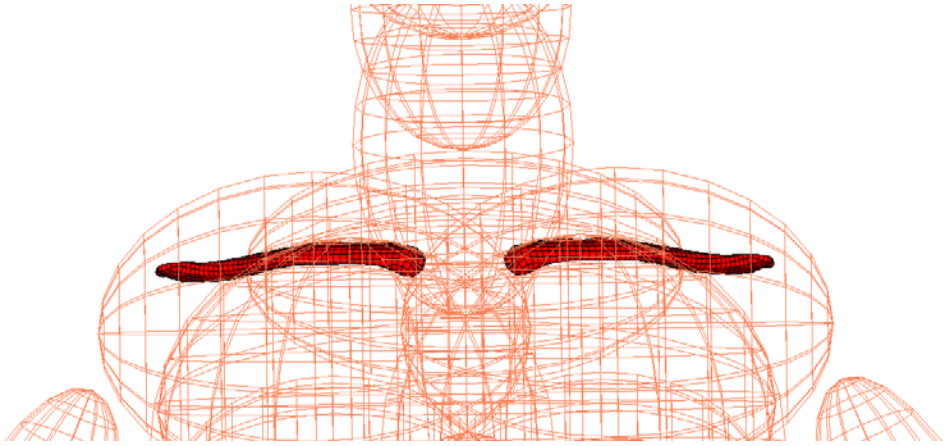

Figure 2-10. Clavicle geometry implemented in parameterized ellipsoid Hybrid III 6-year-old model.

No biomechanical tests were found or provided that could be used to validate the implemented shoulder model.

3 Sensitivity Analysis for Assessment of Biomechanical Parameters

In Chapter 2, the modified and parameterized ellipsoid Hybrid III 6-year-old model in MADYMO was discussed as the base model for improvement of a 6-year-old ATD. In order to arrive at a numerical model of an improved 6-year-old ATD, the design parameters that influence the response of the dummy in typical automotive conditions needs to be known. For this purpose, a design of experiments (DOE) study was performed. The objective of this study was therefore to find key factors that influence the dummy response in typical scenarios relevant for frontal automotive crashes. This chapter starts in Section 3.1 with discussing the chosen crash scenarios and test setups. In Section 3.2, the parameter choices are discussed including the ranges for sensitivity analysis. Section 3.3 details the setup of the design of experiments study resulting in the sensitivity analysis. The results of the latter are discussed in Section 3.4 in the order in which they are performed, first divided over three body regions and finally for whole body response. This chapter ends with the necessary conclusions for interpretation of the results in order to be able to start with the optimization study.

3.1 Crash scenarios and test setups

A sensitivity analysis is useful only when performed in scenarios that are loading the dummy in a similar manner as observed in automotive frontal crashes and when all design parameters that are deemed relevant are tested in a discerning manner. In order to meet these two objectives, a number of scenarios were defined. These consisted first of all of component tests on specific body regions, allowing for a relatively straightforward interpretation of effect of a parameter on the response. Secondly, setups testing whole body response were introduced in order to load the dummy in relevant automotive impact scenarios.

An overview of the setups is provided in Table 3-1 for the component tests and in Table 3-2 for the whole body crash scenarios.

Table 3-1. Component crash scenarios and test setups used for sensitivity analysis.

Interest Area	Test type	Dummy load	Reference
Abdomen	Quasi-static belt load (PEDVE024)	Abdomen stiffness	Kent, 2011
	Dynamic belt load (PEDVE025)	Abdomen stiffness & damping	Kent, 2011
	Dynamic belt load upper abdomen (PEDVE026)	Abdomen stiffness & damping, Ribcage stiffness & damping	Kent, 2011
Thorax	Pendulum impact	Thorax stiffness and damping	Ouyang, 2006 Parent, 2010
	Cardiopulmonary resuscitation (CPR)	Thorax stiffness and damping Back plate contact	Maltese, 2008 Maltese, 2010 Parent, 2010
	Dynamic belt load	Thorax stiffness and damping Back plate contact	Kent, 2009
	Vehicle seat, booster & 3-point belt	Thorax stiffness and damping	Lopez-Valdes, 2011a
Neck	National Biodynamics Laboratory (NBDL) frontal	Neck flexion-extension & tension stiffness & damping Head inertia	Dibb, 2010
	Tension	Neck tension stiffness & damping	Dibb, 2010

Table 3-2. Whole body crash scenarios and test setups used for sensitivity analysis.

Interest Area	Test type	Dummy load	Reference
Whole body	Volunteer low speed sled	Spinal properties Head inertia	Arbogast, 2009 Seacrist, 2010
	Scaled PMHS high speed sled	Spinal properties Head inertia Thorax stiffness & damping Abdomen stiffness & damping	Lopez-Valdes, 2011b
	PMHS shield booster impact	Spinal properties Head inertia Thorax stiffness & damping Abdomen stiffness & damping	Kallieris, 1978 Forbes, 2007

3.1.1 *Abdomen setups*

In order to test the response of the abdomen to compression as a result of belt loading, three simulation setups were developed based on a test setup adopted from Kent (2011). The dummy or human surrogate was placed on a table top and a stiff 40 mm wide belt was fitted on the abdomen at two locations: on the center of the abdomen and high on the abdomen, the latter compressing the lower ribcage as well. Loading was applied either quasi-statically or dynamically.

In Figure 3-1 the simulation setup is shown for the modified and parameterized ellipsoid Hybrid III 6-year-old model with the belt loading on the center of the abdomen. A quasi-static belt pull on both belt ends, as shown in Figure 3-2, was applied. This results in a compression of the abdomen, of which a simulation result is shown in Figure 3-1 (bottom) at time of maximum abdomen deflection.

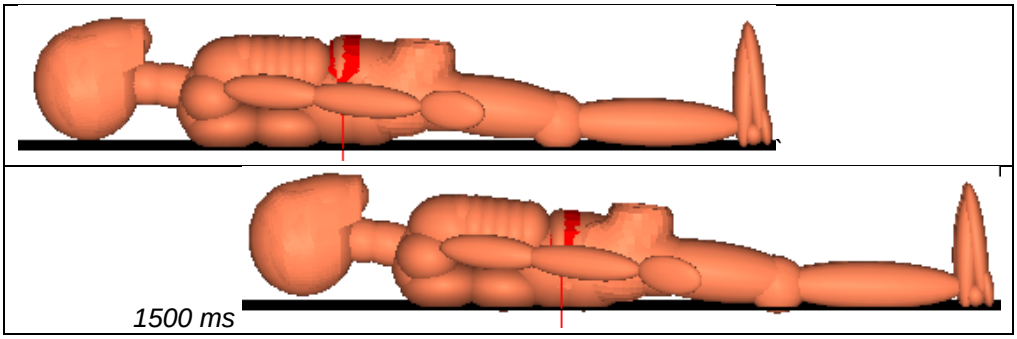

Figure 3-1. Quasi-static abdomen belt load PEDVE024 setups (Kent, 2011) used in sensitivity analysis, initially (top) and at time of maximum abdomen deflection (bottom).

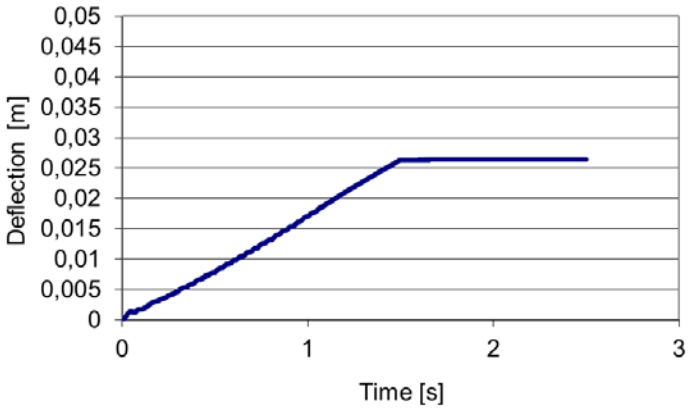

Figure 3-2. Quasi-static abdomen belt load test PEDVE024 (Kent, 2011) belt displacement input function.

In Figure 3-3 the simulation setup is shown for the modified and parameterized ellipsoid Hybrid III 6-year-old model with the belt loading on the center of the abdomen. A dynamic belt pull on both belt ends, as shown in Figure 3-4, was applied. This results in a compression of the abdomen, of which a simulation result is shown in Figure 3-3 (bottom) at time of maximum abdomen deflection.

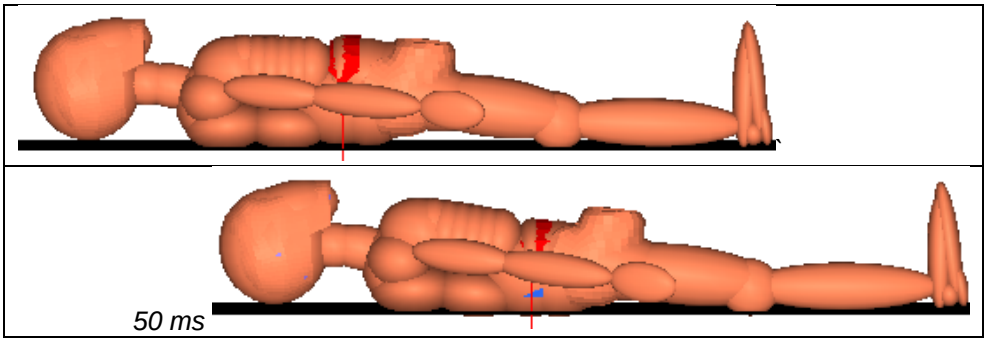

Figure 3-3. Dynamic abdomen belt load PEDVE025 setups (Kent, 2011) used in sensitivity analysis, initially (top) and at time of maximum abdomen deflection (bottom).

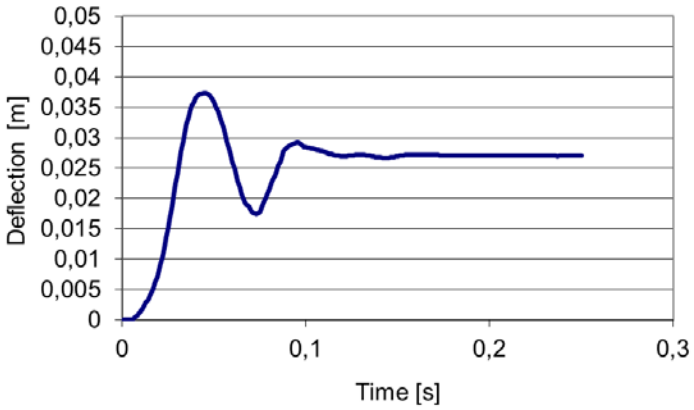

Figure 3-4. Dynamic abdomen belt load test PEDVE025 (Kent, 2011) belt displacement input function.

In Figure 3-5 the simulation setup is shown for the modified and parameterized ellipsoid Hybrid III 6-year-old model with the belt loading high on the abdomen. A dynamic belt pull on both belt ends, as shown in Figure 3-6, was applied. This results in a compression of the abdomen and ribcage, of which a simulation result is shown in Figure 3-5 (bottom) at time of maximum chest/abdomen deflection.

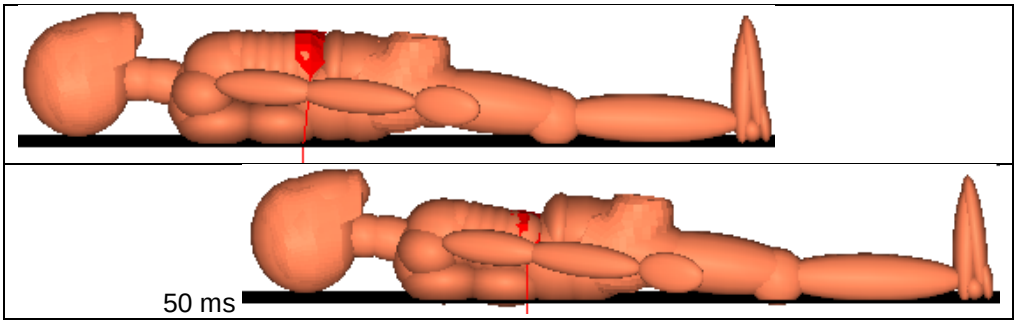

Figure 3-5. Dynamic upper abdomen belt load PEDVE026 setups (Kent, 2011) used in sensitivity analysis, initially (top) and at time of maximum chest/abdomen deflection (bottom).

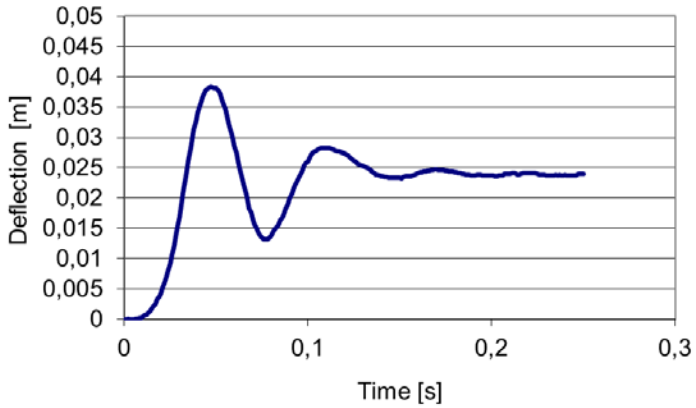

Figure 3-6. Dynamic upper abdomen belt load test PEDVE026 (Kent, 2011) belt displacement input function.

3.1.2 Thorax setups

In order to test the response of the thorax to blunt impact, a simulation setup was developed based on a test setup presented by Ouyang (2006). The dummy or human surrogate was seated on a table top and an impactor weighing 3.5 kg struck the mid-sternum at a velocity of 6.0 m/s. The setup is shown in Figure 3-7 (left) and the response at time of maximum chest deflection is shown in Figure 3-7 (right).

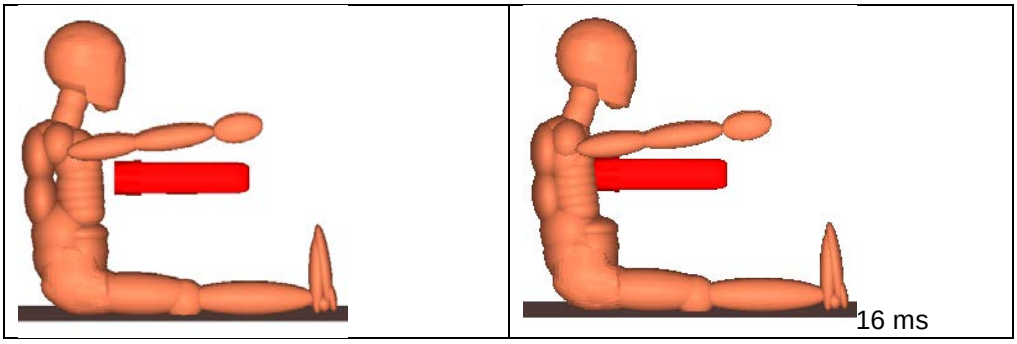

Figure 3-7. Thorax pendulum impact test setup (Ouyang, 2006 / Parent, 2010) as used in sensitivity analysis, initially (left) and at time of maximum chest deflection (right).

An additional setup is based on cardiopulmonary resuscitation (CPR), as published by Maltese (2008, 2010). In Figure 3-8 the simulation setup is shown for the modified and parameterized ellipsoid Hybrid III 6-year-old model with a rigid square box deflecting the thorax. The deflection time history was based on Parent (2010) and is shown in Figure 3-9. The response of the dummy thorax at time of maximum chest compression is shown in Figure 3-8 (right).

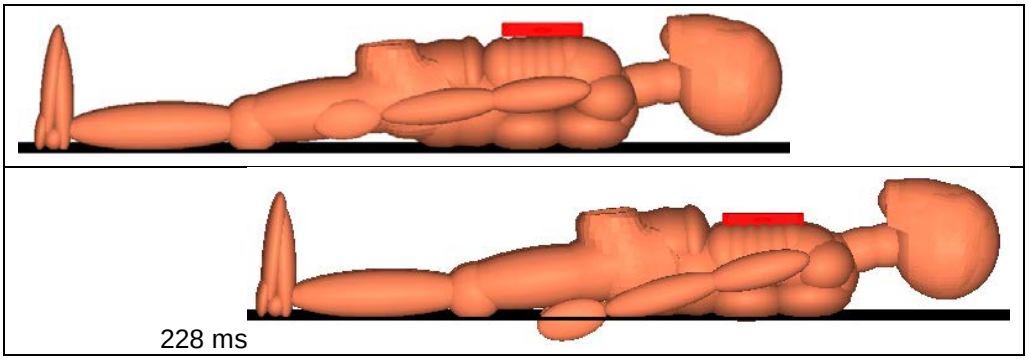

Figure 3-8. Thorax CPR impact test setup (Maltese, 2010) as used in sensitivity analysis, initially (top) and at time of maximum chest deflection (bottom).

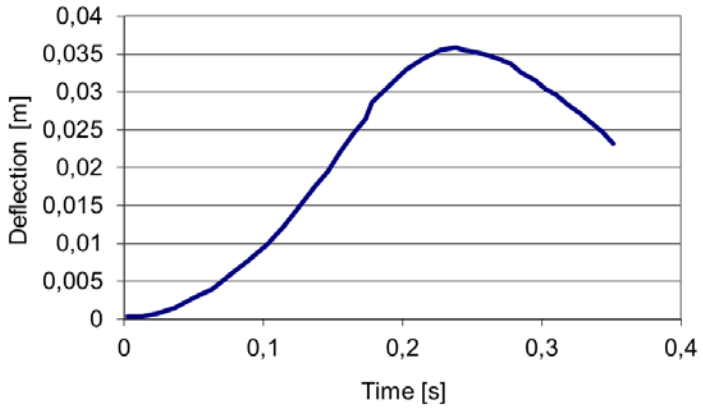

Figure 3-9. CPR thorax compression test (Maltese, 2010 / Parent, 2010) impactor displacement input function.

In order to test the response of the thorax to compression as a result of belt loading, a simulation setup was developed based on a test setup adopted from Kent (2009, 2011). The dummy or human surrogate was placed on a table top and a stiff 40 mm wide belt was fitted over the thorax. In Figure 3-10 the simulation setup is shown for the modified and parameterized ellipsoid Hybrid III 6-year-old model. A dynamic belt pull on both belt ends, as shown in Figure 3-11, was applied. This results in a compression of the thorax, of which a simulation result is shown in Figure 3-10 (bottom) at time of maximum chest deflection.

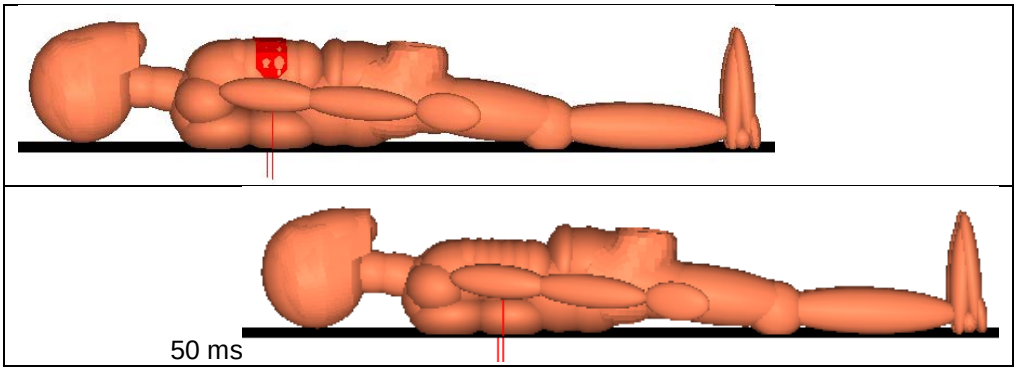

Figure 3-10. Thorax belt load test setup (Kent, 2009) as used in sensitivity analysis, initially (top) and at time of maximum chest deflection (bottom).

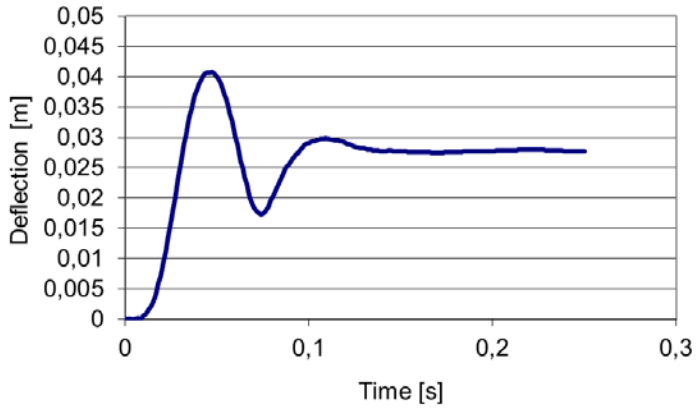

Figure 3-11. Dynamic thorax belt load PEDVE028 (Kent, 2009) test belt displacement input function.

Since realistically for a 6-year-old, chest deflection is typically caused by a 3-point belt in combination with a booster seat. In order to test the sensitivity of the dummy model's chest compression to belt force, a simulation setup was developed and validated based on a 2004 model year Ford Taurus rear bench, a Graco Step 3 Turbobooster high-back booster seat in an Autoliv 3-point belt restraint without force limiting and no pretensioner. This model setup was a replication from one of the hardware sled setups described by Forman (2008). In Figure 3-12, the simulation setup is shown for the modified and parameterized ellipsoid Hybrid III 6-year-old model. The validation results are shown in Appendix B: Ford Taurus rear bench, booster and 3-point belt setup validation. A vehicle acceleration pulse, as shown in Figure 3-13, replicating a frontal crash with 29 km/h ΔV was applied. This results in a dummy forward motion relative to vehicle and booster, and the belt compressing the thorax, of which a simulation result is shown in Figure 3-12 (right) at time of maximum forward head excursion.

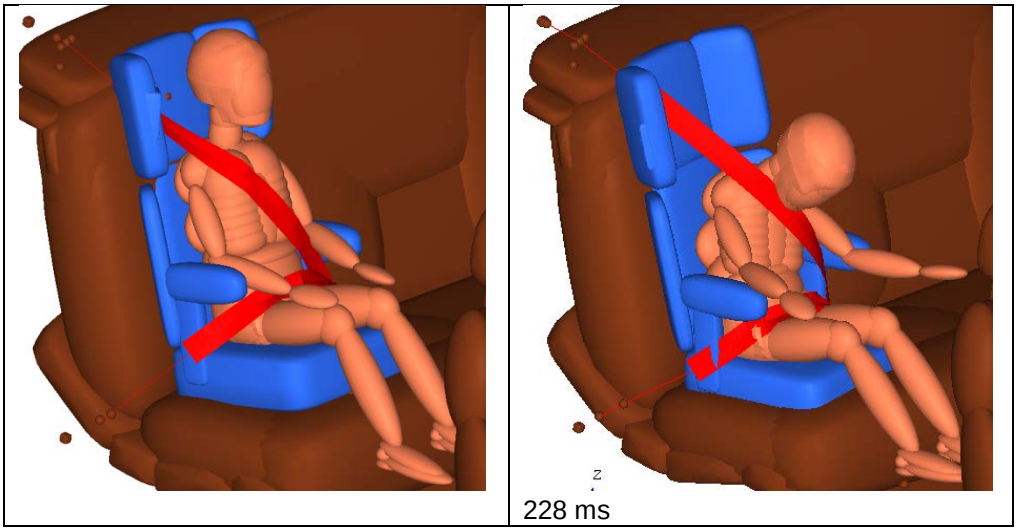

Figure 3-12. Vehicle seat, booster & 3-point belt test setup (Lopez-Valdes, 2011a) as used in sensitivity analysis, initially (left) and at time of maximum forward head excursion (right).

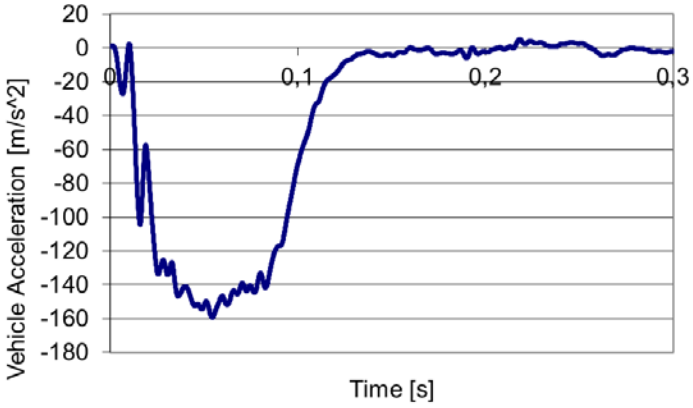

Figure 3-13. Vehicle seat, booster & 3-point belt thorax test (Lopez-Valdes, 2011a) vehicle acceleration pulse with 29 km/h ΔV.

3.1.3 Neck setups

In order to test the response of the neck to flexion as a result of head inertial loading, a simulation setup was developed based on a simulation performed by Dibb (2010). The T1 x-acceleration and rotational y-acceleration measured in adult National Biodynamics Laboratory (NBDL) sled tests was applied to the T1 vertebrae of the 6-year-old human neck model in LS-Dyna (Dibb, 2010). In Figure 3-14 the simulation setup is shown for the modified and parameterized ellipsoid Hybrid III 6-year-old model. The same T1 acceleration and rotational acceleration was applied, as shown in Figure 3-15 and Figure 3-16 respectively. The resulting neck flexion at time of maximum head forward displacement is shown in Figure 3-14 (right).

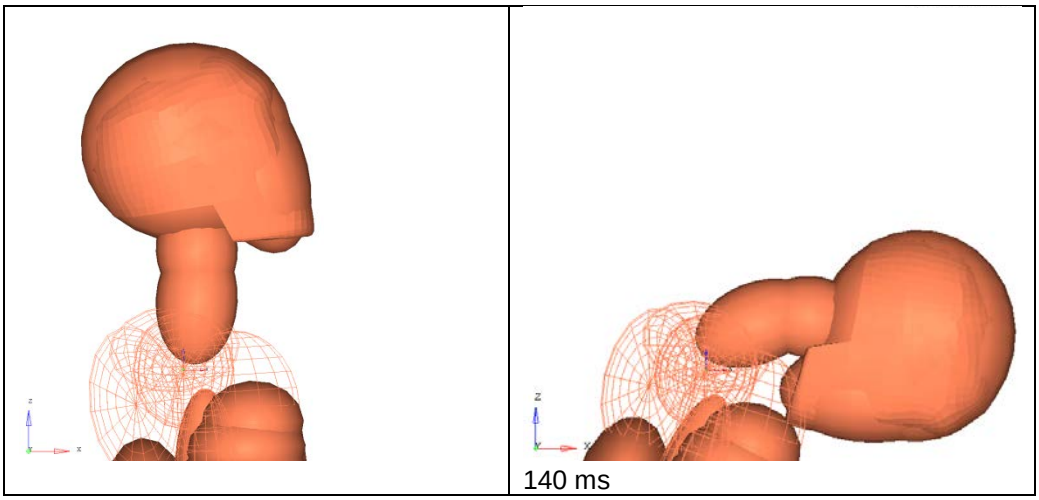

Figure 3-14. NBDL frontal neck test setup (Dibb, 2010) as used in sensitivity analysis, initially (left) and at time of maximum head forward displacement (right).

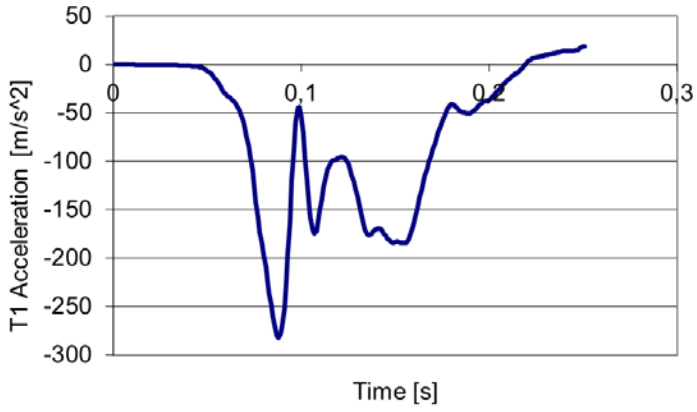

Figure 3-15. NBDL frontal neck test (Dibb, 2010) T1 X-translational acceleration input function.

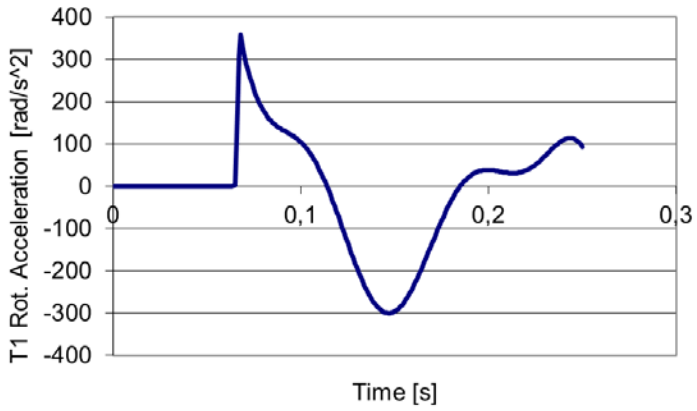

Figure 3-16. NBDL frontal neck test (Dibb, 2010) T1 Y-rotational acceleration input function.

An additional test setup, consisting of applying pure tension to the neck, also based on a simulation performed by Dibb (2010), was developed. A constant loading rate was applied to the head of the 6-year-old human neck model in LS-Dyna (Dibb, 2010). In Figure 3-17 the simulation setup is shown for the modified and parameterized ellipsoid Hybrid III 6-year-old model. A displacement time-history as shown in Figure 3-18 was applied in order to achieve the desired loading rate starting from zero, hence minimizing vibrations due to transient effects. The elongation of the neck at time of maximum head displacement is shown in Figure 3-17 (right).

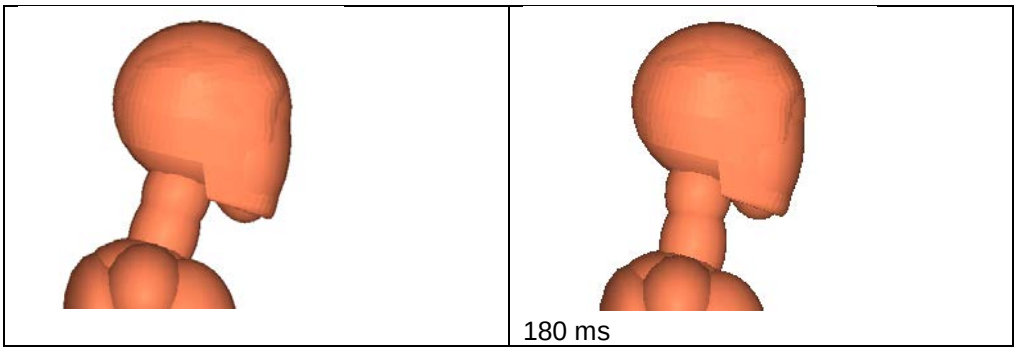

Figure 3-17. Neck tension setup (Dibb, 2010) as used in sensitivity analysis, initially (left) and at time of maximum head displacement (right).

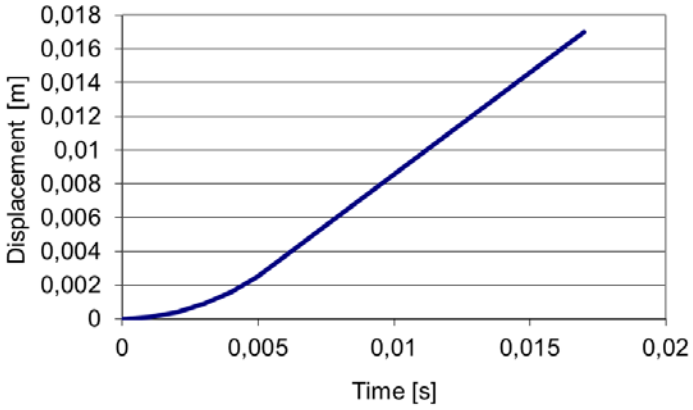

Figure 3-18. Neck tension test (Dibb, 2010) head displacement input function.

3.1.4 Overall setups

Dummy kinematic behavior is of utmost importance in vehicle crashes, especially where correct prediction of head forward displacement is concerned. In order to assess the biofidelity of dummies, whole body setups were created.

The first setup is based on a child volunteer test setup (Arbogast, 2009) in which children of various ages were seated on a rigid seat and restrained by a 3-point belt adapted to attain optimal belt fit for the child. The simulation model of this setup with the modified and parameterized ellipsoid Hybrid III 6-year-old model is shown in Figure 3-19. A sled acceleration pulse was applied as shown in Figure 3-20. The model of this setup was validated against sled tests with a Hybrid III 6-year-old dummy (Seacrist, 2010), of which the results are presented in Appendix C: CHOP sled setup validation. The response of the model at time of maximum forward head excursion is shown in Figure 3-19 (right).

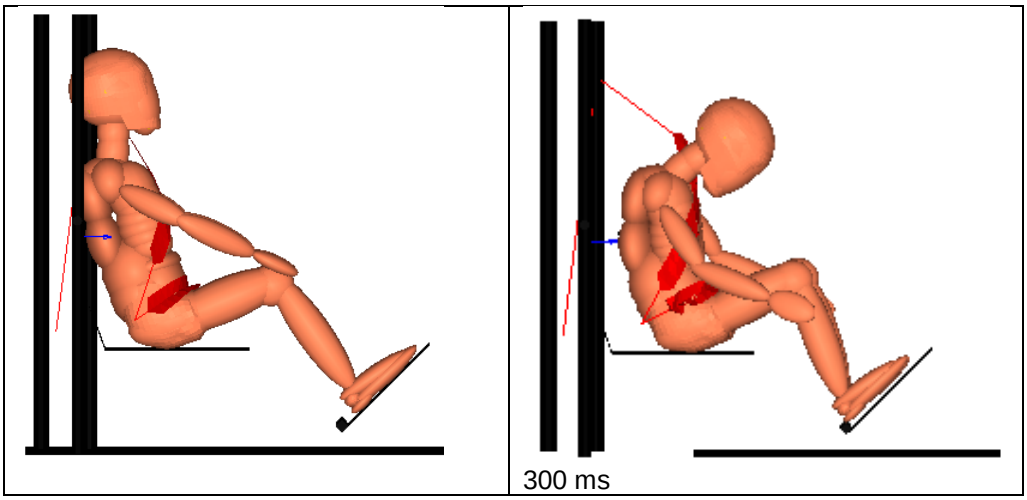

Figure 3-19. Volunteer low speed sled setup (Arbogast, 2009) as used in sensitivity analysis, initially (left) and at time of maximum head excursion (right).

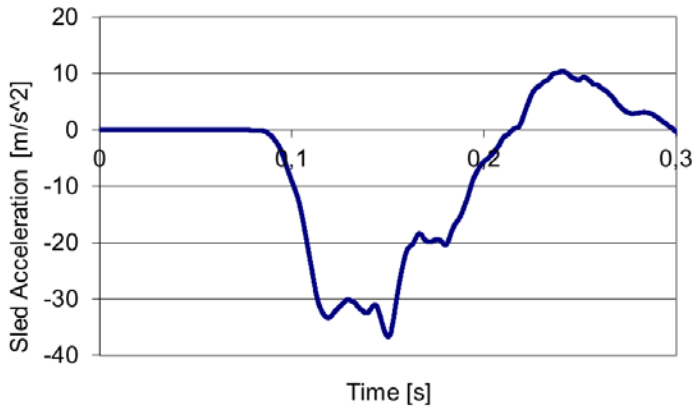

Figure 3-20. Volunteer low speed sled test (Arbogast, 2009) acceleration pulse.

An adaptation of this setup was used to derive the response of a 6-year-old child to higher severity impact (Lopez-Valdes, 2011b). The simulation model was adapted by adding a rigid knee bolster (see Figure 3-21) and by applying a higher severity pulse (see Figure 3-22). The response of the model to the impact at time of maximum forward head excursion is shown in Figure 3-21 (right).

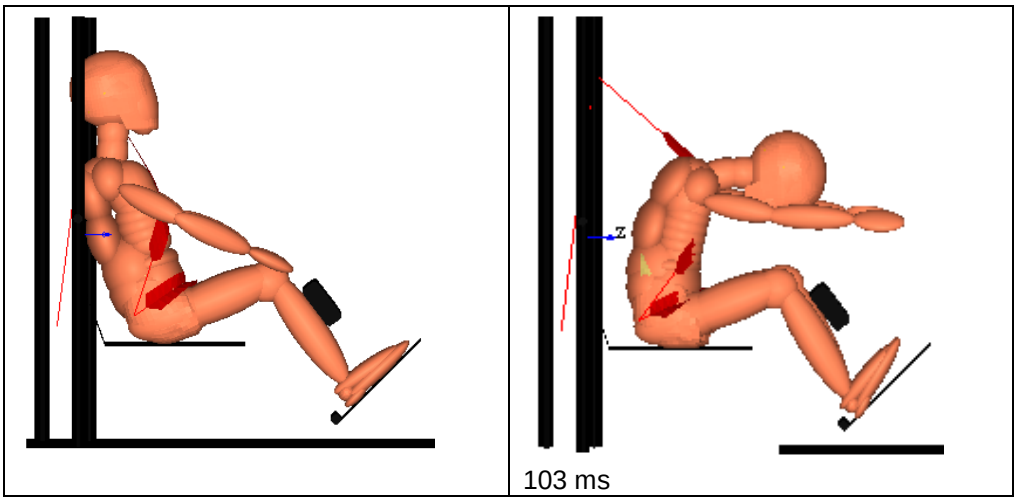

Figure 3-21. Scaled PMHS high speed sled setup (Lopez-Valdes, 2011b) as used in sensitivity analysis, initially (left) and at time of maximum head excursion (right).

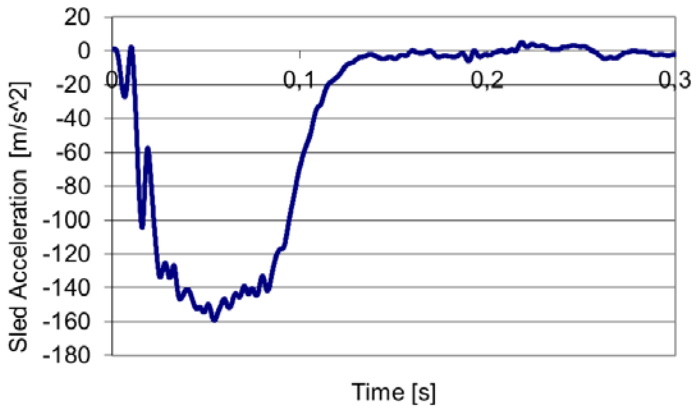

Figure 3-22. Scaled PMHS high speed sled test (Lopez-Valdes, 2011b) acceleration pulse.

The third setup is based on a PMHS test on a vehicle seat with a shield booster (Kallieris, 1978). In an earlier phase of this project the model of this setup was developed and validated (Forbes, 2007). The simulation model of this setup with the modified and parameterized ellipsoid Hybrid III 6-year-old model is shown in Figure 3-23. A sled acceleration pulse was applied as shown in Figure 3-24. The response of the model at time of maximum forward head excursion is shown in Figure 3-23 (right).

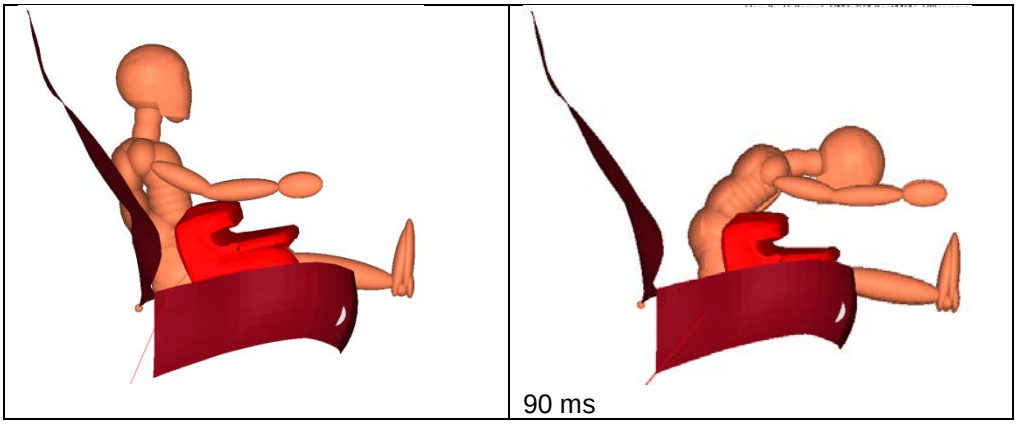

Figure 3-23. PMHS shield booster impact setup (Kallieris, 1978 / Forbes, 2007) as used in sensitivity analysis, initially (left) and at time of maximum head excursion (right).

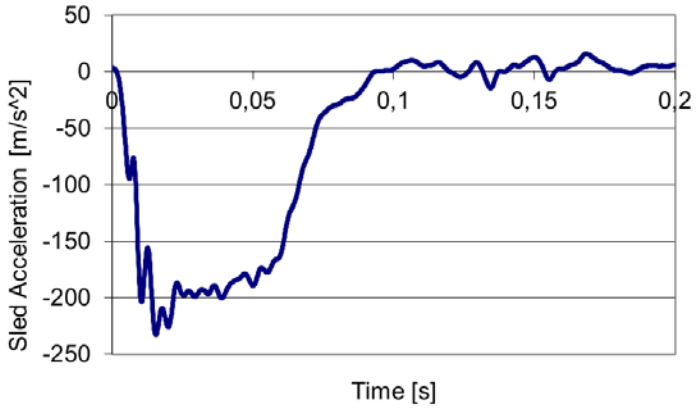

Figure 3-24. PMHS shield booster impact test (Kallieris, 1978 / Forbes, 2007) sled acceleration pulse.

3.2 Parameter choice and ranges

Table 3-3 shows the parameters that could be varied in the parameterized ellipsoid Hybrid III 6-year-old model. The parameterization of the model was largely discussed in Forbes (2007), while some additions were made during the course of the project. Table 3-3 also shows the variation ranges of the parameters for the sensitivity study. These ranges were based on discussions with partners. While input was provided on ranges found in 6-year-old populations, it was not certain that the current normal value in the dummy was anywhere close to that. Therefore, the ranges were not based on the ranges observed among child populations. Instead, scale factors and dimensional scaling values that were anticipated to cover the expected difference between the current Hybrid III 6-year-old and actual 6-year-old children were defined.

Table 3-3. Overview of parameters and scaling values for sensitivity study

Interest Area	Parameter	Scale down	Normal	Scale up
Abdomen	Abdominal stiffness	0.5	1.0	2.0
	Abdominal damping	0.1	1.0	10.0
	Pelvis flesh stiffness	0.5	1.0	2.0
Thorax	Rib stiffness anterior-posterior direction (1)	0.5	1.0	2.0
	Rib stiffness lateral direction	0.5	1.0	2.0
	Rib damping (3)	0.1	1.0	10.0
	Rib flesh stiffness (4)	0.5	1.0	2.0
	Thorax / shoulder flesh stiffness (5)	0.5	1.0	2.0
	Sternum stiffness (6)	0.5	1.0	2.0
	Sternum damping (7)	0.1	1.0	10.0

Interest Area	Parameter	Scale down	Normal	Scale up
Neck / Spine	Head mass	0.667	1.0	1.5
	Head center of gravity X-direction	-20 mm	0 mm	20 mm
	Head center of gravity Y-direction	-20 mm	0 mm	20 mm
	Neck joint stiffness flexion-extension	0.5	1.0	2.0
	Neck joint damping flexion-extension	0.1	1.0	10.0
	Neck joint stiffness lateral bending	0.5	1.0	2.0
	Neck joint damping lateral bending	0.1	1.0	10.0
	Neck tensile stiffness	0.5	1.0	2.0
	Neck tensile damping	0.1	1.0	10.0
	Neck upper joint z-position	-20 mm	0 mm	20 mm
	Neck middle joint z-position	-20 mm	0 mm	20 mm
	Neck lower joint z-position	-20 mm	0 mm	20 mm
	Lumbar joint rotational stiffness flexion-extension and lateral	0.5	1.0	2.0
	Lumbar joint rotational damping flexion-extension and lateral	0.1	1.0	10.0
	Lumbar joint shear stiffness posterior-anterior and lateral	0.5	1.0	2.0
	Lumbar joint shear damping posterior-anterior and lateral	0.1	1.0	10.0
	Lumbar joint z-position	-20 mm	0 mm	20 mm
	Thoracic joint rotational stiffness flexion-extension	0.5	1.0	2.0
	Thoracic joint rotational damping flexion-extension	0.1	1.0	10.0
	Thoracic joint z-position	-20 mm	0 mm	20 mm

In order to add clarification to the thorax parameters, a schematic overview of the thorax structure, based on Parent (2010), is shown in Figure 3-25. The numbers behind the parameters in Table 3-3 correspond to the numbers in the schematic below.

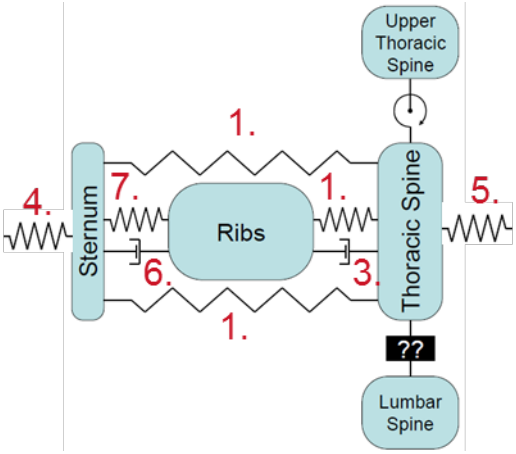

Figure 3-25. Schematic of thorax structure in modified and parameterized ellipsoid Hybrid III 6-year-old model, as adopted from Parent (2010).

3.3 Design of sensitivity study

The sensitivity study is performed in four different groups which are defined by body region (abdomen, thorax, neck and overall setups). Only the parameters which have influence on the specific interest area of the simulation setups (see Table 3-3) are varied for the abdomen, thorax and neck setups. For the whole body crash scenario setups, all the parameters are varied. As such, for every parameter two sensitivity scores are determined; 1) a sensitivity score for the specific body region is calculated and 2) a sensitivity score for the whole body crash setups is determined. Simulations are performed where in each simulation one parameter is varied, while all others are kept at the normal value. Variations exist of scaling upwards and downwards according to the values denoted in Table 3-3.

In general, the sensitivity of a parameter (S_{par}) is determined by the sensitivity equation,

$$S_{par} = \frac{\sum_{i=1}^{n} S_{sim,i} * W_{sim,i}}{\sum_{i=1}^{n} W_{sim,i}},$$

which is dependent on the sensitivity of the parameter in all n simulations ($S_{sim,i}$ is the parameter sensitivity for the i^{th} simulation) and the specific weighting factors ($W_{sim,i}$) of the simulations. The simulation sensitivity is dependent on the parameter sensitivity of all n different plots ($S_{plot,i}$ is the sensitivity for the i^{th} plot) or responses of an experiment and the specific weighing factors ($W_{plot,i}$) of the specific plots,

$$S_{sim} = \frac{\sum_{i=1}^{n} S_{plot,i} * W_{plot,i}}{\sum_{i=1}^{n} W_{plot,i}}.$$

The different plots which are used in the sensitivity study are force-time plots (F-t), force-displacement plots (F-d), displacement-time plots (d-t), rotational acceleration-time plots (α-t) and trajectories (z-x). The plot sensitivity is dependent on the sensitivity of the parameters on all n different signals ($S_{signal,i}$) is the sensitivity for the i^{th} signal) of the plots and their weighting factors ($W_{signal,i}$) and is given by the following equation,

$$S_{plot} = \frac{\sum_{i=1}^{n} S_{signal,i} * W_{signal,i}}{\sum_{i=1}^{n} W_{signal,i}} .$$

The signal sensitivity of a parameter is defined by the error diversity of the signal in the parameterized MADYMO simulations to the experimental data from literature. Four different sensitivity signals are used to determine the sensitivity of a parameter (overall sensitivity, peak height sensitivity, peak time sensitivity and slope sensitivity). The signal sensitivity is given by the following equation,

$$S_{signal,i} = \sum_{i=1}^{n-1} \frac{|Signal_{error}(i) - Signal_{error}(i+1)|}{n-1} ,$$

where $Signal_{error}(i)$ is the signal error for scaling factor *i*. The four different signal sensitivities are determined from four different signal errors (overall error, peak height error, peak time error and slope error).

The overall error (R_{error}) is determined out of the mean difference between the simulation outcome ($X_{sim,i}$) and the experimental data ($X_{exp,i}$) at all *i* data points and is normalized by the mean of the experimental data,

$$R_{error} = \frac{\sum_{i}^{n} \frac{X_{exp,i} - X_{sim,i}}{mean(X_{exp})}}{n} .$$

The peak height error (P_{error}) is given by the relative difference between the peak height of the simulation (P_{sim}) and the experimental data (P_{exp}),

$$P_{error} = \frac{P_{exp} - P_{sim}}{P_{exp}} .$$

The peak time error (T_{error}) is given by the relative difference between the peak time of the simulation (T_{sim}) and the experimental data (T_{exp}),

$$T_{error} = \frac{T_{exp} - T_{sim}}{T_{exp}} .$$

The slope error ($Slope_{error}$) is given by the relative difference between the slope of the simulation ($Slope_{sim}$) and the experimental data ($Slope_{exp}$),

$$Slope_{error} = \frac{Slope_{exp} - Slope_{sim}}{Slope_{exp}} .$$

Not every sensitivity signal will be used to calculate the sensitivity response of a parameter for every simulation. Table 3-4 shows the signals, plots and the weighting factors of the experiments which are used to calculate the sensitivity score of a parameter. All experiments were weighted equally, except for the Taurus booster setup. This setup was given lower weighting since it was deemed too complex to provide a direct relation between parameters and dummy response.

Table 3-4. Overview of simulations, plots, signals and weighing factors for sensitivity study.

Interest area	Simulation	W_sim	Plots	W_plot	Signal	W_signal
Abdomen	Quasi-static abdomen belt PEDVE024 (Kent, 2011)	1	F-t	1	Overall	1
					Peak height	1
	Dynamic abdomen belt PEDVE025 (Kent, 2011)	1	F-t	1	Overall	1
					Peak height	1
	Dynamic upper abdomen belt PEDVE026 (Kent, 2011)	1	F-t	1	Overall	1
					Peak height	1
Thorax	Thorax belt load (Kent, 2009)	1	F-t	1	Overall	1
					Peak height	1
	CPR thorax compression (Maltese, 2010)	1	F-d	1	Slope	1
	Thoracic pendulum (Ouyang, 2006 / Parent, 2010)	1	F-t	1	Overall	1
					Peak height	1
					Peak time	1
			d-t	1	Overall	1
					Peak height	1
					Peak time	1
	Taurus booster setup (Lopez-Valdes, 2011a)	0,5	F-d	1	Slope	1
Neck	Neck tensile (Dibb, 2010)	1	F-d	1	Peak height	1
	NBDL frontal neck test (Dibb, 2010)	1	d-t	1	Overall	1
					Peak height	1
					Peak time	1
			α-t	1	Overall	1
					Peak height	1
					Peak time	1
Overall	Frontal impact volunteer (Arbogast, 2009)	1	Head top trajectory	1	Overall	1
					Peak height X	1
			Nasion trajectory	1	Overall	1
			Opisthocranion trajectory	1	Overall	1
			C4 trajectory	1	Overall	1
			T1 trajectory	1	Overall	1
			Iliac crest trajectory	1	Overall	1
			Shoulderbelt force	1	Overall	1
					Peak height X	1
					Peak time	1
			Lapbelt force	1	Overall	1
					Peak height X	1
					Peak time	1
	Frontal impact high speed scaled (Lopez-Valdes, 2011b)	1	Head COG trajectory	1	Overall	1
					Peak height X	1
			T1 trajectory	1	Overall	1
			T8 trajectory	1	Overall	1
			Pelvis trajectory	1	Overall	1
	Frontal impact HIII/PMHS (Kallieris, 1978 / Forbes, 2007)	1	Head trajectory	1	Overall	1
					Peak height X	1
			Knee trajectory	1	Overall	1
			Left shoulderbelt force	1	Overall	1
					Peak height X	1
					Peak time	1
			Right shoulderbelt force	1	Overall	1
					Peak height X	1
					Peak time	1

3.4 Sensitivity analysis results

As mentioned in Section 3.3, two sensitivity scores are determined. The scores for the specific interest regions and overall setups are summarized in Table 3-5. Parameter sensitivity scores which are higher than the mean sensitivity score for a body region are marked yellow. In the following sections the results of the four body regions are discussed in more detail.

Table 3-5. Sensitivity scores for interest regions and overall setups.

Interest region	Parameter	Sensitivity score interest region	Sensitivity score overall setups
Abdomen	Abdominal stiffness	0,385	0,009
	Abdominal damping	0,044	0,005
	Pelvis flesh stiffness	0,196	0,015
Thorax	Rib stiffness anterior-posterior direction	0,819	0,011
	Rib stiffness lateral direction	0,001	0,001
	Rib damping	0,313	0,007
	Rib flesh stiffness	0,087	0,000
	Thorax / shoulder flesh stiffness	0,035	0,000
	Sternum stiffness	0,054	0,002
	Sternum damping	0,043	0,003
Neck / Spine	Head mass	0,188	0,079
	Head centre of gravity X-direction	0,089	0,023
	Head centre of gravity Y-direction	0,184	0,025
	Neck joint stiffness flexion-extension	0,072	0,059
	Neck joint damping flexion-extension	0,156	0,099
	Neck joint stiffness lateral bending	0,000	0,002
	Neck joint damping lateral bending	0,000	0,002
	Neck tensile stiffness	2,254	0,004
	Neck tensile damping	6,399	0,003
	Neck upper joint z-position	0,327	0,041
	Neck middle joint z-position	0,304	0,030
	Neck lower joint z-position	0,014	0,021
	Lumbar joint rotational stiffness flexion-extension and lateral	0,000	0,032
	Lumbar joint rotational damping flexion-extension and lateral	0,000	0,051
	Lumbar joint shear stiffness posterior-anterior and lateral	0,000	0,007
	Lumbar joint shear damping posterior-anterior and lateral	0,000	0,002
	Thoracic joint rotational stiffness flexion-extension	0,000	0,050
	Thoracic joint rotational damping flexion-extension	0,000	0,055
	Thoracic joint z-position	0,005	0,032
	Lumbar joint z-position	0,003	0,045

3.4.1 Abdomen

The abdominal stiffness is the most sensitive parameter of interest region abdomen. Also, the pelvis flesh stiffness scores above the mean sensitivity, while the abdominal

damping is a less sensitive parameter. Figure 3-26 shows the results of the simulations with a varying abdominal stiffness (scaling factors 0.5 - 1.0 - 2.0). Three belt tests are simulated as described in Section 3.1.1. The abdominal stiffness is highly sensitive for the static experiment and the lower abdominal belt load experiment. Figure 3-27 shows the results of the sensitivity simulations for the abdominal damping. Note that while the parameter abdominal damping has a relatively low sensitivity score compared with abdominal stiffness, the peak height of both dynamic belt tests raise equally for both abdominal stiffness as well as abdominal damping. The low (scale factor 0.5) and normal (scale factor 1.0) abdominal damping simulation result in almost equal belt forces. In the dynamic lower belt test, stiffness influences both initial peak as well as constant force level later in the experiment, while obviously damping only influences the peak. There is very low sensitivity of any parameter to the upper belt load tests, since the belt effectively loads the ribcage of the dummy instead of the abdomen.

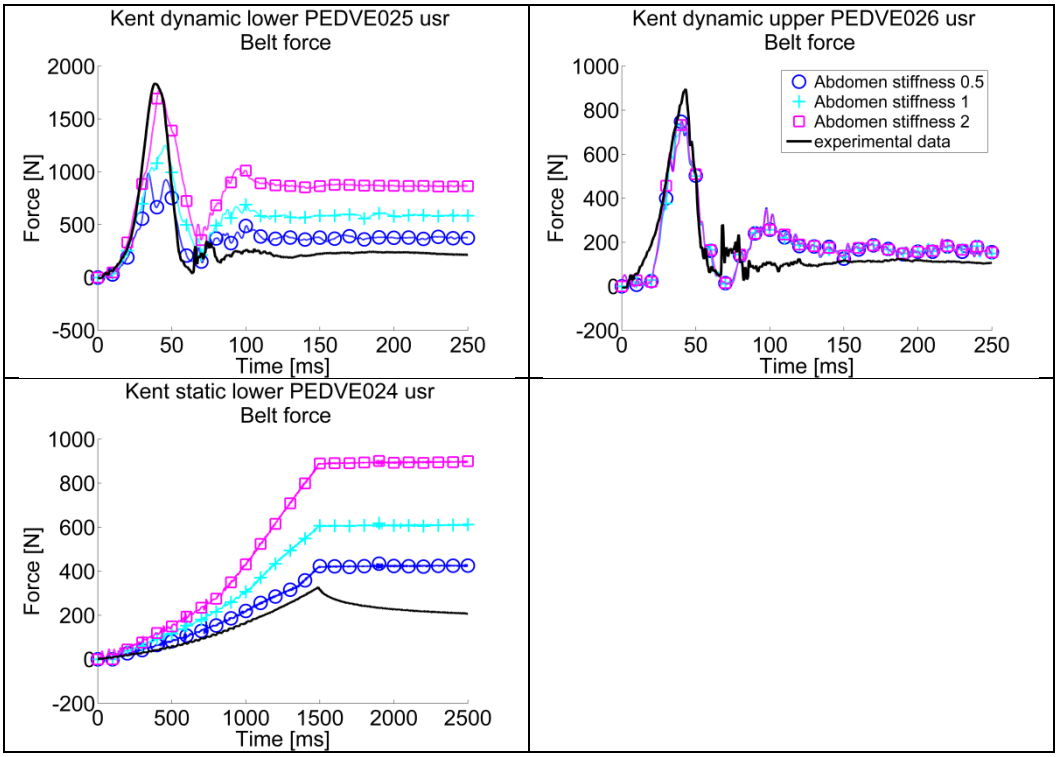

Figure 3-26. Results of sensitivity simulations with parameter abdominal stiffness for abdomen region.

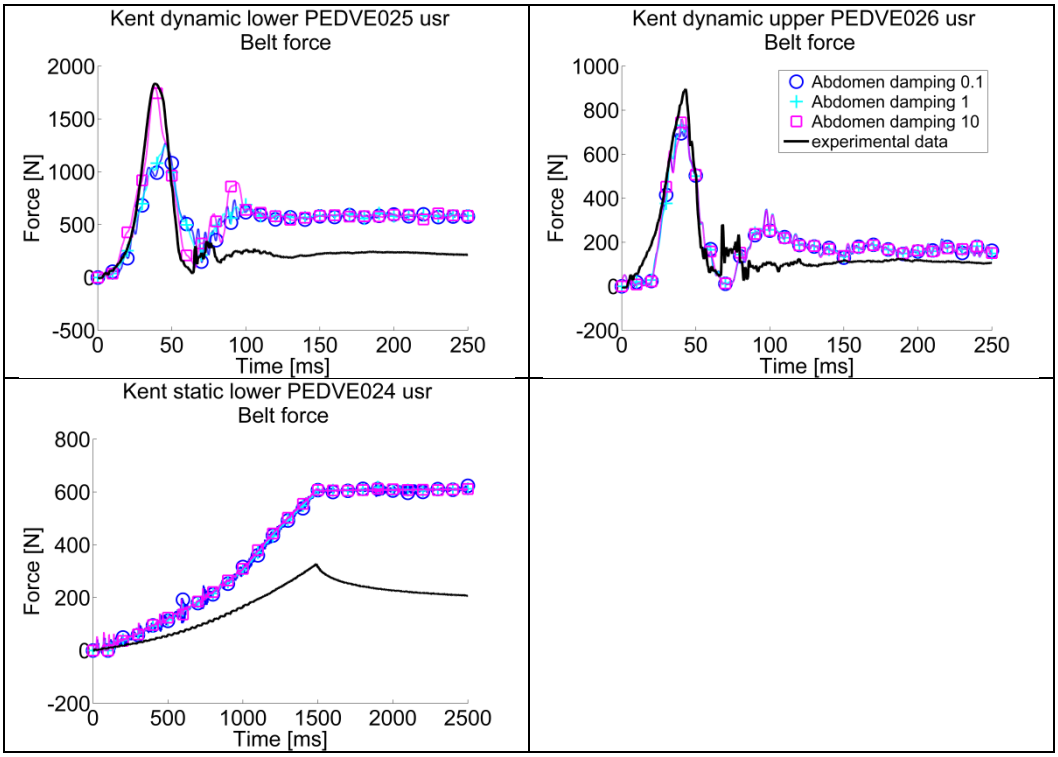

Figure 3-27. Results of sensitivity simulations with parameter abdominal damping for abdomen region.

3.4.2 Thorax

For the thorax interest region, rib damping and rib stiffness in anterior posterior direction are the most sensitive parameters, while the rib stiffness in lateral direction shows almost no sensitivity. The sensitivity of the other parameters are comparable. Figure 3-28 shows the results of the sensitivity simulations with the rib stiffness in anterior-posterior direction. The rib stiffness has a relative high sensitivity for all experiments. As was also seen for the abdominal damping in the abdomen sensitivity results, the rib damping has especially high sensitivity by scaling the damping up (see Figure 3-29). Scaling the rib damping down shows only differences for the thoracic pendulum simulations. In the dynamic belt test, stiffness influences both initial peak as well as constant force level later in the experiment, while obviously damping only influences the peak.

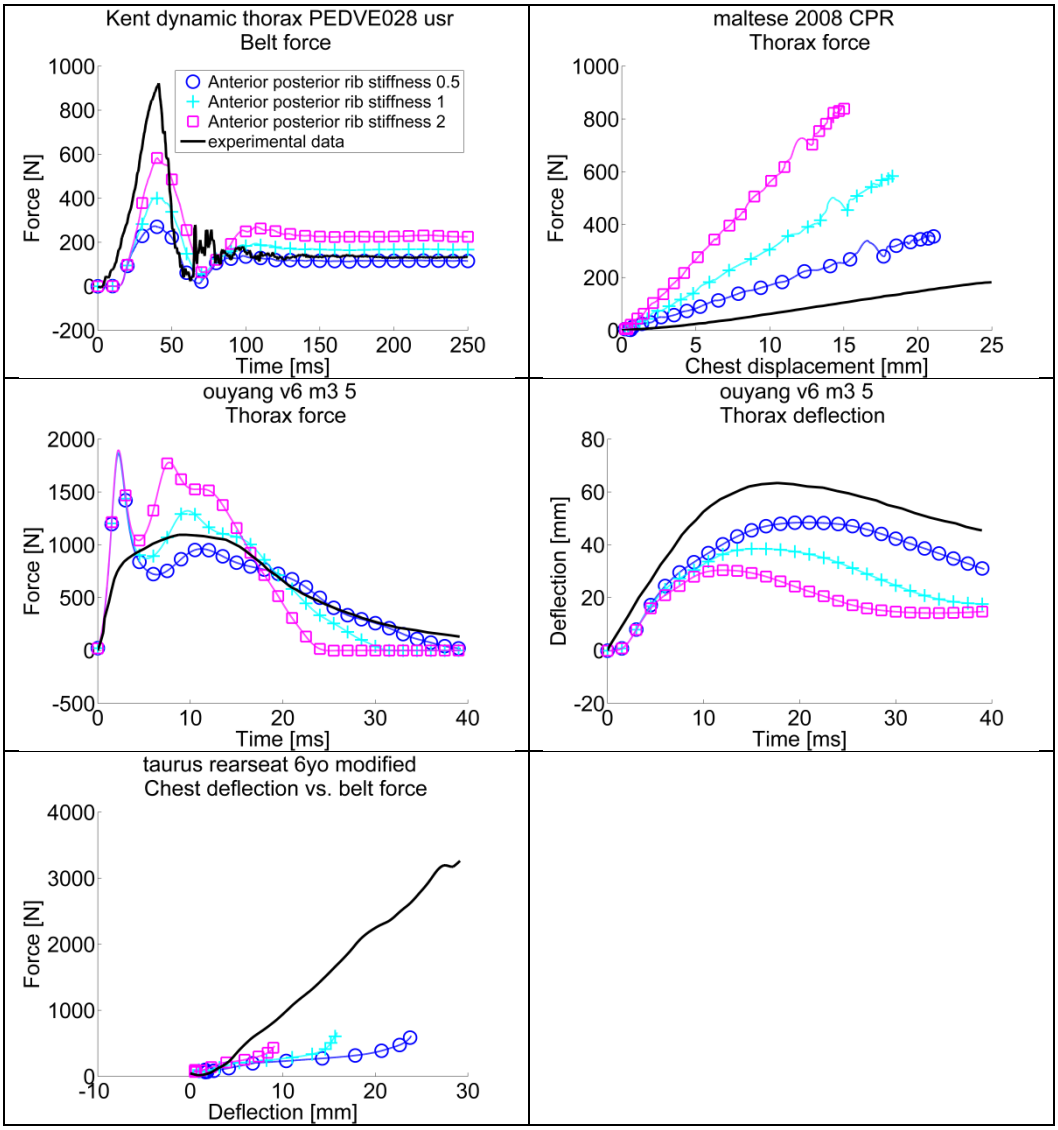

Figure 3-28. Results of sensitivity simulations with parameter rib stiffness anterior-posterior for thorax region.

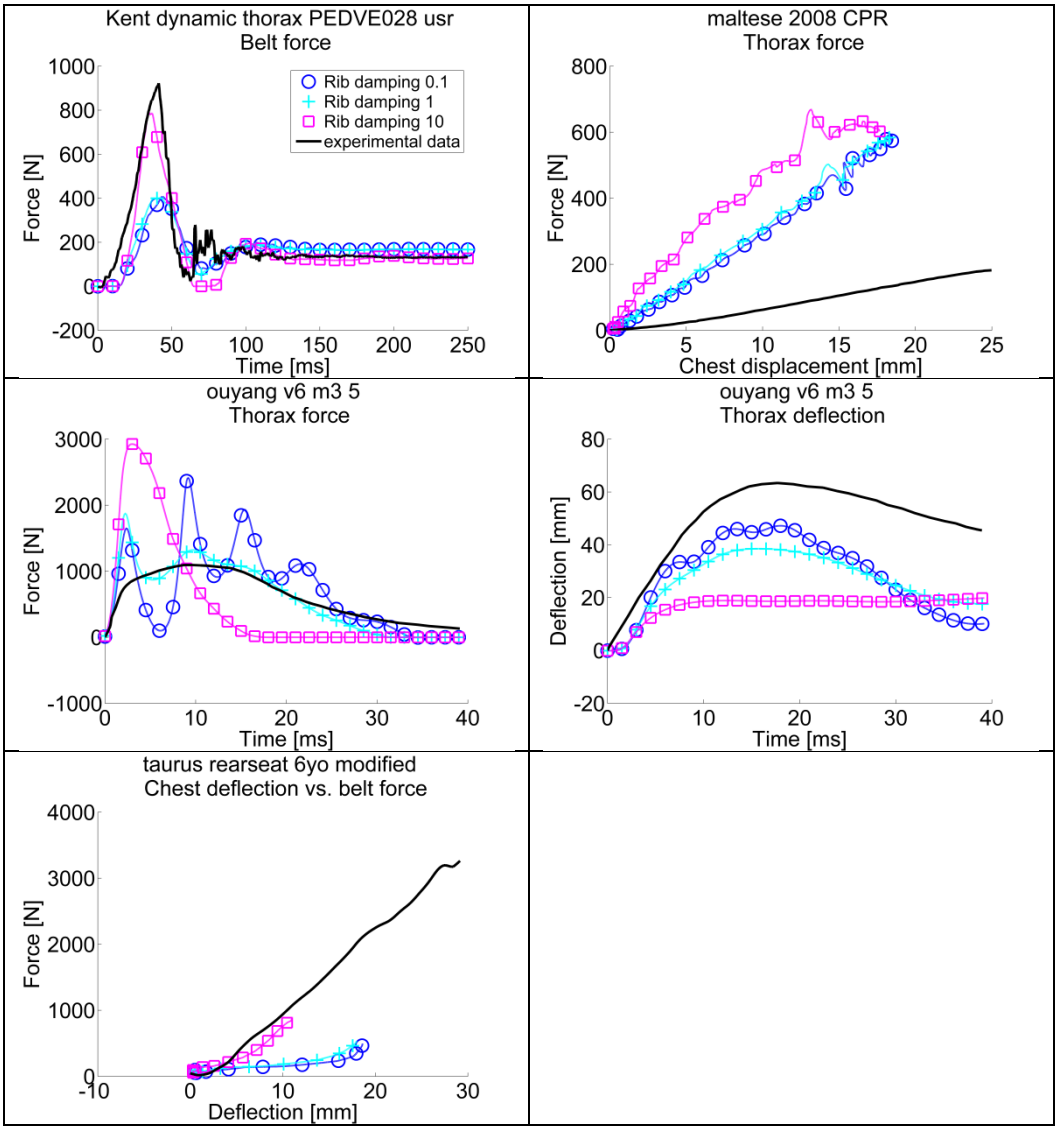

Figure 3-29. Results of sensitivity simulations with parameter rib damping for thorax region.

3.4.3 *Neck and spine*

Table 3-5 shows that the neck tensile stiffness and damping are the only parameters that score above the mean sensitivity for the neck interest region. However, the head mass, head center of gravity, neck joint stiffness and damping for flexion-extension and neck joint z-positions are also relatively sensitive parameters. Figure 3-30 shows that the neck tensile stiffness is especially sensitive for the neck tension simulation. The tensile neck stiffness is less sensitive for the NBDL simulation. This also applies for the neck tensile damping. The other parameters mentioned above are more equally sensitive for the tensile and NBDL simulations.

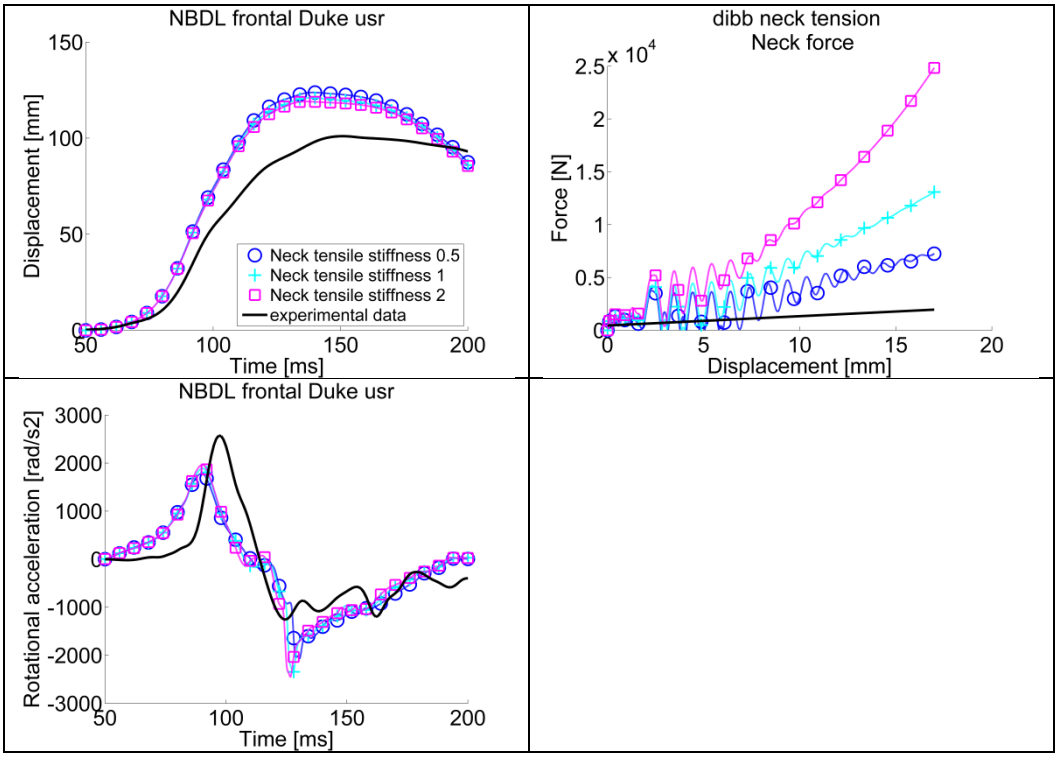

Figure 3-30. Results of sensitivity simulations with parameter neck tensile stiffness for neck region.

3.4.4 *Overall*

For the overall setups, in general, parameters have relatively lower sensitivity scores than for the specific body region simulations. The most sensitive parameters are found in the neck/spine region. Especially, the head mass, head center of gravity, neck joint stiffness and damping flexion-extension, lumbar joint stiffness and damping flexion-extension and thoracic joint stiffness and damping flexion-extension have a high sensitivity to the overall test setups. While the neck tensile stiffness and damping are very sensitive for the neck simulations, the neck tensile parameters are less sensitive for the overall setups. Also, the lumbar, thoracic and neck joint z-positions were sensitive parameters. However, by varying these parameters the length of the spine / neck changes. As such, the scaling of these parameters has limited significance since the anthropometry of the dummy is assumed to be fairly representative of a 6-year-old. Figure 3-31 shows the sensitivity results of the most sensitive parameter, the neck joint damping flexion-extension.

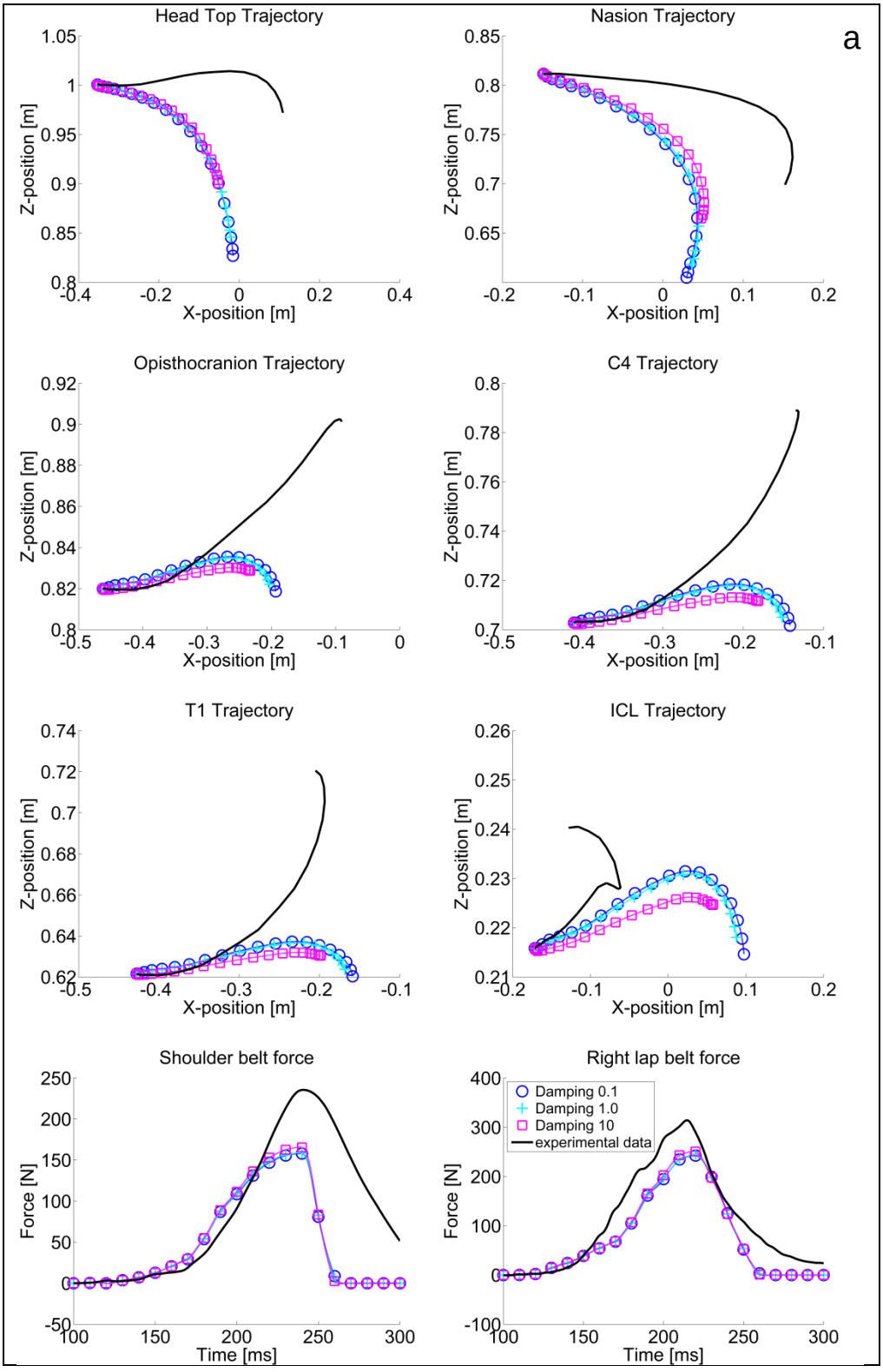
a
Head Top Trajectory
Nasion Trajectory
Opisthocranion Trajectory
C4 Trajectory
T1 Trajectory
ICL Trajectory
Shoulder belt force
Right lap belt force
Z-position [m]
X-position [m]
Force [N]
Time [ms]
Damping 0.1
Damping 1.0
Damping 10
experimental data

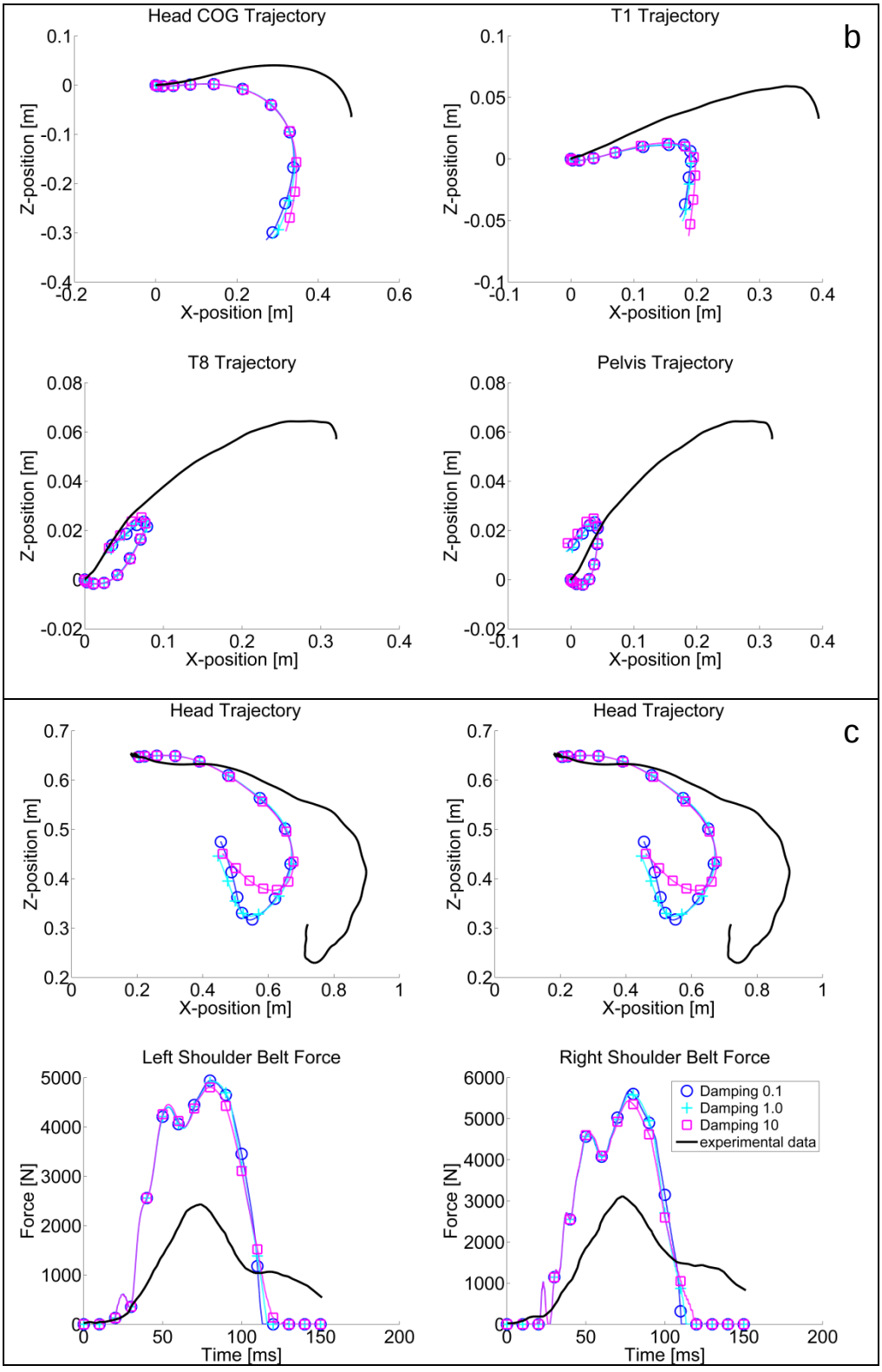

Figure 3-31. Results of sensitivity simulations with parameter neck joint damping flexion-extension for overall setups (cell a: Volunteer low speed sled; cell b: Scaled PMHS high speed sled; cell c: PMHS shield booster impact).

3.5 Conclusion

In Task 1 a sensitivity analysis was performed with the updated model to assess which parameters are of what influence on which response. In this section the results of the sensitivity study are discussed separately for every interest region.

3.5.1 Abdomen

Both the abdomen and pelvis flesh stiffness parameters had high sensitivity to the abdominal experiments. To create a more biofidelic dummy model, the stiffness values should be reduced, especially based on the quasi-static experiment. Because the abdomen damping, with generally lower sensitivity, had a high sensitivity to the peaks of the dynamic experiments, the abdominal damping should be increased to reach the peak values of the dynamic experiments.

3.5.2 Thorax

The rib stiffness in anterior-posterior direction and rib damping showed high sensitivity. Only the rib stiffness had a high sensitivity response for all simulations. To reach the experimental outcome, the rib stiffness in anterior-posterior direction should be lowered. Increasing the rib damping could have a positive effect on the belt experiments (Kent and Taurus setup). All other parameters had a less sensitive response. However, the sternum damping and sternum stiffness could be reduced to reach the results of the CPR and thoracic pendulum experiments and the contact stiffness values could eventually be increased to reach the outcome of the belt load experiment.

3.5.3 Neck and spine

The neck tensile stiffness and damping were the most sensitive neck parameters. One of these neck tensile parameters should be reduced to reach the neck tensile stiffness of the neck tensile experiment. The experimental response of the frontal neck test could be reached by lowering the positions of the neck joints and by placing the head center of gravity in posterior direction or by scaling the neck flexion-extension stiffness and damping.

3.5.4 Overall

Almost all parameters had a lower sensitivity for the overall setups as for the interest area setups. This can be explained because the overall setups evaluate more kinematic responses, which are generally more indirectly linked to the parameters than the mechanical responses of the specific component simulations. The most sensitive parameters in the overall simulations were the head mass, head center of gravity, neck joint stiffness and damping flexion-extension, lumbar joint stiffness and damping flexion-extension and thoracic joint stiffness and damping flexion-extension. In order to achieve more upward motion of the dummy torso and reduced downward motion of the head, the neck, lumbar and thoracic joint flexion-extension stiffness and damping could be increased to get less spinal rotation in flexion-extension. However, it is believed that a stiffer spine does not add biofidelity to the dummy. In addition, the upward motion is more biofidelic with a stiffer spine, but it hardly helps in creating forward excursion. Changing the mass and the center of gravity position of the head should improve the kinematic response of the dummy model. However, it was decided to not change these

parameters because they were qualified as fairly correct. Also, the lumbar, thoracic and neck joint z-positions were sensitive parameters. However, by varying these parameters the length of the spine or neck changes and thereby the length of the total dummy model. So, the scaling of these parameters is limited and the ranges are too small to change the kinematical response of the dummy. Therefore, it was proposed not to change these parameters.

3.5.5 Discussion

The body region setups provided sensitive parameters and directions for parameter changes, while the overall setups showed sensitive to most similar parameters, although to a smaller degree. In the overall setups, it was expected that neck tensile stiffness would be sensitive, however, it was not. Most likely this was due to the current stiffness being one or two orders of magnitude too large.

Differences between parameterized HIII model and the biomechanical tests may not only be due to the limited biofidelity of the parameterized HIII but also due to differences in model setups, even where validation of the setup was performed.

4 Optimization Study for Response Requirements for Future ATDs

In Task 1 (reported in Chapter 3), a sensitivity analysis was performed with the updated and parameterized model to assess which parameters are of what influence on which response. The results of this sensitivity study are used as input for the optimization study (Task 2), which will be discussed in this chapter. This chapter starts in Section 4.1 by discussing the chosen crash scenarios and test setups for the optimization study. In Section 4.2, the parameter choices are discussed. Section 4.3 details the optimization method. The results of the latter are discussed in Section 4.4 and concluded in Section 4.5.

4.1 Crash scenarios and test setups

It was decided to partially change the optimization simulation matrix in comparison to the simulation matrix that was used for the sensitivity study. More and different loading scenarios were included to get more variation in loading rates. An overview of the setups is provided in Table 4-1 for the component tests and in Table 4-2 for the whole body crash scenarios. The scenarios in shaded cells were added relative to those used for the sensitivity study and will be discussed in more detail in the remainder of this section. Regarding the other setups, for a description it is referred to Chapter 3.

Table 4-1. Component crash scenarios and test setups used for optimization study.

Interest Area	Test type	Dummy load	Reference
Abdomen	Quasi-static belt load (PEDVE024)	Abdomen stiffness	Kent, 2011
	Dynamic belt load (PEDVE025)	Abdomen stiffness & damping	Kent, 2011
	Dynamic belt load (PAC1.16)	Abdomen stiffness & damping (high penetration rate)	Kent, 2006
Thorax	Pendulum impact	Thorax stiffness and damping	Ouyang, 2006 Parent, 2010
	CPR	Thorax stiffness and damping Back plate contact	Maltese, 2008 Maltese, 2010 Parent, 2010
	Distributed dynamic belt load (PEDVE029 and PEDVE030)	Thorax stiffness and damping Back plate contact	Kent, 2009
	Diagonal dynamic belt load (PEDVE033 and PEDVE034)	Thorax stiffness and damping Back plate contact	Kent, 2009
	Scaled PMHS high speed sled (Belt load vs. Chest deflection)	Thorax stiffness & damping	Lopez-Valdes, 2011b
Neck	NBDL frontal	Neck flexion-extension & tension stiffness & damping Head inertia	Dibb, 2010
	Tension	Neck tension stiffness & damping	Dibb, 2010

Table 4-2. Whole body crash scenarios and test setups used for sensitivity analysis.

Interest Area	Test type	Dummy load	Reference
Whole body	Volunteer low speed sled	Spinal properties Head inertia	Arbogast, 2009 Seacrist, 2010
	Scaled PMHS high speed sled	Spinal properties Head inertia Thorax & abdomen stiffness & damping	Lopez-Valdes, 2011b
	PMHS shield booster impact	Spinal properties Head inertia Thorax & abdomen stiffness & damping	Kallieris, 1978 Forbes, 2007

4.1.1 *High rate abdomen belt setup*

To optimize the abdominal characteristics for both low and high rate belt penetration a new dynamic belt load scenario was added for the optimization study. This setup is adopted from Kent (2006) and has the same setup as the abdomen belt test for the sensitivity study (see Figure 3-3). Only the dynamic belt pull on both belt ends is changed, representing a higher loading rate as in comparable test PEDVE025, as shown in Figure 4-1.

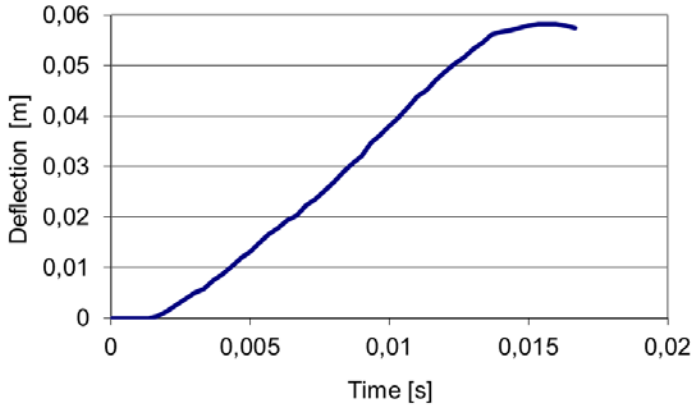

Figure 4-1. High rate dynamic abdomen belt load test PAC1.16 (Kent, 2006) belt displacement input function.

4.1.2 *Thorax belt setups*

It was decided to add distributed and diagonal thorax belt load scenarios for the optimization study. Diagonal belt loading was decided to be more representative for real world crash scenarios and with a distributed belt the thorax characteristics could be better determined. Both belt loading setups are adopted from Kent (2009). The

distributed and diagonal belt load setups for the thorax region are shown in Figure 4-2 and Figure 4-3, respectively.

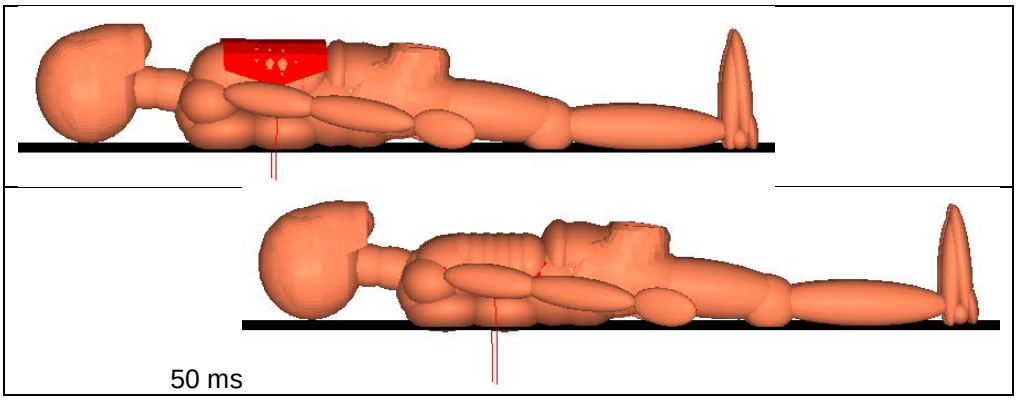

Figure 4-2. Thorax distributed belt load test setup (Kent, 2009) as used in optimization analysis, initially (top) and at time of maximum chest deflection (bottom).

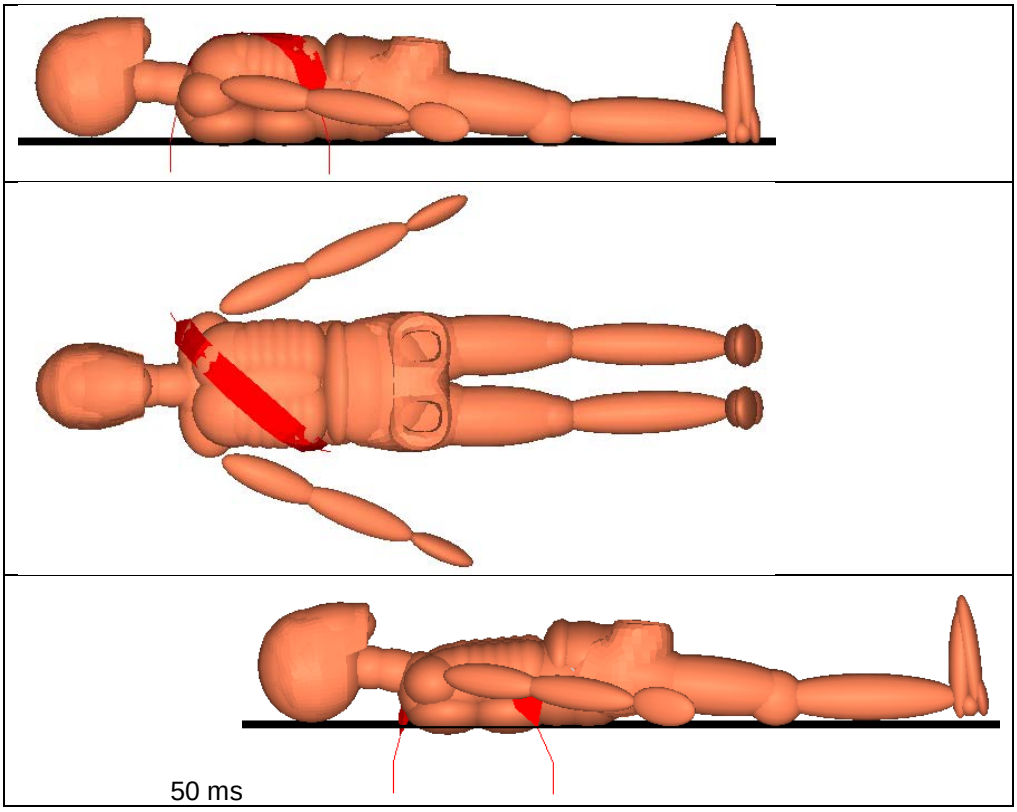

Figure 4-3. Thorax diagonal belt load test setup (Kent, 2009) as used in optimization analysis, initially (top and middle) and at time of maximum chest deflection (bottom).

For both thorax belt load setups, two different dynamic belt displacement experiments are simulated. Figure 4-4 and Figure 4-5 show the dynamic belt pulls for the distributed

belt setup and Figure 4-6 and Figure 4-7 show the pulls for the diagonal belt load scenarios.

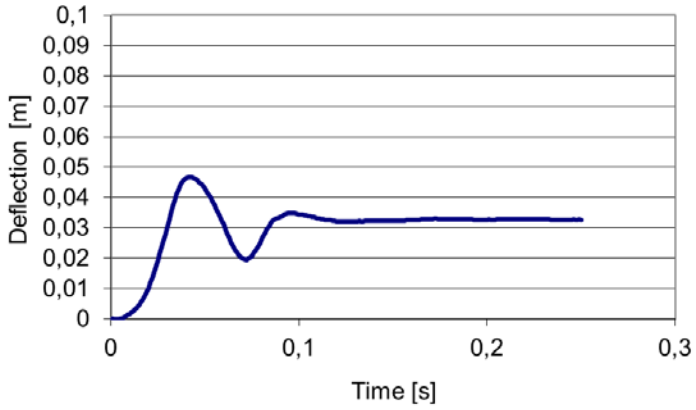

Figure 4-4. Dynamic thoracic distributed belt load test PEDVE029 (Kent, 2009) belt displacement input function.

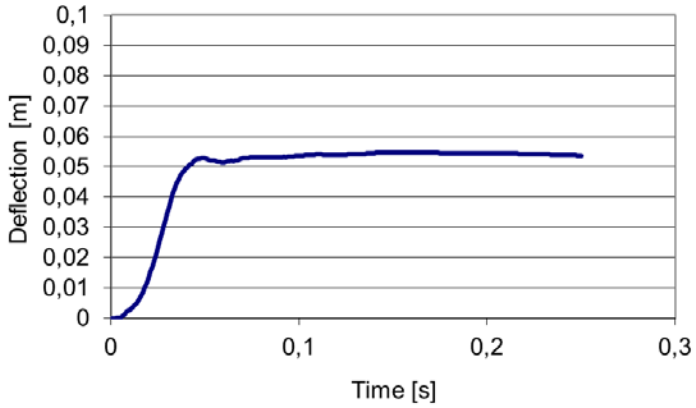

Figure 4-5. Dynamic thoracic distributed belt load test PEDVE030 (Kent, 2009) belt displacement input function.

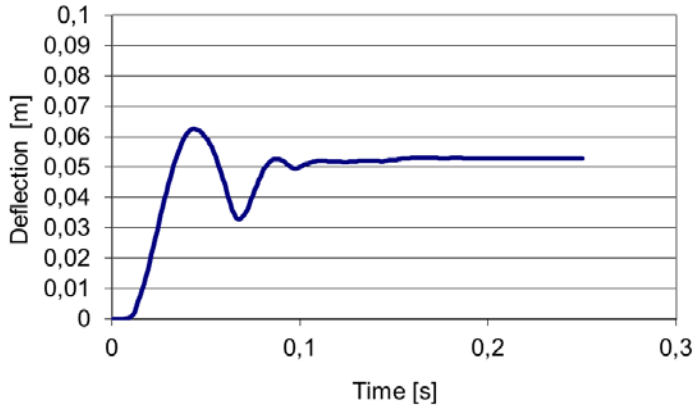

Figure 4-6. Dynamic thoracic diagonal belt load test PEDVE033 (Kent, 2009) belt displacement input function.

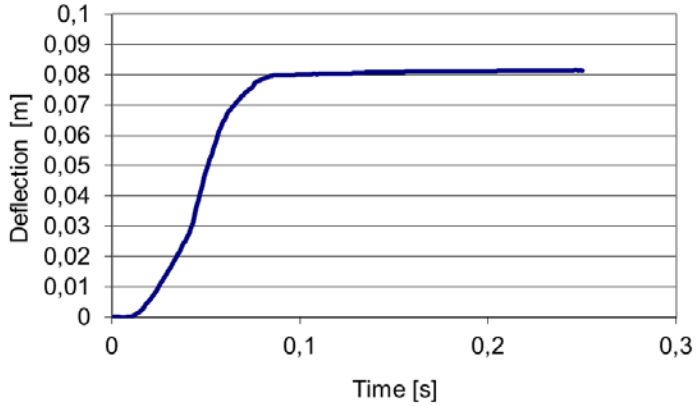

Figure 4-7. Dynamic thoracic diagonal belt load test PEDVE034 (Kent, 2009) belt displacement input function.

4.1.3 Thorax high speed sled setups

Because the belt force and chest displacement of the Ford Taurus rear bench simulation setup (Lopez-Valdes, 2011a) is less accurate because of the influence of the booster on the belt forces, as discussed in Chapter 3, the relatively more simplified PMHS high speed sled test setup (Lopez-Valdes, 2011b) is included to optimize the thorax region parameters. This setup is as described in Section 3.1.4. The shoulder belt force and chest deflection results are used to optimize the thorax parameters.

4.2 Parameter choice and limits

After analyzing the results of the sensitivity study (Section 3.4 and 3.5), it was decided which parameters are used to optimize the parameterized ellipsoid Hybrid III 6-year-old

model. Because the neck and spine parameters are sensitive in both the whole body setups and the head/neck setups, the neck and spine parameters are optimized with the neck and overall setup simulations. Table 4-3 gives an overview of the parameters that are optimized and their scaling factors at the start of the optimization.

Table 4-3. Overview of parameters and start scaling values for optimization study.

Interest Area	Parameter	Start value
Abdomen	Abdominal stiffness	1.0
	Abdominal damping	1.0
	Pelvis flesh stiffness	1.0
Thorax	Rib stiffness anterior-posterior direction	1.0
	Rib damping	1.0
	Rib flesh stiffness	1.0
	Thorax / shoulder flesh stiffness	1.0
	Sternum stiffness	1.0
	Sternum damping	0.01
Neck / Overall	Neck joint stiffness flexion-extension	1.0
	Neck joint damping flexion-extension	1.0
	Neck tensile stiffness	1.0
	Neck tensile damping	1.0
	Lumbar joint rotational stiffness flexion-extension and lateral	1.0
	Lumbar joint rotational damping flexion-extension and lateral	1.0
	Thoracic joint rotational stiffness flexion-extension	1.0
	Thoracic joint rotational damping flexion-extension	1.0

The abdominal parameters are optimized first, followed by the optimization of the thoracic parameters and then the neck and spine parameters. Because the optimization algorithm, which is described in the next section, can optimize up to five parameters at a time within acceptable computation time, the optimization of the thorax is performed in two steps. First, the rib stiffness, rib damping, rib flesh stiffness, shoulder flesh stiffness and sternum stiffness are optimized. In the second optimization step the sternum damping will be optimized. The optimization of the neck/spine parameters is also performed in two steps. The latter optimization starts with the optimization of the neck parameters (neck tensile stiffness and damping and neck joint flexion-extension stiffness and damping). After the neck parameters the lumbar joint rotational stiffness and damping and thorax joint rotational stiffness and damping are optimized. At last, the neck parameters are optimized again with the optimized lumbar and thorax joint parameters.

4.3 Design of optimization study

As mentioned before, the optimization study is performed in three different groups which are defined by body region (abdomen, thorax and neck/spine). The abdomen and thorax parameters are optimized by the abdomen and thorax setups, respectively, and the neck/spine parameters are optimized by the neck and overall setups. To optimize the dummy parameters, a gradient descent optimization algorithm is used. This algorithm searches for a local minimum of the objective function.

The objective function (F_{obj}) is dependent on the errors of the n different simulations ($E_{sim,i}$ is the error of the i^{th} simulation) of the interest area setups compared with experimental responses and their weighting factors ($W_{sim,i}$). The objective function is given by

$$F_{obj} = \frac{\sum_{i=1}^{n} E_{sim,i} * W_{sim,i}}{\sum_{i=1}^{n} W_{sim,i}} .$$

The simulation error is given by

$$E_{sim} = \frac{\sum_{i=1}^{n} E_{plot,i} * W_{plot,i}}{\sum_{i=1}^{n} W_{plot,i}} ,$$

where $E_{plot,i}$ is the error of the different plots (or responses) of a simulation and $W_{plot,i}$ is the weighting factor. The different plots which are used in the optimization study are force-time plots, force-displacement plots, displacement-time plots, rotational acceleration-time plots and trajectories plots. The error of a plot is dependent on the error of the n different signals ($E_{signal,i}$ is the error of the i^{th} signal) of the plots and their weighting factors ($W_{signal,i}$) and is given by the following equation,

$$E_{plot} = \frac{\sum_{i=1}^{n} E_{signal,i} * W_{signal,i}}{\sum_{i=1}^{n} W_{signal,i}} .$$

Four different signals are used to determine the error of a plot (overall error, peak height error, peak time error and slope error). The overall error (R_{error}) is determined out of the mean difference between the simulation outcome ($X_{sim,i}$) and the experimental data ($X_{exp,i}$) of all n data points and is normalized by the mean of the experimental data,

$$R_{error} = \frac{\sum_{i}^{n} \frac{\left| X_{exp,i} - X_{sim,i} \right|}{mean(X_{exp})}}{n} .$$

The overall error of the trajectories is determined out of the overall error of the x-displacement vs. time and z-displacement vs. time responses. The peak height error (P_{error}) is given by the relative difference between the peak height of the simulation (P_{sim}) and the experimental data (P_{exp}),

$$P_{error} = \frac{\left| P_{exp} - P_{sim} \right|}{P_{exp}} .$$

The peak time error (T_{error}) is given by the relative difference between the peak time of the simulation (T_{sim}) and the experimental data (T_{exp}),

$$T_{error} = \frac{|T_{exp} - T_{sim}|}{T_{exp}} .$$

The slope error ($Slope_{error}$) is given by the relative difference between the slope of the simulation ($Slope_{sim}$) and the experimental data ($Slope_{exp}$),

$$Slope_{error} = \frac{|Slope_{exp} - Slope_{sim}|}{Slope_{exp}} .$$

Not every signal is used to determine the error of a plot. Table 4-4 provides an overview of the signals, plots and the weighting factors of the experiments which are used to optimize the parameters. Various weighting factors were introduced based on relevance and quality of various signals, plots and tests.

For the abdomen, focus was laid on high rate tests, hence providing quasi-static tests with a lower weighting factor of 0.5 as well as the peak value of the low rate test.

For the thorax, the simulation weighting was determined by the relevance of the type of loading. A full-scale frontal impact belt loading scenario was deemed most realistic, hence most important. The diagonal belt loading component setup was second most important, followed by distributed belt. Pendulum and CPR impacts were weighted at the lowest values respectively, due to the type of loading being less realistic in automotive frontal impact. When three signals were used for one setup, signal weighting was reduced such that the overall weighting remained constant.

For the neck tests, the NBDL neck flexion test and specifically the head displacement response was deemed most important, together with the tensile test. Both tests have high and unique sensitivity of parameters in relevant loading rates, which cannot be overtaken by any of the overall tests. From the overall tests, the high speed scaled sled test was deemed most relevant due to its realistic loading range, even though these are created based on scaling. The volunteer sled tests were weighted lower due to the lower loading rate, while the shield booster setup was considered less relevant due to the absence of a harness belt system. In all tests, weighting was such that head trajectory was most important.

Table 4-4. Overview of simulations, plots, signals and weighing factors for optimization study.

Interest area	Simulation	W_sim	Plots	W_plot	Signal	W_signal
Abdomen	Quasi-static abdomen belt PEDVE024 (Kent, 2011)	0,5	F-t	1	Overall	1
					Peak height	1
	Low rate dynamic abdomen belt PEDVE025 (Kent, 2011)	1	F-t	1	Overall	1
					Peak height	0,5
	High rate dynamic abdomen belt PAC1.16 (Kent, 2006)	1	F-t	1	Overall	1
					Peak height	1
Thorax	Distributed thorax belt PEDVE029 (Kent, 2009)	0,7	F-t	1	Overall	1
					Peak height	1
	Distributed thorax belt PEDVE030 (Kent, 2009)	0,7	F-t	1	Overall	1
					Peak height	1
	Diagonal thorax belt PEDVE033 (Kent, 2009)	0,8	F-t	1	Overall	1
					Peak height	1
	Diagonal thorax belt PEDVE034 (Kent, 2009)	0,8	F-t	1	Overall	1
					Peak height	1
	CPR thorax compression (Maltese, 2010)	0,2	F-d	1	Slope	1
	Thoracic pendulum (Ouyang, 2006 / Parent, 2010)	0,5	F-t	1	Overall	1
					Peak height	0,5
					Peak time	0,5
			d-t	1	Overall	1
					Peak height	0,5
					Peak time	0,5
	Frontal impact high speed scaled (Lopez-Valdes, 2011b)	1	F-d	1	Slope	1
Neck / Overall	Neck tensile (Dibb, 2010)	1	F-d	1	Slope	1
	NBDL frontal neck test (Dibb, 2010)	1	d-t	1	Overall	1
					Peak height	0,5
					Peak time	0,5
			α-t	0,5	Overall	1
					Peak height	0,5
					Peak time	0,5
	Frontal impact volunteer (Arbogast, 2009)	0,5	Head top trajectory	0,5	Overall	1
					Peak height X	1
			Nasion trajectory	0,25	Overall	1
			Opisthocranion trajectory	0,25	Overall	1
			C4 trajectory	0,5	Overall	1
			T1 trajectory	0,5	Overall	1
			Iliac crest trajectory	0,5	Overall	1
			Shoulderbelt force	0,25	Overall	1
					Peak height X	1
					Peak time	1
			Lapbelt force	0,25	Overall	1
					Peak height X	1
					Peak time	1
	Frontal impact high speed scaled (Lopez-Valdes, 2011b)	1	Head COG trajectory	1	Overall	1
					Peak height X	1
			T1 trajectory	0,5	Overall	1
			T8 trajectory	0,5	Overall	1
			Pelvis trajectory	0,5	Overall	1
	Frontal impact HIII/PMHS (Kallieris, 1978 / Forbes, 2007)	0,3	Head trajectory	1	Overall	1
					Peak height X	1
			Knee trajectory	0,5	Overall	1
			Left shoulderbelt force	0,25	Overall	1
					Peak height X	1
					Peak time	1
			Right shoulderbelt force	0,25	Overall	1
					Peak height X	1
					Peak time	1

4.4 Results

In this section, first, the scaling factors determined by the optimization algorithm study are discussed. Table 4-5 gives an overview of the scaling parameters after performing the optimization algorithm. However, based on biomechanical expertise, manual adjustments were made after performing the optimization algorithm. These results are summarized in Table 4-6. Secondly, the results for every interest area are discussed in more detail in Sections 4.4.1 to 4.4.3. In these sections, the responses of the optimized parameterized ellipsoid Hybrid III 6-year-old model are compared with the responses of the parameterized ellipsoid Hybrid III 6-year-old model before optimization and with the experimental responses.

Table 4-5. Overview of parameter scaling factors after performing optimization algorithm.

Interest Area	Parameter	Scaling factor
Abdomen	Abdominal stiffness	0.12662
	Abdominal damping	1.1492
	Pelvis flesh stiffness	0.14853
Thorax	Rib stiffness anterior-posterior direction	1.0016
	Rib damping	5.2185
	Rib flesh stiffness	7.9507
	Thorax / shoulder flesh stiffness	9.5814
	Sternum stiffness	0.15655
	Sternum damping	0.005
Neck / Spine	Neck joint stiffness flexion-extension	0.16128
	Neck joint damping flexion-extension	0.044194
	Neck tensile stiffness	0.16128
	Neck tensile damping	0.022097
	Lumbar joint rotational stiffness flexion-extension and lateral	17.0859
	Lumbar joint rotational damping flexion-extension and lateral	50
	Thoracic joint rotational stiffness flexion-extension	50
	Thoracic joint rotational damping flexion-extension	50

All scaling factors that are determined by the optimization algorithm for the abdomen and thorax area seem to be realistic in terms of order of magnitude. The lowering of the sternum damping (200 times decreased) is at the cut off from a defined constraint in the optimization algorithm; however, this large reduction is expected from sensitivity study. Also, the decrease of the neck tensile and neck flexion-extension parameters is expected.

The increased lumbar and thoracic joint rotational parameters are also in line with the conclusions from the sensitivity analysis. It was concluded that increased lumbar and

thoracic joint rotational stiffness introduces more realistic upward motion of the dummy, while it unfortunately does not help in creating more realistic forward excursion. However, as already mentioned in Section 3.5.4, it is believed that a stiffer spine does not add biofidelity to the dummy. This is shown in Figure 4-8A, where the kinematics of the optimized parameterized ellipsoid Hybrid III 6-year-old model during the scaled PMHS high speed sled simulation are given for T=100 ms and T=150 ms. During this simulation no flexion is observed in the spine. This was considered not biofidelic (Sherwood, 2003). Therefore, the scaling of the lumbar and thoracic joint rotational parameters is performed by analyzing the kinematics of the whole body crash scenario simulations. Figure 4-8B and C show the optimized parameterized ellipsoid Hybrid III 6-year-old model with original (not scaled) lumbar and thoracic joint rotational parameters and with ten times decreased lumbar and thoracic joint rotational parameters, respectively. As the difference in kinematic response between original spine rotational characteristics and decreased spine rotational characteristics is negligible (as shown in Figure 4-9) and both models result in more biofidelic responses compared to the model with optimized rotational scaling factors, it was decided to leave the lumbar and thoracic joint rotational parameters at 1.0. Nevertheless, Figure 4-9 shows that the model with all optimized parameters results in higher head forward excursion than the original model before optimization. The manually adjusted and final scaling factors are shown in Table 4-6. The responses in all optimization setups of the parameterized ellipsoid Hybrid III 6-year-old model with these scaling factors are discussed in the remainder of this section.

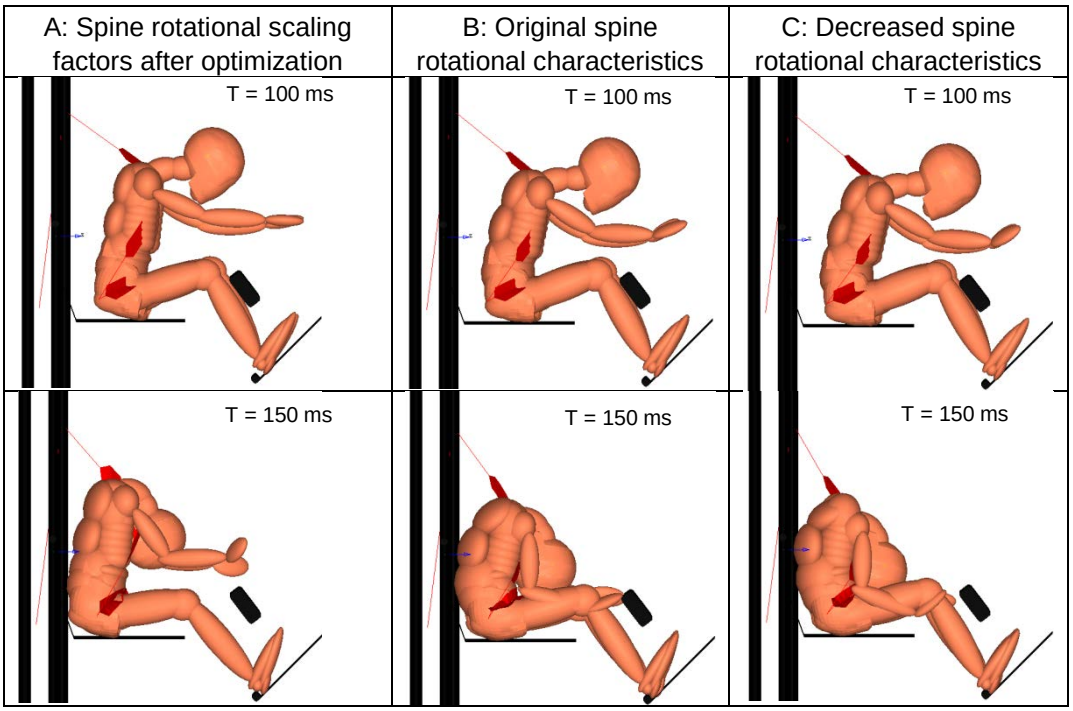

Figure 4-8. Kinematics of the scaled PMHS high speed sled (Lopez-Valdes, 2011b) simulation at 100 ms and 150 ms with optimized parameterized ellipsoid Hybrid III 6-year-old model (left), optimized parameterized ellipsoid Hybrid III 6-year-old model with original spine rotational characteristics (middle) and optimized parameterized ellipsoid Hybrid III 6-year-old model with decreased spine rotational characteristics (right).

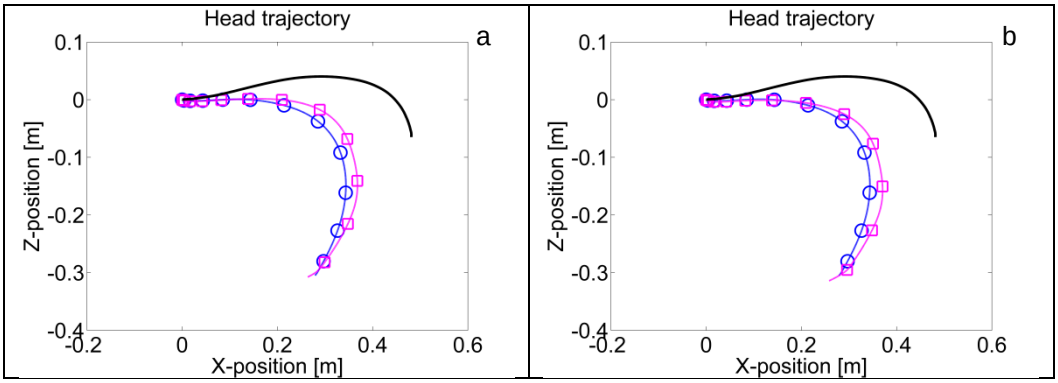

Figure 4-9. Head trajectory of the scaled PMHS high speed sled (Lopez-Valdes, 2011b) simulations with optimized parameterized ellipsoid Hybrid III 6-year-old model with original spine rotational characteristics (a, squares), optimized parameterized ellipsoid Hybrid III 6-year-old model with decreased spine rotational characteristics (b, squares), Hybrid III 6-year-old model before optimization (circles) and experimental data (black)

Table 4-6. Overview of final scaling factors of parameters, after manual adjustment.

Interest Area	Parameter	Scaling factor
Abdomen	Abdominal stiffness	0.12662
	Abdominal damping	1.1492
	Pelvis flesh stiffness	0.14853
Thorax	Rib stiffness anterior-posterior direction	1.0016
	Rib damping	5.2185
	Rib flesh stiffness	7.9507
	Thorax / shoulder flesh stiffness	9.5814
	Sternum stiffness	0.15655
	Sternum damping	0.005
Neck / Spine	Neck joint stiffness flexion-extension	0.16128
	Neck joint damping flexion-extension	0.044194
	Neck tensile stiffness	0.16128
	Neck tensile damping	0.022097
	Lumbar joint rotational stiffness flexion-extension and lateral	1.0
	Lumbar joint rotational damping flexion-extension and lateral	1.0
	Thoracic joint rotational stiffness flexion-extension	1.0
	Thoracic joint rotational damping flexion-extension	1.0

4.4.1 Abdomen

Three different simulation setups were used to perform the optimization of the abdomen parameters. Two dynamic belt load tests and a quasi-static belt load experiment were simulated. The optimization algorithm decreases the abdominal stiffness and pelvis

flesh stiffness with a factor of 8 and 7, respectively. The abdominal damping is increased with almost 15%.

The responses of the simulations with optimized and not optimized parameterized ellipsoid Hybrid III 6-year-old model and experimental data of high rate dynamic belt load test, low rate dynamic belt load test and quasi-static belt load test are shown in Figure 4-10. After optimization, the peak of the high rate dynamic belt load response of the optimized Hybrid III model was still more than 200% too high. However, the response was significantly improved compared with the model before optimization. Also, the peak response of the optimized model in the low rate dynamic belt load test was too high and even worse than the not optimized model. However, the overall response of the optimized Hybrid III model was improved. The response of the optimized Hybrid III 6-year-old dummy model was significantly improved for the quasi-static belt load test compared with the not optimized 6-year-old Hybrid III dummy model.

In Appendix A: Abdomen parameter optimization, the optimization results of the abdomen prior to final optimization with other parameters are shown. This indicates that if optimization on abdomen parameters only would be performed, better optimization fit would be achieved.

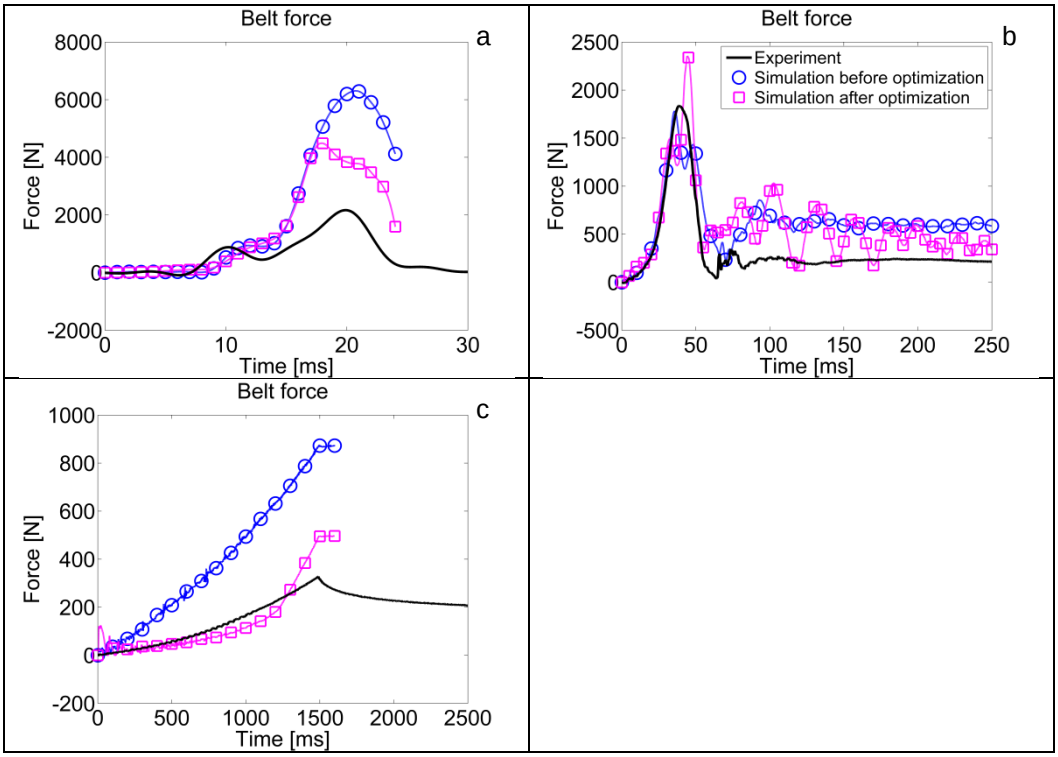

Figure 4-10. Response of the simulations with optimized parameterized ellipsoid Hybrid III 6-year-old model (blocks) and Hybrid III 6-year-old model before optimization (circles) and experimental data (black) of high rate dynamic belt load test PAC1.16 (Kent, 2006) (a), low rate dynamic belt load test PEDVE025 (Kent, 2011) (b) and quasi-static belt load test PEDVE024 (Kent, 2011) (c).

4.4.2 Thorax

Seven different simulations were performed for the optimization of the thoracic parameters. Four dynamic belt load tests, a pendulum test, a CPR loading test and a full scale shoulder belt load test were simulated. The optimization algorithm hardly altered the rib stiffness, but increased the rib flesh stiffness and thorax-shoulder stiffness almost 8 and more than 9 times, respectively. The rib damping was increased with more than 500%. The sternum stiffness was decreased more than 6 times and the sternum damping was decreased to 0.5% of the original value. However, for the sternum damping scaling, the lower limit of the optimization algorithm was reached.

Figure 4-11 gives the response of the parameterized ellipsoid Hybrid III 6-year-old model before and after optimization for the belt load tests and the scaled PMHS high speed sled test. The response of the simulation of the scaled PMHS high speed sled test was improved, as Figure 4-11e shows. The chest deflection vs. belt force response of the optimized Hybrid III model fits well between the upper and lower corridor of the experimental data. The increased rib damping, rib flesh stiffness and thorax/shoulder flesh stiffness coefficients caused a rise of the force peaks of the belt load responses. Only the experimental force peak of one distributed belt load test (PEDVE030, Figure 4-11b) was not reached by the optimized model. For all other belt load tests the peaks of the responses of the optimized dummy simulations were similar to the peaks of the experimental data. The experimental force values of the later, more static, part of the belt load tests was reached for test PEDVE029 (Figure 4-11a) and PEDVE033 (Figure 4-11c). The higher belt forces of the experimental data at the later part of test PEDVE030 (Figure 4-11a) and PEDVE034 (Figure 4-11c) were not reached by the simulations with the optimized parameterized ellipsoid Hybrid III 6-year-old model. However, the responses at the peak phase and static end phase of all belt load tests were improved after optimization, especially for lower force tests PEDVE029 and PEDVE033.

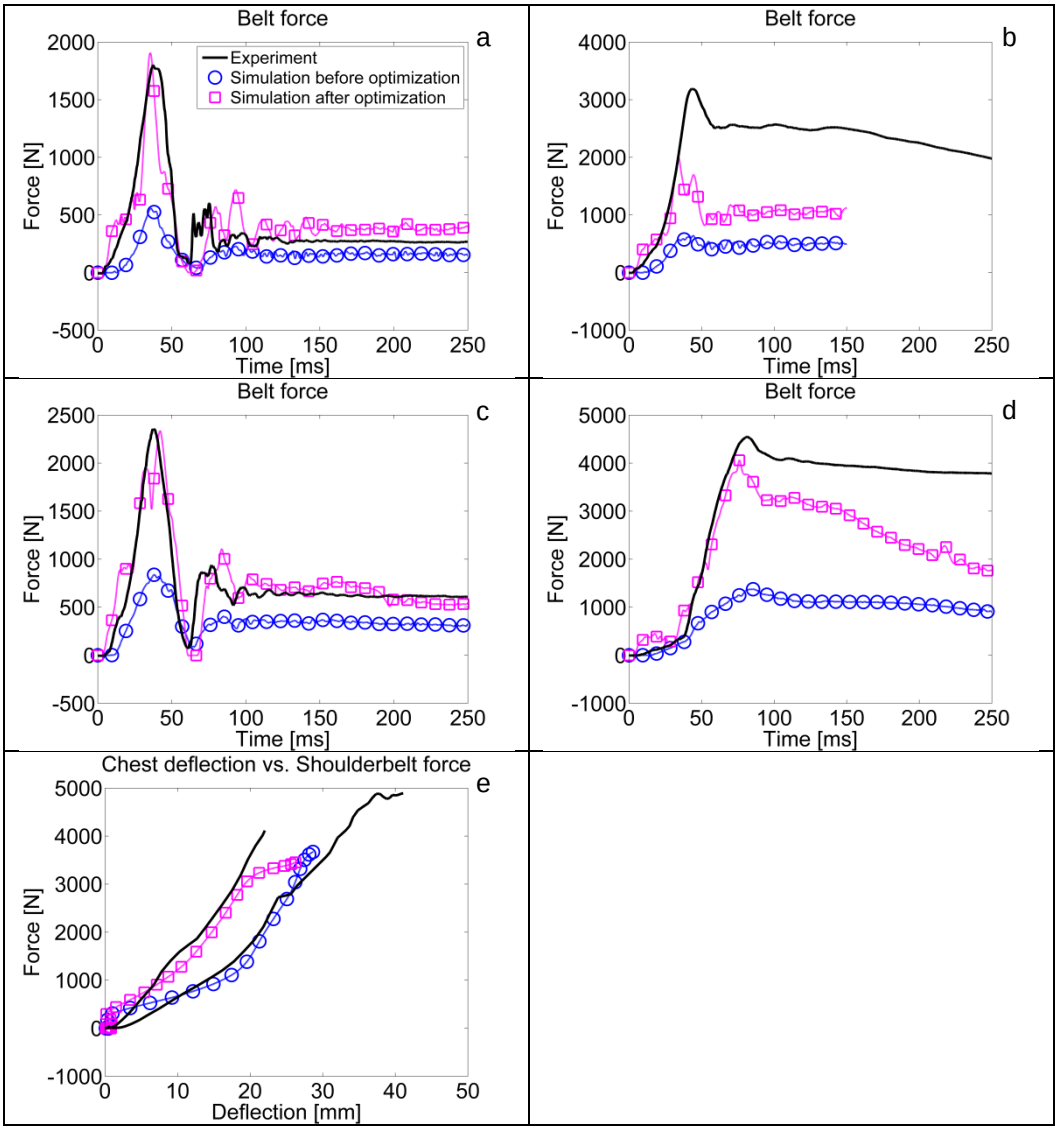

Figure 4-11. Response of the simulations with optimized parameterized ellipsoid Hybrid III 6-year-old model (blocks) and Hybrid III 6-year-old model before optimization (circles) and experimental data (black) of the distributed belt load tests (Kent, 2009) (a: PEDVE029 and b: PEDVE030), diagonal belt load tests (Kent, 2009) (c: PEDVE033 and d: PEDVE034) and chest deflection vs. shoulder belt force of the scaled PMHS high speed sled test (Lopez-Valdes, 2011b) (e).

Figure 4-12 gives the responses of the parameterized ellipsoid Hybrid III 6-year-old model before and after optimization for the thorax pendulum test setup and CPR impact test setup, which both have lower weighting factors. The responses of both test setups were not improved after optimization. The increased rib damping and rib contact stiffness caused an early force peak for the pendulum test. Furthermore, the maximum chest deflection was not reached and a fluctuation was introduced. The CPR impact response also showed an early peak and the force which was needed to reach 25 mm chest deflection was more than 400% too high.

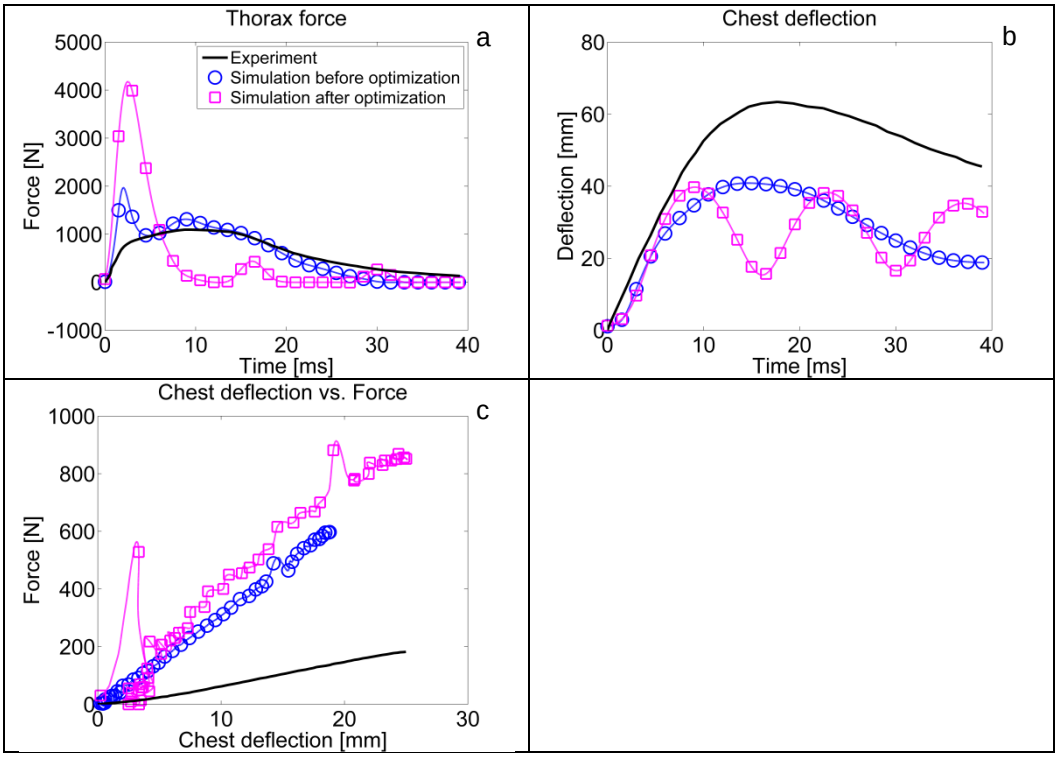

Figure 4-12. Response of the simulations with optimized parameterized ellipsoid Hybrid III 6-year-old model (blocks) and Hybrid III 6-year-old model before optimization (circles) and experimental data (black) of the thoracic pendulum test (Ouyang, 2006 / Parent, 2010) (force-time (a) and displacement-time (b) response) and CPR test (Maltese, 2010) (c).

4.4.3 Neck and spine

Five different simulation setups were used to perform the optimization of the neck and spine parameters. Two neck test setups and three full body sled test setups were simulated. The optimized neck tensile stiffness and damping are decreased to 16% and 2% of the original parameter values, respectively. Also the neck flexion-extension stiffness and damping parameters were decreased after optimization. These parameters were optimized to values that are 6 and 22 times lower than the parameter value before optimization, respectively. The spine rotational parameters were significantly increased by the optimization algorithm. However, as already mentioned in this section, the lumbar and thoracic joint rotational stiffness and damping were set back to their original values after analyzing the kinematics of the full body sled test simulations.

Figure 4-13 gives the responses of the parameterized ellipsoid Hybrid III 6-year-old model after and before optimization for the neck setup simulations. The decreased neck tensile stiffness caused a significant decrease of the neck tensile test response. After optimization, the Hybrid III 6-year-old model had a response equal to the experimental data. The NBDL frontal test responses of the dummy before and after optimization were changed to a smaller extent. The head rotational acceleration fits better with the experimental data after optimization. However, the response of the head displacement

was worse after optimization. The error on the maximum head displacement was increased.

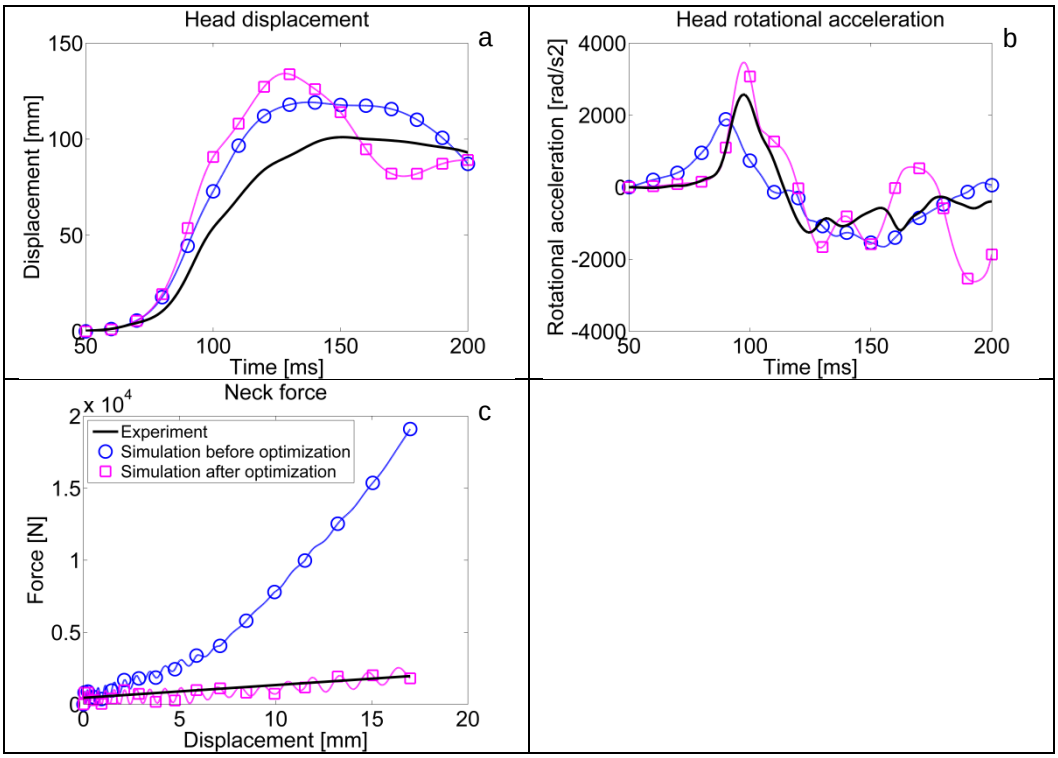

Figure 4-13. Response of the simulations with optimized parameterized ellipsoid Hybrid III 6-year-old model (blocks) and Hybrid III 6-year-old model before optimization (circles) and experimental data (black) of the NBDL frontal test (Dibb, 2010) (a: head displacement-time and b:head rotational acceleration) and neck tensile test (Dibb, 2010) (c).

Figure 4-14 gives the responses of the two dummy models during the PMHS high speed sled test simulation. The trajectories of the head, T1 and T8 vertebra and pelvis were improved after optimization, but did not reach the frontal x-displacement of the experimental data. The experimental data described a frontal displacement that is 150 to 250 mm larger. The trajectory of the T1 vertebra was almost not changed after optimization. Also, the frontal displacement of the T1 vertebra was not reached by the optimized parameterized ellipsoid Hybrid III 6-year-old model.

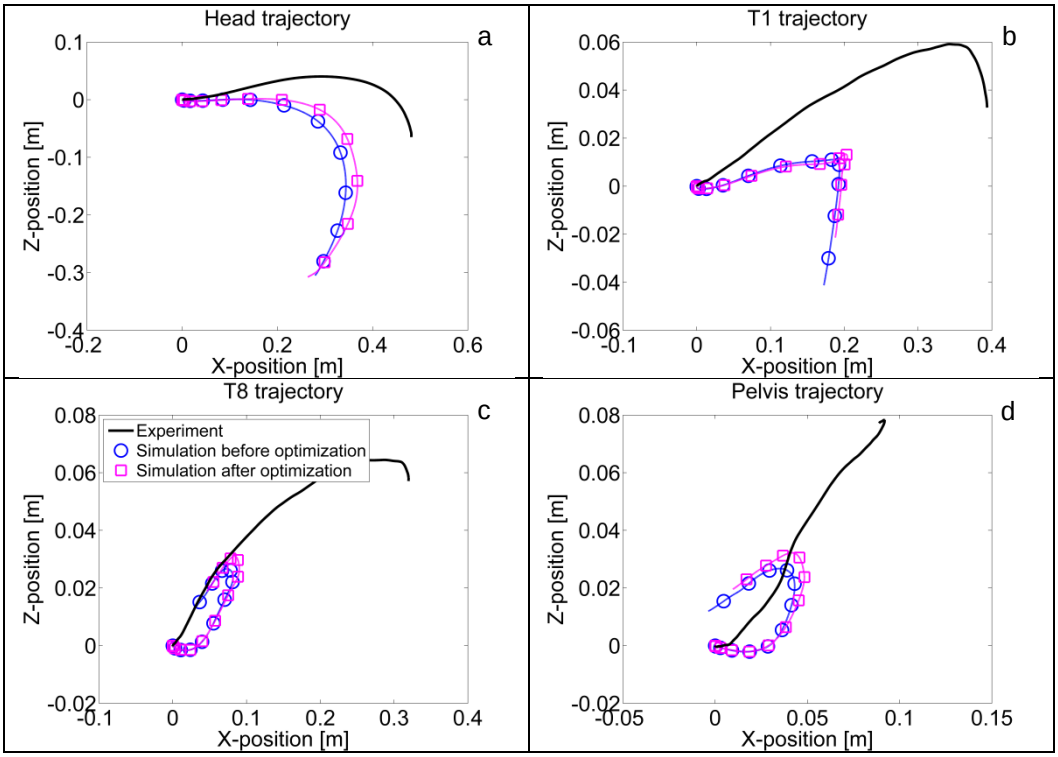

Figure 4-14. Response of the simulations with optimized parameterized ellipsoid Hybrid III 6-year-old model (blocks) and Hybrid III 6-year-old model before optimization (circles) and experimental data (black) on the scaled PMHS high speed sled test (Lopez-Valdes, 2011b) (a: Head trajectory, b: T1 trajectory, c: T8 trajectory and d: Pelvis trajectory).

Figure 4-15 gives the responses of the two dummy models during the volunteer low speed sled test. Like the trajectories of the high speed sled test simulations, the optimized parameterized ellipsoid Hybrid III 6-year-old model did not reach the experimental trajectories for the low speed sled test. The head of the Hybrid III moved 350 mm forward, while the x-displacement of the experimental data described a forward head displacement of almost 600 mm. The head of both the dummy models rotated in a downwards direction, which was hardly observed in the experimental data. The C4 and T1vertebra had similar frontal displacements as the experimental data. However, the C4 and T1vertebra did not displace upwards like the experimental data. In contrast with the vertebra and head displacement, the pelvis moved 200 mm more forward than the experimental volunteer data. Furthermore, the belt forces were significantly lower for the simulations with both Hybrid III models compared with the belt forces of the experiments with volunteers. The optimization of the parameterized ellipsoid Hybrid III 6-year-old model hardly improved the responses of the low speed volunteer test simulations.

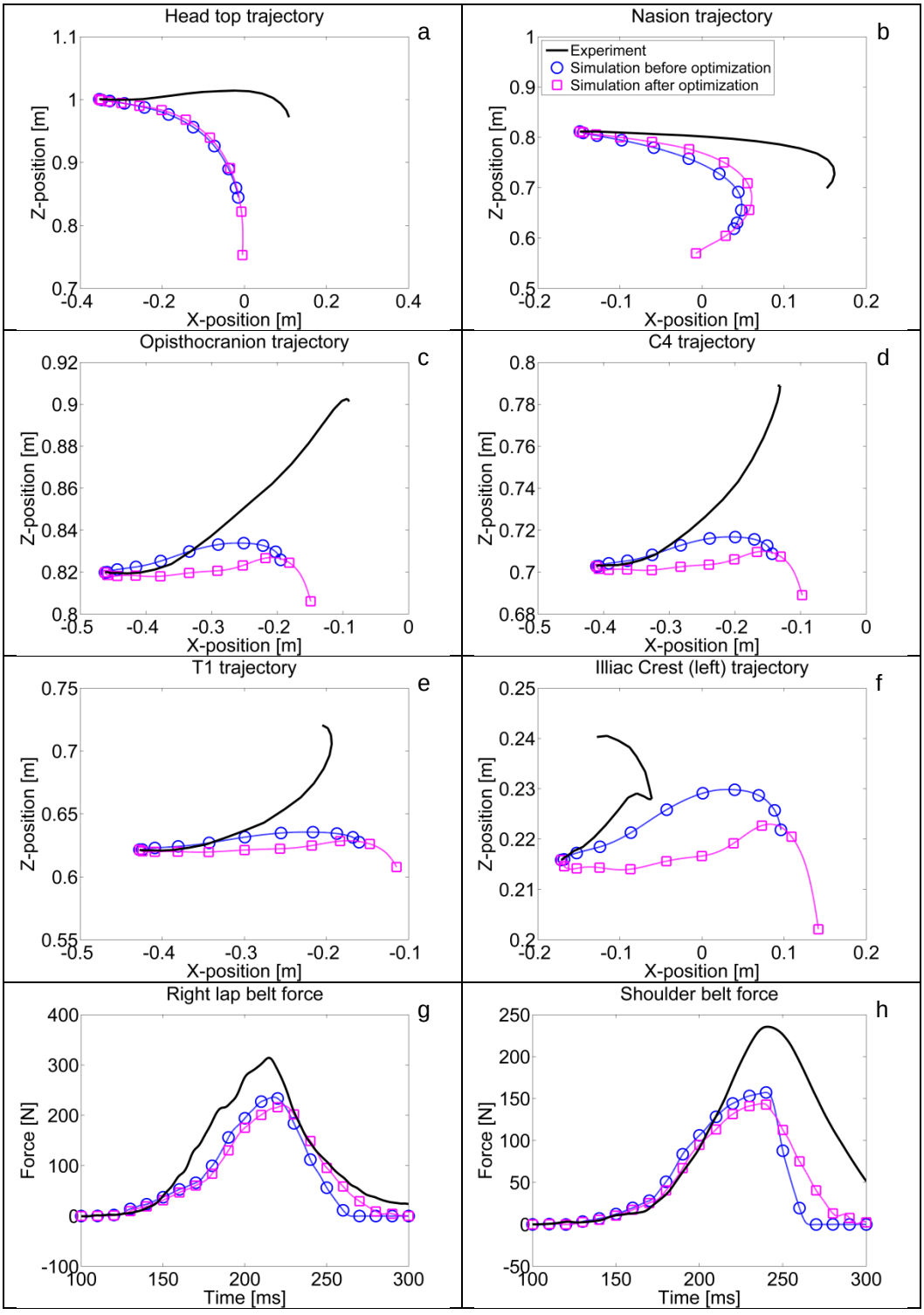

Figure 4-15. Response of the simulations with optimized parameterized ellipsoid Hybrid III 6-year-old model (blocks) and Hybrid III 6-year-old model before optimization (circles) and experimental data (black) on the volunteer low speed sled test (Arbogast, 2009) (a: Head top trajectory, b: Nasion trajectory, c: Opisthocranion trajectory, d: C4 trajectory, e: T1 trajectory, f: Left iliac crest trajectory, g: Lap belt force and h: Shoulder belt force).

Figure 4-16 gives the responses of the two dummy models during the PMHS shield booster impact test. Like the other full scale sled test simulations, the head x-displacement of the optimized parameterized ellipsoid Hybrid III 6-year-old model did not reach the experimental frontal movement in the PMHS shield booster impact test simulation. The difference in head movement was more than 200 mm. Also the z-displacement of the experimental data was not reached. In contrast with the belt forces of the high speed sled test simulations, the belt forces found in the PMHS shield booster impact simulations were higher than the experimental belt forces. The optimization of the parameterized ellipsoid Hybrid III 6-year-old model did not improve the responses of the PMHS shield booster impact simulations.

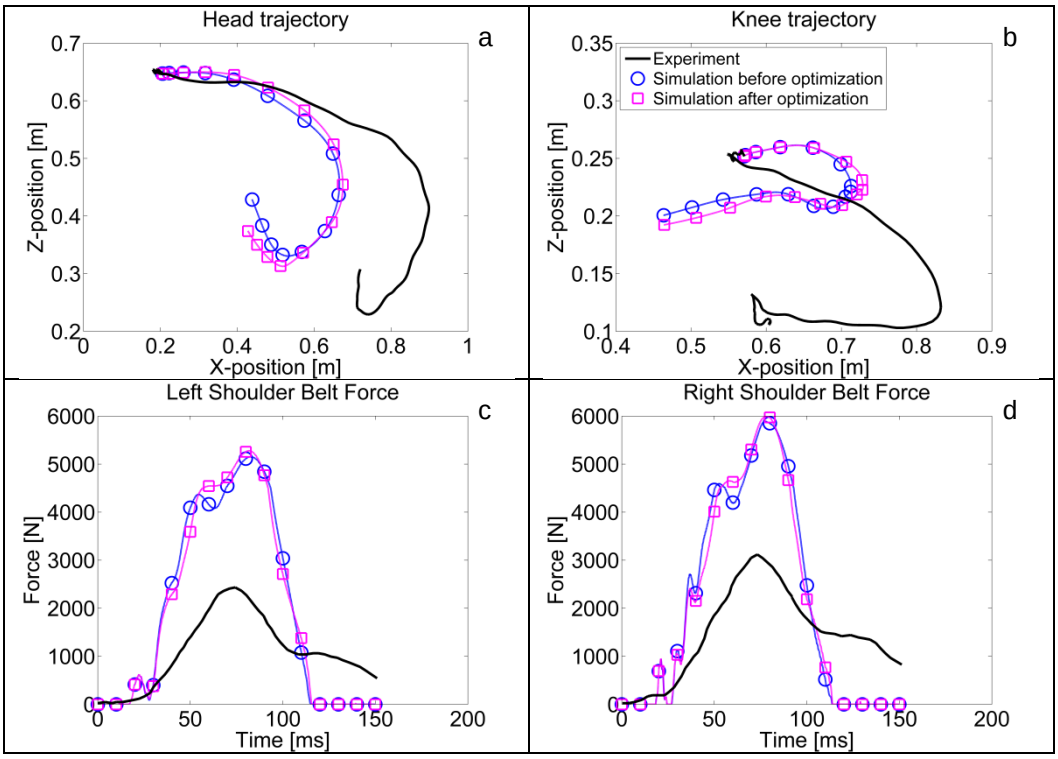

Figure 4-16. Response of the simulations with optimized parameterized ellipsoid Hybrid III 6-year-old model (blocks) and Hybrid III 6-year-old model before optimization (circles) and experimental data (black) on the PMHS shield booster impact test (Kallieris, 1978 / Forbes, 2007) (a: Head trajectory, b: Knee trajectory, c: Left shoulder belt force and d: right shoulder belt force).

As already described at the start of this section, the scaling of the lumbar and thoracic joint rotational parameters was performed by analyzing the kinematics of the whole body crash scenario simulations. The lumbar and thoracic joint rotational stiffness and damping was increased by the optimization algorithm (see Table 4-5). The responses of the dummy model, optimized by the optimization algorithm, during the PMHS high speed sled test simulation are given in Figure 4-17. This figure shows that the optimization had no effect on the frontal displacement, but the z-displacement of the dummy model was improved. However, the kinematic response of the improved model

was proposed as not biofidelic (as seen in Figure 4-8). That figure shows that the increased spine parameters cause no spine bending.

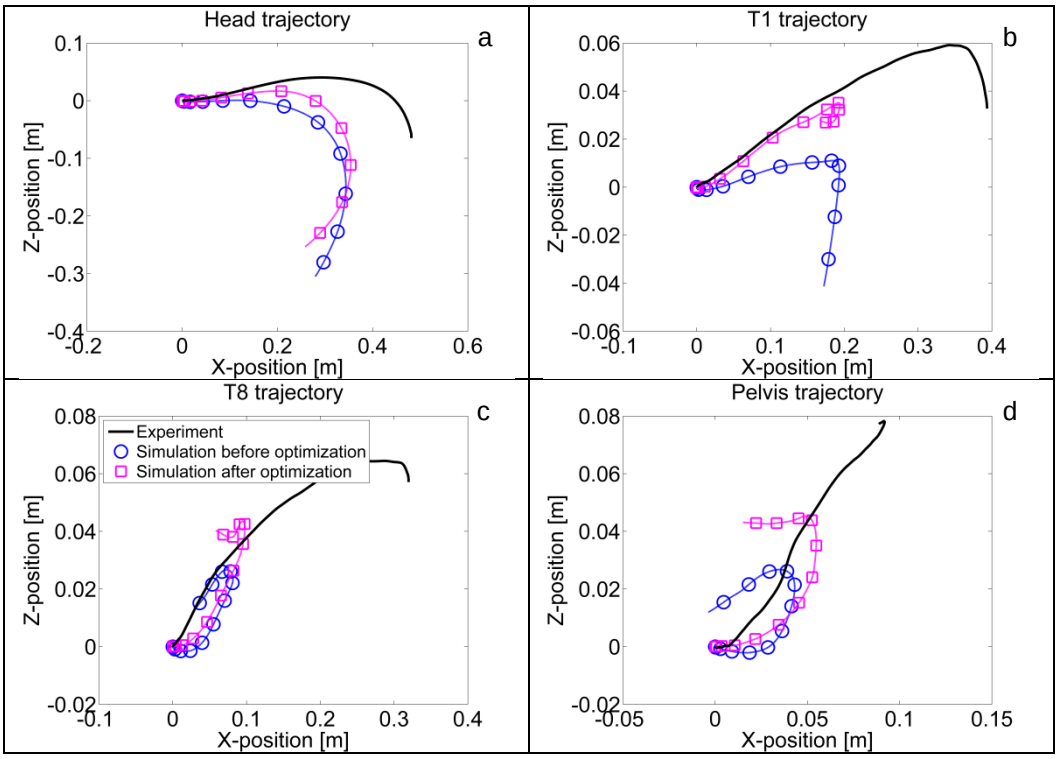

Figure 4-17. Response of the simulations with parameterized ellipsoid Hybrid III 6-year-old model with increased spinal parameters (blocks) and Hybrid III 6-year-old model before optimization (circles) and experimental data (black) on the scaled PMHS high speed sled test (Lopez-Valdes, 2011b) (a: Head trajectory, b: T1 trajectory, c: T8 trajectory and d: Pelvis trajectory).

4.5 Discussion

In Task 2 an optimization study was performed with the parameterized ellipsoid Hybrid III 6-year-old model. In this section the results of the optimization study are discussed.

4.5.1 Abdomen

The responses of the parameterized ellipsoid Hybrid III 6-year-old model from the abdomen belt load tests improved after optimization. Especially, the results of the quasi-static and high rate abdomen belt tests improved significantly. The responses of the Hybrid III dummy in the low rate dynamic test were different but not improved or got worse after optimization. The belt force response showed more fluctuations after optimization. This could be explained by the increase of the thorax / shoulder flesh stiffness parameter that not only influenced the outcome of the thorax simulations but also the outcome of the abdomen belt load tests. Furthermore, the Hybrid III dummy model was not again settled during optimization, while the table-dummy contact parameters changed during optimization. Due to this, the dummy bounced slightly

during the belt load test. This also caused the fluctuation in the responses for the dynamic belt test simulations.

4.5.2 Thorax

The responses of the parameterized ellipsoid Hybrid III 6-year-old model from the thoracic belt load tests improved significantly after optimization. However, the responses from the CPR and pendulum simulations were worse after optimization. This can be explained by the rib damping parameter that was significantly increased. Therefore, the force peaks of the belt load tests were reached by the optimized Hybrid III dummy model, but this also caused the pendulum and CPR impactor to bounce back from the chest (see Figure 4-12). Because the weighting factors of the belt load simulations were higher than the weighting factors of the CPR impactor and thorax pendulum tests, the parameters were more optimized towards the responses of the belt load simulations.

4.5.3 Neck and spine

The responses of the parameterized ellipsoid Hybrid III 6-year-old model from the neck test setups improved significantly after optimization. The neck tensile and neck flexion-extension stiffness and damping parameters were significantly decreased by the optimization algorithm. However, with the decrease of the neck parameters, the responses of the parameterized ellipsoid Hybrid III 6-year-old model from the whole body sled test setups did not improve. It was expected that decreasing the neck and spine parameters should cause the spinal bending that was required to reach the forward displacement of the head and vertebra, which were found in the experimental data. Nevertheless, the lumbar and thoracic joint rotational stiffness and damping were increased by the optimization algorithm. This had no effect on the frontal displacement, but the z-displacement of the dummy model improved (see Figure 4-17). However, the kinematic response of the improved model was proposed as not biofidelic as can be seen in Figure 4-8. That figure shows that the increased spine parameters caused no spine bending. Therefore, as already mentioned in Section 4.4, after analyzing the kinematics of the sled test setups the lumbar and thoracic joint rotational stiffness and damping were scaled back to the original values. The spine rotational parameters were not decreased because this also did not improve the kinematic responses of the whole body sled test setup.

4.6 Conclusion

After analyzing the results of the optimization study, it can be concluded that the optimization algorithm was largely able to reach the biomechanical responses of the specific body region tests (abdomen, thorax and neck) by scaling the parameters of the specific interest regions (abdomen, thorax and neck). Due to weighting and desiring one set of parameters for all tests, some test matched better than others. Nevertheless, some parameters of the thorax body region influenced the responses of the abdomen region setups. Therefore, after the optimization of all body regions, it is recommended that a final optimization cycle be performed to improve the optimization of the parameters. In this way, the influence of all parameters on specific body region setups is taken into account.

While this optimization study provided qualitative results on the ability of the model to meet the biomechanical responses and with which parameters, the level at which the objective function was met was not quantified in the report. The objective function and its minimization in the various optimization steps would be an applicable measure to do so.

The experimental (kinematic) responses of the whole body sled test setups could not be reached by optimization of the chosen parameters of the ellipsoid Hybrid III 6-year-old model. This can be explained by the parameter choice which was described in Section 3.2. Even after introduction of flexion compliance in the thoracic spine, the spine remained quite rigid. There were almost no tensile spine parameters that could be scaled. The neck tensile stiffness was decreased by more than 80%, while all other spine tensile parameters could not be changed. Decreasing the spinal tensile stiffness as well as the spinal shear stiffness could cause more frontal head displacement.

The too rigid spinal configuration of the parameterized dummy model may also affect the interaction with the shoulder belt. A more flexible spine could crouch more under the belt, hence not load the belt as much. This may result in lower friction restraint offered by the belt, resulting in more forward T1 and head excursion.

An additional explanation for the failed optimization of the whole body setup responses could be the MADYMO model of the Hybrid III 6-year-old dummy in the scaled PMHS high-speed sled test (Lopez-Valdes, 2011b). As described in Appendix B, the kinematic response of the head and spine of the hardware Hybrid III 6-year-old dummy was quite different from that of the MADYMO model of the standard 6-year-old dummy in the volunteer low-speed sled setup (Seacrist, 2010). The head and T1 forward excursions were substantially lower at 200 mm and 60 mm respectively, while the pelvis trajectory, belt forces and dummy neck loads of the hardware test setup were in good agreement with those of the MADYMO model. The degree of neck flexion in the simulation at 150 ms after impact (refer to Figure 4-9) seems unrealistically high, which may be caused by the severity of this test being higher than the validation range of the current dummy model.

An additional limitation on the accuracy of the results may lie in the fact that the scaled PMHS high-speed sled tests (Lopez-Valdes, 2011b) resulted in scaled responses. If different scaling techniques were applied, the head displacement data was typically lower (Lopez-Valdes, 2011b) and therefore possibly closer to that predicted by the simulation.

5 Biofidelity Test Corridor Development

5.1 Introduction

The modified and parameterized ellipsoid Hybrid III 6-year-old model, with the inclusion of the optimized parameters obtained in Chapter 4, was developed to serve as a design brief of a future dummy. While the parameters and responses presented in the prior chapters in this report could benefit future dummy design, it may be more useful to use the optimized model for the development of biofidelity test corridors. Biofidelity test corridors are here defined as a range of responses of a dummy to a simplified laboratory environment test setup. These biofidelity test responses in turn can be used by dummy manufacturers in designing ATDs. As such, the objective of this task is to develop biofidelity test responses that a future 6-year-old frontal impact ATD should meet in order to be biofidelic.

While the task description supposes corridors to be developed representing a certain range, the current study did not develop ranges of dummy responses, due to lack of data. As such, biofidelity test responses are generated, as opposed to biofidelity test corridors.

5.2 Selection of biofidelity tests

As discussed, biofidelity tests are tests that are fairly simple in their setup allowing ATD manufacturers to test and certify ATDs in a repeatable, reproducible and cost-effective manner. In order to do so, first an evaluation of current biofidelity tests was performed, since adaptation of available setups is a method to maintain the above goals.

Part 572 (NHTSA, 2000), applicable to the current Hybrid III 6-year-old dummy, requires the following types of tests:

- Head drop test from 376 mm height, with criteria for peak acceleration, oscillations, lateral acceleration and time of peak. Since head properties have not been altered relative to the current Hybrid III 6-year-old dummy model, this test is not relevant for this study.
- Neck (and head) flexion pendulum test at 4.95 m/s impact velocity, with criteria for neck moment, neck angle and time of rebound.
- Neck (and head) extension pendulum test at 4.3 m/s impact velocity, with criteria for neck moment, neck angle and time of rebound.
- Thorax probe impact at 6.71 m/s with 2.86 kg impactor. Criteria include probe force, sternum displacement and hysteresis.
- Torso flexion test at 45 degrees of quasi-static deformation, with criteria for applied force and return angle.
- Knee probe impact at 2.1 m/s with 0.82 kg impactor, with criteria for probe force, sternum displacement, hysteresis. Since lower extremities were outside the scope of this study, this test is not relevant for this study.

In addition to Part 572 tests, biofidelity tests developed for the THOR dummy (Gesac, 2005), were evaluated for their applicability. The only test that was considered relevant and not included via other means was the following:

- Head probe impact at 2.0 m/s and 23.4 kg impactor with criteria for peak force and time of peak. In order to make this test representative for a 6-year-old, the impactor mass is scaled to 2.86 kg.

Another ATD for a 6-year-old in frontal impact is the Q6 dummy. Its biofidelity requirements are similar to those defined in Part 572. However, a few differences exist of which a relevant one is discussed below:

- Besides a 6.7 m/s thorax probe impact test, a test at reduced velocity of 4.3 m/s is also performed.

For adult frontal ATDs the development of so-called Gold Standard test setup is currently being performed, with the objective to develop a test setup that assesses the complete dummy in a representative test while maintaining a high degree of repeatability and reproducibility at acceptable cost. It consists of a rigid seat sled setup with a traditional 3-point belt restraint without a retractor, subject to a standardized crash pulse (Shaw, 2009). The test setup used for high-speed sled tests, based on Lopez-Valdes (2011b), is used as a Gold Standard setup adapted for a 6-year-old.

In addition to current ATD biofidelity tests, some of the biomechanical tests used in this study (see Chapters 3 and 4) are candidates for becoming a biofidelity test meeting the typical criteria as well. Especially, dynamic belt load setups for abdomen and thorax are relevant as they are more comparable to modern automotive loading conditions when compared to the pendulum impactor tests.

From the above overview, biofidelity tests were defined for the current study as shown in Table 5-1 for the relevant body regions and in Table 5-2 for whole body setups. For the Part 572 test, thresholds were available. For other tests they were not derived or presented.

Table 5-1. Body region biofidelity test setups, criteria and current standardized thresholds for a 6-year-old ATD in frontal impact (*N.A.* for non-applicable).

Interest Area	**Test type**	**Criteria & *Threshold***	**Reference**
Abdomen	Dynamic belt load (PEDVE025)	Peak belt force *NA* Hold belt force *NA*	Kent, 2011
Thorax	Diagonal dynamic belt load (PEDVE033)	Peak belt force *NA* Hold belt force *NA*	Kent, 2009
	Pendulum test 6.7 m/s and 2.86 kg	Chest deflection *38-46 mm* Peak force *1500 N*	Part 572 (NHTSA, 2000)
	Pendulum test 4.3 m/s and 2.86 kg	Chest deflection *NA* Peak force *NA*	Part 572 (NHTSA, 2000)
Spine	Torso flexion test	Peak force *147-200 N*	Part 572 (NHTSA, 2000)
Neck	Neck flexion pendulum test 4.95 m/s	Head rotation *74-92°* Occ.con. moment *27-33 Nm* Decay to 5 Nm *103-123 ms*	Part 572 (NHTSA, 2000)
	Neck extension pendulum test 4.3 m/s	Head rotation *85-103°* Occ.con. moment *-19 to -24 Nm* Decay to 5 Nm *123-147 ms*	Part 572 (NHTSA, 2000)
Head	Head pendulum test 2.0 m/s and 2.86 kg	Peak force *NA*	THOR (Gesac, 2005)

Table 5-2. Whole body biofidelity test setups, criteria and current standardized thresholds for a 6-year-old ATD in frontal impact (*N.A.* for non-applicable).

Interest Area	**Test type**	**Criteria & *Threshold***	**Reference**
Whole body	Rigid seat, 3pt belt, sled test 40 km/h and 15G	Head CG excurs. *NA* T1 excursion *NA* T8 excursion *NA* Pelvis excursion *NA* Up. Neck Fx *NA* Up. Neck Fz_t *NA* Up. Neck My_e *NA* Up. Neck My_f *NA* Lumbar Fz_t *NA*	Lopez-Valdes, 2011b

In the following sections, the above setups and the results are discussed. For each setup, a simulation is performed with the optimized model as well as with the standard MADYMO Hybrid III 6-year-old model for comparison.

5.3 Results

5.3.1 Abdomen dynamic belt load (PEDVE025)

The table top test setup with a horizontal belt and a belt displacement function as defined in PEDVE025 test was used. The belt force response is shown in Figure 5-1. It is shown that the new (optimized) dummy model shows a lower initial loading force peak as well as a lower constant hold loading force compared to the old (original) Hybrid III 6-year-old model. These responses are slightly different compared to those presented in Figure 4-10, since in these simulations the spine was locked and since any hardware dummy test will have a flexible spine as well. A suitable criterion for the optimized dummy model would be around 700 N peak force and 150 N hold force, given the prescribed belt displacement function.

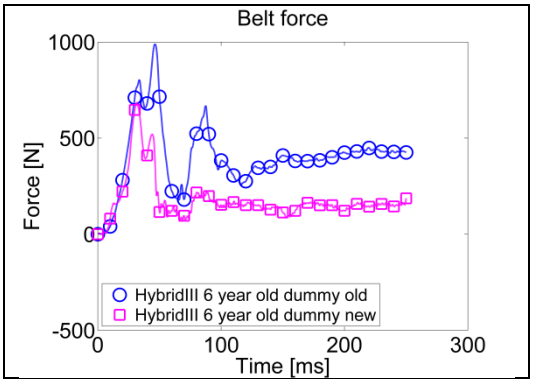

Figure 5-1. Abdomen dynamic belt load test

5.3.2 *Thorax diagonal dynamic belt load (PEDVE033)*

The table top test setup with a diagonal belt and a belt displacement function as defined in PEDVE033 test was used. The belt force response is shown in Figure 5-1. It is shown that the new (optimized) dummy model shows a substantially higher initial loading force peak as well as a higher constant hold loading force compared to the old (original) Hybrid III 6-year-old. These responses are slightly different compared to those presented in Figure 4-11, since in these simulations the spine was locked and since any hardware dummy test will have a flexible spine as well. A suitable criterion for the optimized dummy model would be around 2200 N peak force and 700 N hold force, given the prescribed belt displacement function.

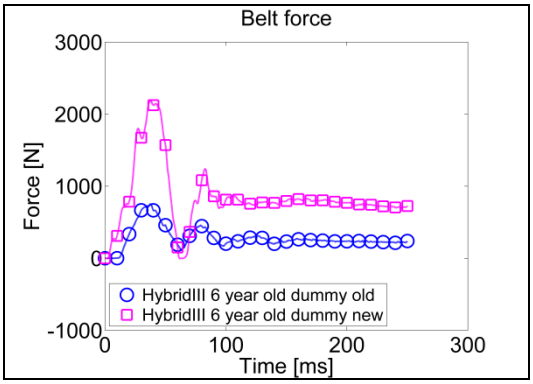

Figure 5-2. Thorax diagonal dynamic belt load tests

5.3.3 *Thorax pendulum impact*

The thorax pendulum test with 2.86 kg pendulum impactor as defined in Part 572 (NHTSA, 2000) was performed at velocities of 6.7 m/s and 4.3 m/s. The resulting pendulum force and chest deflection are shown in Figure 5-3. It is shown that the new (optimized) dummy model shows a substantially higher initial loading force peak at equal levels of deflection for both velocities. It should be noted that the new (optimized) model displays undercritical damping in the deflection characteristic, where kinematics shows that the impactor repeatedly contacts and loses contact with the thorax after the first loading peak. A suitable criterion for the optimized dummy model in the 4.3 m/s test

would be around 25 mm chest deflection and 3300 N peak force. For the 6.7 m/s test, a suitable criterion for the optimized dummy model would be around 40 mm chest deflection and 4300 N peak force. While similar chest deflection is found as required by Part 572 (i.e. in between 38-46 mm), force levels are substantially higher than required by Part 572 (i.e. maximum 1500 N). While the optimized dummy model is supposed to be more biofidelic, in the optimization to this test low weighting was attributed. As such, this specific response may not be biofidelic. This was compromised since this type inertial impactor loading is not considered representative anymore. Therefore, it is questionable whether this setup should be proposed for a future dummy.

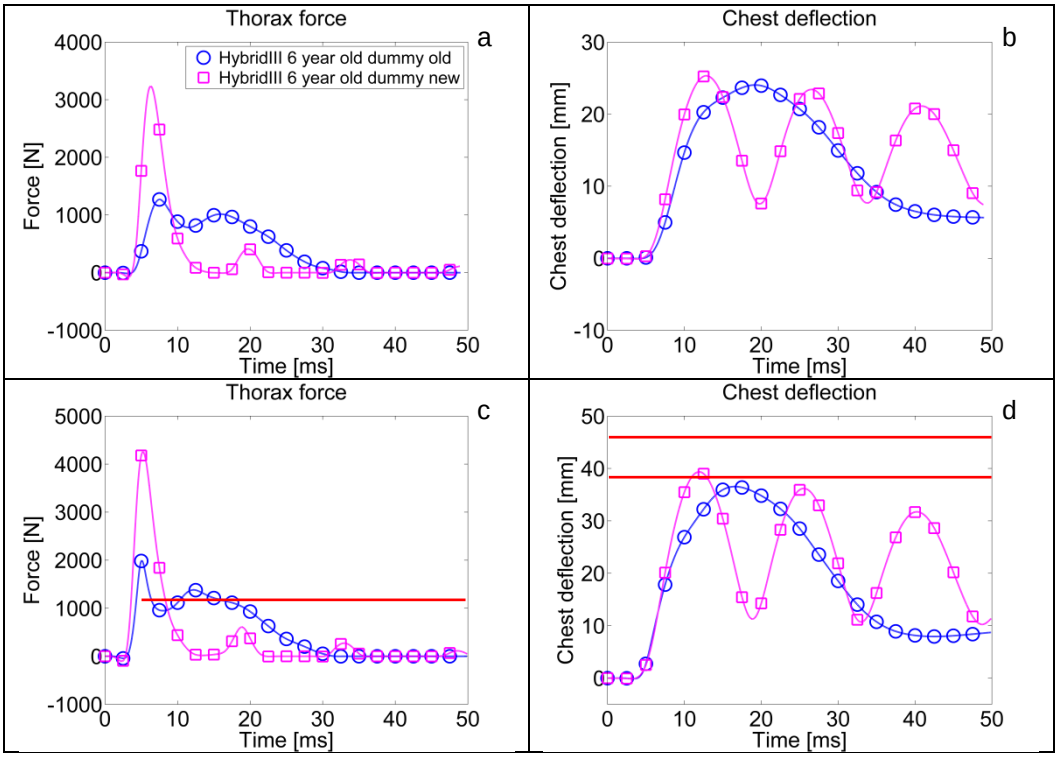

Figure 5-3. Thorax pendulum test with 4.3 m/s impact velocity (a: Force and b: Chest displacement) and with 6.7 m/s impact velocity (c: Force and d: Chest displacement), thresholds in red.

5.3.4 Torso flexion test

The torso flexion test requiring 45° of applied flexion, as defined in Part 572, (NHTSA, 2000) was performed as well. The resulting traction force versus torso flexion is shown in Figure 5-4. It is shown that the new (optimized) dummy model shows a substantially lower force peak at 45° of applied flexion. The achieved force of 183 N would be a suitable criterion, and is in between the range as required by Part 572 (i.e. in between 147-200 N). It should be noted that the original (old) dummy model reaches much higher force levels. This raises doubts about the ability to correctly implement this test numerically. It is not clearly stated in Part 572 whether at the initial position of 22°, the dummy is preloaded or not. In the current simulation, the 45° of applied flexion are from a non-preloaded condition.

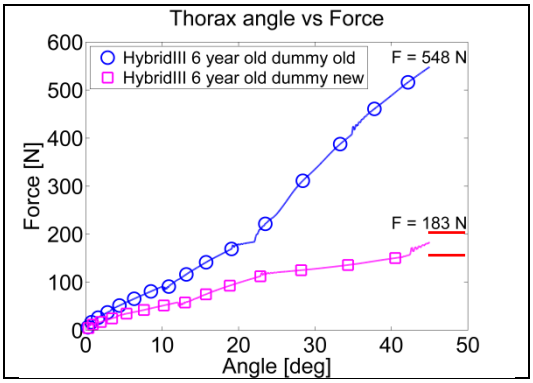

Figure 5-4. Torso flexion test, thresholds in red

5.3.5 *Neck (and head) pendulum test*

The neck (and head) pendulum test as defined in Part 572 (NHTSA, 2000) was performed as prescribed with impact velocities of 4.95 m/s in flexion and 4.3 m/s in extension. The resulting head rotation and occipital condyle moment are shown in Figure 5-5. It is shown that the new (optimized) dummy model shows a substantially more compliant neck response. While higher degrees of head rotation are observed, the occipital condyle moments are generally lower.

A suitable criterion for the optimized dummy model in the flexion test would be to allow around 153° head rotation and 28 Nm occipital condyle moment. Head rotation values are substantially higher than required by Part 572 (i.e. in between 74-92°), while occipital condyle moments are within the range required (i.e. in between 27-33 Nm). The decay to 5 Nm occurs at around 165 ms after impact, which is substantially later than required (i.e. in between 103-123 ms).

A suitable criterion for the optimized dummy model in the extension test would be to allow around 227° head rotation and 16 Nm occipital condyle moment. Head rotation values are substantially higher than required by Part 572 (i.e. in between 85-103°), while occipital condyle moments are just below the range required (i.e. in between -19 to -24 Nm). The decay to 5 Nm occurs at around 240 ms after impact, which is substantially later than required (i.e. in between 123-147 ms). It should however be noted that the optimization of the dummy model did not focus on neck extension, but merely on neck tension and flexion.

It should be noted that for both flexion and extension tests the optimized dummy model's head rotation values are so large that impact of the head with the pendulum may occur. In order to eliminate this unrealistic interaction, it may be advisable to reduce the impact velocity of the pendulum test.

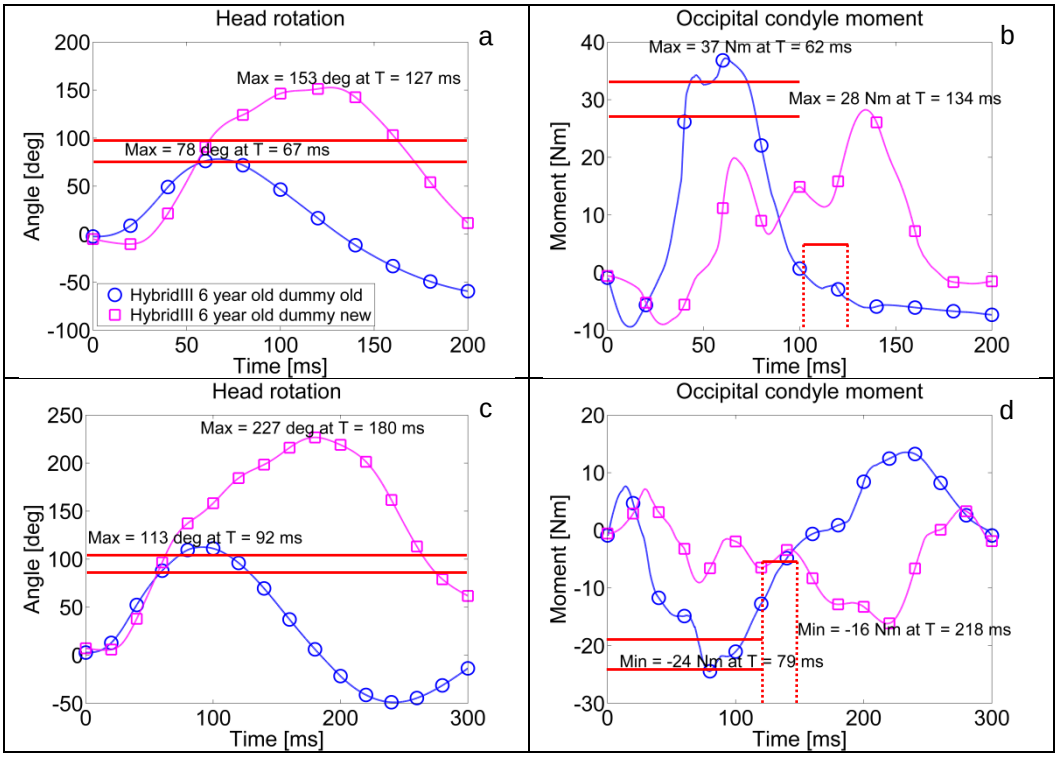

Figure 5-5. Pendulum flexion (a: head rotation and b: occipital condyle moment) and pendulum extension (c: head rotation and d: occipital condyle moment), thresholds in red.

5.3.6 Head pendulum test

The head pendulum test with 2.86 kg pendulum impactor as defined for THOR adult dummy (Gesac, 2005) was performed at velocities of 2.0 m/s. The response for the new (optimized) dummy model was very similar to that of the old (original) dummy model, as is shown in Figure 5-6. This response is primarily determined by head contact properties and slightly by neck stiffness and damping. A suitable criterion for the optimized dummy model would be to reach 2300 N impactor force. However, it should be noted that head contact properties were not optimized for biofidelity in this study.

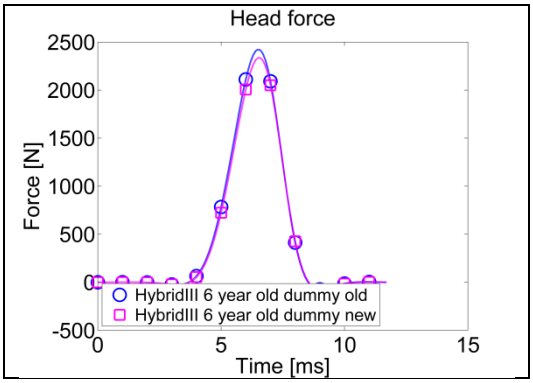

Figure 5-6. Head pendulum test.

5.3.7 Whole body rigid seat and 3-point belt sled test

As mentioned in the introduction in section 5.1, this setup was equal to the setup used for high-speed sled tests in sensitivity and optimization, based on Lopez-Valdes (2011b). The pulse used represents a 40 km/h ΔV at approximate peak acceleration of 15 G, as shown in Figure 5-7.

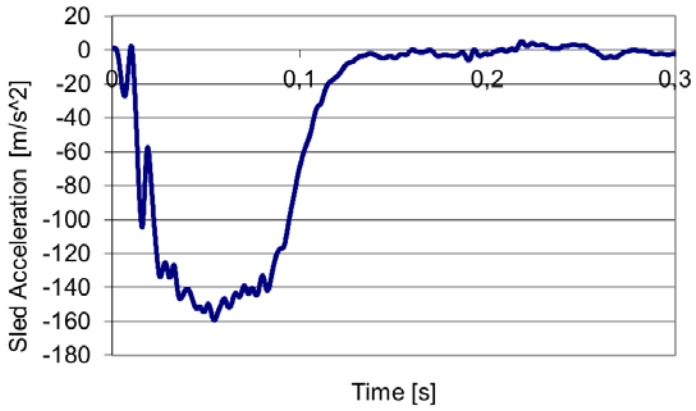

Figure 5-7. Scaled PMHS high speed sled test acceleration pulse.

The resulting trajectories for the dummy models are shown in Figure 5-9. Trajectories are plotted based on dummy model accelerometer measurements in head center of gravity, T1, T8 and in the pelvis. Loads in the dummy model consist of upper neck axial force, anterior-posterior shear force and neck flexion-extension moment, lower neck axial force and lumbar axial force. The response for the new (optimized) dummy model resulted in more forward excursion for head, T1 and T8 compared to the old (original) dummy model. For pelvis, T8 and T1 more forward excursion was combined with more upward excursion.

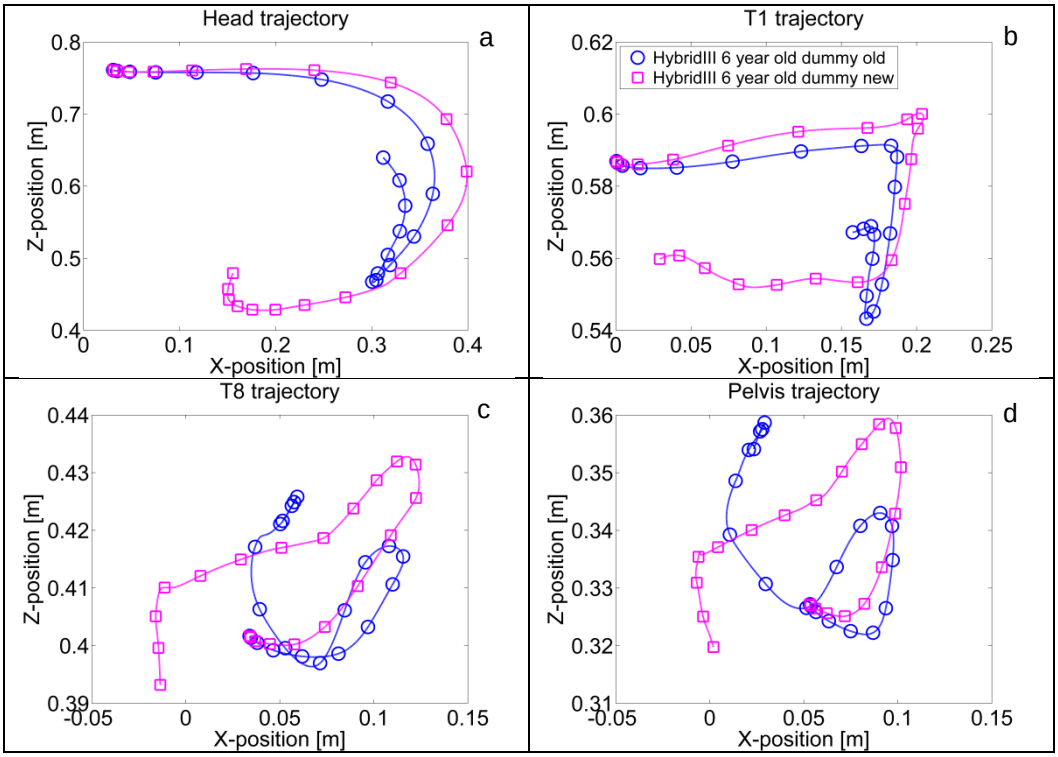

Figure 5-8. Scaled PMHS high speed sled test (a: Head trajectory, b: T1 trajectory, c: T8 trajectory, d: Pelvis trajectory).

The resulting loads in the dummy model are shown in Figure 5-9. The loads in the upper neck were higher in the new (optimized) dummy model for all neck shear force (Fx), neck axial force (Fz) and neck flexion-extension moment (My). The loads in the upper neck were higher in the new (optimized) dummy model for Fx and Fz, however, the new (optimized) dummy model shows hardly any My. Lumbar spine axial force remained largely similar. Suitable criteria for the upper neck would be around -1600 N Fx, 1900 N Fz in tension, -38 Nm in neck extension and 24 Nm in neck flexion. A suitable lumbar tensile force criterion would be 900 N.

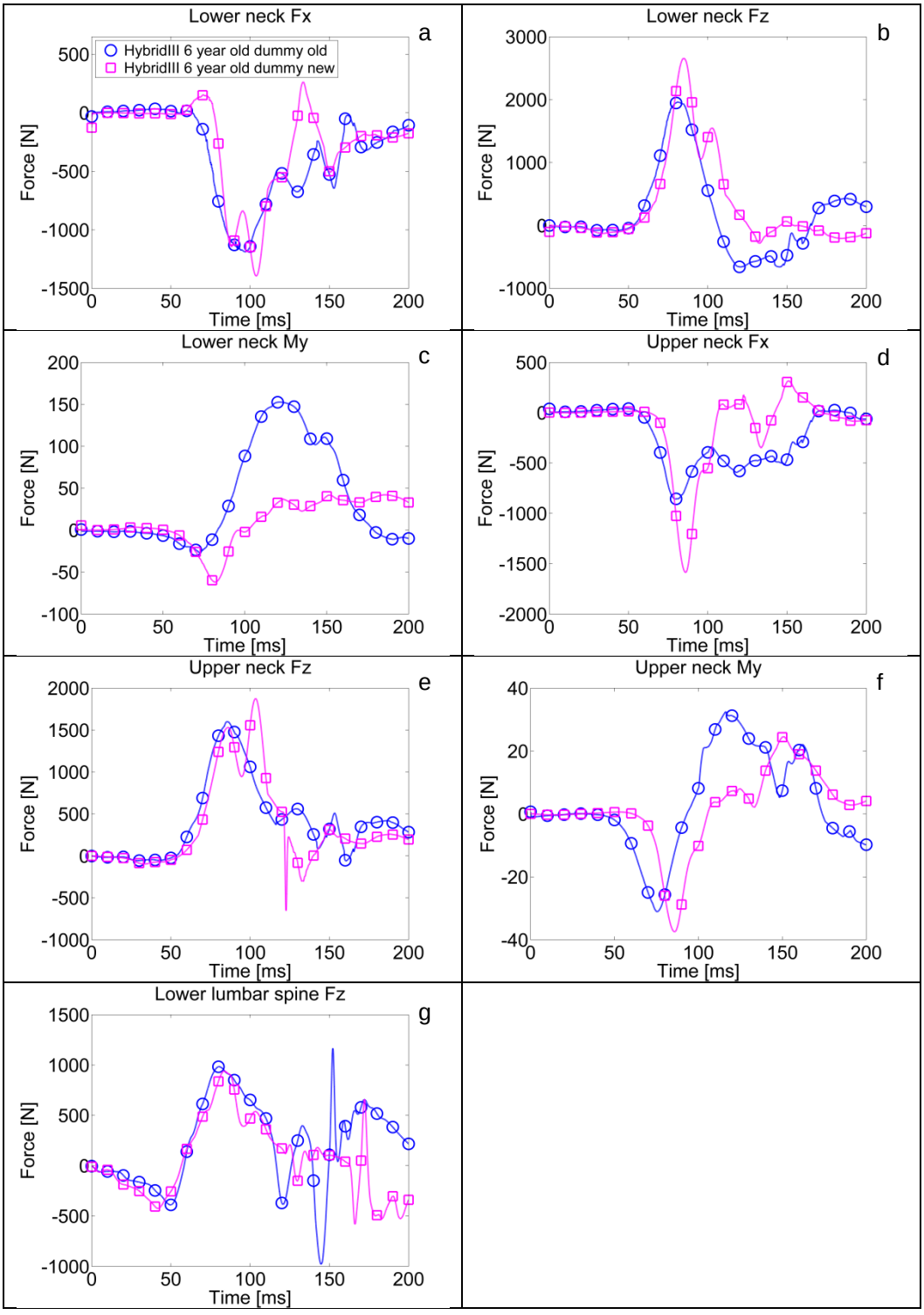

Figure 5-9. Scaled PMHS high speed sled test (a: Upper neck Fx, b: Upper neck Fz, c: Upper neck My, d: Lower neck Fx, e: Lower neck Fz, f: Lower neck My and g: Lumbar spine Fz).

5.4 Conclusion

Biofidelity test responses for a future ATD representing a 6-year-old in frontal impact crashes were developed based on existing standards and biomechanical tests developed by partners within this project. These responses consist of deterministic responses of the optimized parameterized 6-year-old dummy model, obtained in Chapter 4 in the test setups described in Table 5-3 for relevant body regions and in

Table 5-4 for whole body setups. For the whole body setup, it is important to note that the optimization did not result in the targeted whole body kinematics. Hence, the whole body test setup criteria and thresholds are likely to change once a more optimized model is obtained.

Table 5-3. Body region biofidelity test setups, criteria and proposed thresholds for a 6-year-old ATD in frontal impact.

Interest Area	**Test type**	**Criteria & *Threshold***	**Reference**
Abdomen	Dynamic belt load (PEDVE025)	Peak belt force *700 N* Hold belt force *150 N*	Kent, 2011
Thorax	Diagonal dynamic belt load (PEDVE033)	Peak belt force *2200 N* Hold belt force *700 N*	Kent, 2009
	Pendulum test 6.7 m/s and 2.86 kg	Chest deflection *40 mm* Peak force *4300 N*	Part 572 (NHTSA, 2000)
	Pendulum test 4.3 m/s and 2.86 kg	Chest deflection *25 mm* Peak force *3300 N*	Part 572 (NHTSA, 2000)
Spine	Torso flexion test	Peak force *183 N*	Part 572 (NHTSA, 2000)
Neck	Neck flexion pendulum test 4.95 m/s	Head rotation *153°* Occ.con. moment *28 Nm* Decay to 5 Nm *165 ms*	Part 572 (NHTSA, 2000)
	Neck extension pendulum test 4.3 m/s	Head rotation *227°* Occ.con. moment *-16 Nm* Decay to 5 Nm *240 ms*	Part 572 (NHTSA, 2000)
Head	Head pendulum test 2.0 m/s and 2.86 kg	Peak force *2300 N*	THOR (Gesac, 2005)

Table 5-4. Whole body biofidelity test setups, criteria and proposed thresholds for a 6-year-old ATD in frontal impact.

Interest Area	**Test type**	**Criteria & *Threshold***	**Reference**
Whole body	Rigid seat, 3pt belt, sled test 40 km/h and 15G	Head CG excurs. *400 mm* T1 excursion *210 mm* T8 excursion *125 mm* Pelvis excursion *100 mm* Up. Neck Fx *-1600 N* Up. Neck Fz_t *1900 N* Up. Neck My_e *-38 Nm* Up. Neck My_f *24 Nm* Lumbar Fz_t *900 N*	Lopez-Valdes, 2011b

While the existing standards typically allow ranges within certain criteria should lie, currently deterministic responses and threshold values are proposed. For an extension of these responses to corridors and for the extension of threshold values to ranges, more insight needs to be obtained regarding 1) variability in hardware parameters, 2) variability in input load, 3) variability within 6-year-old populations, 4) the effects of these on the response and 5) acceptability by all stakeholders. Once these variables are quantified, they can be implemented in further parameterization of the simulation setups and via stochastic simulations the desired corridors and ranges can be obtained.

While the tests based on existing standards have well-described test setups, for the additional setups both the test setup and the input load may need to be further defined and generalized. For the belt load setups at least belt attachment points and input load function need to be further defined and generalized, in order to be able to implement it in hardware setups. For the sled setup, the rigid seat, knee bolster, foot well and seat belt need to be defined, as well as the development of a more generic acceleration pulse. For this, hardware design involvement is required, which was outside of the scope of this study.

Since some dummy model properties have changed quite dramatically, some existing biofidelity test setups resulted in undesirable behavior. Mainly the neck pendulum tests result in unrealistic amounts of neck flexion and extension, such that it is proposed to reduce the input energy (or initial velocity) of these tests. Also, the thorax pendulum test resulted in unrealistic behavior with the new thoracic properties; however, due to the low weighting that was attributed to this setup, this setup may not be representative for a future dummy anymore.

6 Conclusions and Recommendations

In this project, the primary objective was to develop a numerical anthropometric test device that could serve as a design brief for a future ATD representing a 6-year-old child in frontal impact. The basis for the numerical ATD was the MADYMO Hybrid III 6-year-old model, which is a validated multi-body model representing the hardware Hybrid III 6-year-old.

6.1 Dummy Model Design Updates

This model was updated with the following body segment models with higher levels of flexibility and/or expected biofidelity:

- A rigid pelvis block and abdomen component with updated geometry for improved lap belt interaction.
- An additional thoracic spine degree of freedom, allowing flexion and extension at the mid thoracic spine level.
- A shoulder with more deformation modes, allowing relative motion of the gleno-humeral joint relative to the spine and with a representative clavicle geometry for improved belt interaction.

The updates were based on data provided by research partners in the project. In discussion with partners these updates were deemed necessary and sufficient in order to create a model that could represent the desired level of biofidelity of a 6-year-old child in frontal impact. No component validation data was available or provided that would allow for a body segment validation on the updated segment models.

6.2 Sensitivity Analysis for Assessment of Biomechanical Parameters

After the updates were applied, the model was parameterized to be able to perform sensitivity and optimization studies that would help to arrive at the future ATD design brief. The choice of parameters was defined based on available parameters in the updated Hybrid III 6-year-old model and agreed upon by the partners in the project. The ranges within these parameters that would need to be varied were not based on biomechanical studies quantifying human variability, but merely based on engineering judgment. Human variability data, even though only sparsely available, would have been useful if the initial set of parameters in the model was within the range of human variability. However, for most parameters it most likely wasn't, since the base model of the Hybrid III 6-year-old dummy is based on a scaled Hybrid III 50th percentile dummy, both with limited biofidelity due to 1) the scaling and 2) the simplified hardware representation requiring lumped and hence non-biofidelic parameters. Engineering judgment allows for choosing substantially wide ranges such that the biofidelic response most likely lies within the range.

The updated and parameterized Hybrid III 6-year-old model was then used in sensitivity analysis. This consisted of finding relations between dummy parameter variations and sensitivities in output response in a supposedly comprehensive range of test setups. In performing this analysis, insight was obtained in which parameters influenced which

responses in what test conditions. In total, 9 body region test setups were defined, as well as 3 different whole body test setups. Body region setups were defined for abdomen, thorax and neck independently. They had the purpose to quantify the performance of a dummy in specific and controlled experiments, while whole body setups are better at quantifying the final performance requirement in automotive frontal impact testing. The following sensitivities were observed:

- In the abdomen, both abdomen and pelvis flesh stiffness values would need to be reduced to meet quasi-static force response at the applied levels of belt displacement. In order to meet higher force peaks at high belt loading rates, abdominal damping needed to be increased.
- The thorax model in the updated and parameterized Hybrid III 6-year-old dummy model is similar to a Lobdell-like model with a number of springs and dampers in series, each representing a lumped structure in the thorax. From this model, the most sensitive parameters were the stiffness of the ribs and the accompanying damping parameter. Basically, stiffness would need to be reduced and damping be increased. However, setups representing inertially loaded impacts required reductions of stiffness and damping in the sternum, while belt loaded impacts required increases of contact stiffness properties.
- For the neck, it was known that the dummy parameters represented a far less compliant structure than that of a 6-year-old child. This was immediately clear for neck tensile stiffness and flexion-extension properties. Sensitivity to geometrical parameters, such as neck joint locations and head mass were found as well; however, based on input from partners it was concluded that these should not be altered for later optimization.
- In the whole body setups, lower sensitivity to parameter variations was observed. The parameters that were most sensitive were parameters in the lumbar, thoracic and lumbar spine. Again, geometrical parameters were chosen not to be proposed for optimization. Stiffness parameters had positive as well as adverse effects. Stiffening the spine allowed for more upward motion of the dummy in all three sled tests, which was observed in the biomechanical responses as well. A stiffer spine did, however, have negligible effects on forward motion of the dummy, as did a more compliant spine. The fact that a more compliant spine does not create the desired forward motion, may be due to the chosen test setups with 3-point belts restraining the dummy from displaying torso flexion or due to limitations in the validation of the models of the sled setups.

6.3 Optimization Study for Response Requirements for Future ATDs

Based on the results from the sensitivity analysis, an optimization study was initiated. The same body region and whole body setups were used with some modifications resulting from progressed insight. For abdomen and thorax alternative loading rates were added, to optimize for rate sensitivity. For optimization of the relation between belt force and chest deflection, the more simplified scaled PMHS high-speed sled setup was used. Compared to the earlier booster seat setup, this setup may show increased sensitivity. The scaled PMHS high-speed sled setup poses a more direct interaction between shoulder belt and thorax due to the absence of a high-back booster seat, which adds time-variant load on the shoulder belt. A gradient descent optimization

algorithm was used which searches for a local minimum of the objective function for multiple parameter variations at the same time. Weighting factors were defined and agreed upon by the partners to stress important test setups, responses and signals. Results were generated from the optimization algorithm itself; however, based on observed interdependency and undesirable local minima, manual adjustments were made. The interdependency was observed for thorax and abdomen body regions. The undesirable local minimum was observed in the earlier discussed stiffer spine for more upward dummy motion. The final results were presented by comparing the response of the optimized model after manual adjustments with the response of the MADYMO Hybrid III 6-year-old model. The final model differed from the baseline model in relative terms as follows:

- The abdominal stiffness values were reduced by an order of magnitude 10, while abdominal damping was increased by 15 percent.
- The thorax was optimized predominantly towards belt loaded setups by reducing sternum stiffness and by increasing contact stiffness used in the model, as sensitivity analysis indicated. The parameter with highest sensitivity however, the rib stiffness, was kept constant in the optimization. Similarly, damping parameters were varied substantially but not all in the same direction.
- Since neck and spine parameters influence neck body region setups as well as whole body setups, the optimization for these was grouped as well. As concluded from the sensitivity analysis, the optimization algorithm reduced neck flexion-extension and tension stiffness and damping substantially. Also in line with findings from sensitivity analysis, spinal parameters were increased by the optimization algorithm; however, it was decided to set them at 1.0 for the final model. This was decided since a further reduction did not improve the kinematics towards the desired more forward excursion of the upper torso and head.

In general, the optimization algorithm largely managed to improve the response of the updated and parameterized Hybrid III 6-year-old model. However, the trajectories of the upper torso and head in the whole body sled setups were not met. The final optimized model never displayed the amount of forward excursion observed in the biomechanical tests. This is partially attributed to differences between the model of the seat and belt setup from the experimental setup, as validation showed. Moreover, the parameterized model still had limited amount of degrees of freedom to allow for the biomechanical response to be replicated. In the absence of kinematic data showing biofidelic human motion in frontal impact, it is anticipated that more spinal flexion bending and spinal axial extension occur in reality which alters the interaction with the 3-point belt such that more head forward excursion is achieved. Shoulder flexibility, although introduced in the updated model, could also result in more forward excursion. However, the latter was not parameterized and as such not optimized. The optimization study resulted in an optimized version of the updated and parameterized Hybrid III 6-year-old model, which is a final deliverable of the project as well.

6.4 Biofidelity Test Corridor Development

The optimized model can be used by partners in further definition of a design brief for a future dummy, where currently not specified in the Statement of Work. However, for hardware ATD design, a numerical model is difficult to ‘meet’ in terms of characteristics.

As such, biofidelic responses were generated in biofidelity test setups that were deemed representative and implementable in hardware environments at acceptable cost. These responses were based on existing hardware dummy biofidelity setups, such as pendulum tests and based on tests from the optimization study that were deemed more representative such as belt load tests and whole body sled tests. For each test, responses were generated and criteria were proposed. This allows the designer of a more biofidelic ATD to focus on these setups and the criteria rather than focus on the specific parameters in the optimized model. Some setups with the optimized model resulted in undesirable behavior, which would demand an adaptation of the test setup, something that is to be decided with the partners in the project when hardware implementation is being devised.

6.5 Recommendations

While this study largely met the objectives, recommendations for future research can be made based on the above findings and conclusions:

- Component validation and dummy biofidelity optimization for body regions for which it was not performed, such as shoulder and pelvis.
- An extension of the flexibility of the spine of the dummy model, including a detailed kinematic analysis comparing dummy response to biomechanical subject response (e.g. child volunteer, PMHS or any other) in whole body sled setups.
- Conduct a similar sensitivity and optimization study using a 6-year-old child human model. Perhaps, the head excursions can be better optimized with the human model than with the Hybrid III dummy model
- A more detailed validation of the sled setups based on standard Hybrid III 6-year-old test, including a more detailed specification of the experimental setup in order to more accurately model it. This will reduce current uncertainty in the reason why the forward excursion is not met. It may be due to limited flexibility, or due to differences between model and experimental setup.
- A final optimization loop on all setups and all parameters could be performed to fine-tune responses and to resolve interdependencies observed.
- Currently, deterministic biofidelity test responses are generated, while if human variability data comes available and when agreement between stakeholders is achieved on allowable tolerances, these responses can be extended to corridors, as is common for dummy response requirements.
- In the hardware implementation of the biofidelity test setups and future use of the optimized updated and parameterized Hybrid III 6-year-old model, questions may arise that can be resolved with parameter studies with the developed numerical models.

7 References

Arbogast, K. B., Chen, I., Nance, M. L., Durbin, D., & Winston, F.K.(2004) Predictors of pediatric abdominal injury risk, Stapp Car Crash Journal 48: 479-494.

Arbogast K.A., Balasubramanian S., Seacrist T., Maltese M.R., Garcia-Espana J.F., Hopely T., Constans E., Lopez-Valdes F.J., Kent R., Tanji H., Higuchi K. (2009). Comparison of kinematic responses of the head and spine for children and adults in low-speed frontal sled tests. *Stapp Car Crash Journal. Vol. 53*, pp. 329-372.

Dibb, A. T. (2010). Pediatric Head and Neck Dynamic Response: A Computational Study. Ph.D. Dissertation, Duke University, Department of Biomedical Engineering.

Forbes, P.A. (2007). Development of child human body models and simulated testing environments for the improvement of child safety. TNO report TNO-033-HM-2007-00311..

Forman, J., Michaelson, J., Kent, R., Kuppa, S., & Bostrom, O. (2008, Occupant restraint in the rear seat: ATD responses to standard and pre-tensioning, force-limiting belt restraints. *Annu. Proc. Assoc. Adv. Automotive Med., 52*:141–154.

GESAC [General Engineering and Systems Analysis Company]. (2005, March). Biomechanical Response Requirements of the THOR NHTSA Advanced Frontal Dummy (Revision 2005.1), (Report No. GESAC-05-03). Boonsboro, MD: Author. Available at www.nhtsa.gov/DOT/NHTSA/NVS/Biomechanics%20&%20Trauma/THOR-NT%20Advanced%20Crash%20Test%20Dummy/thorbio05_1.pdf.

Ivarsson, B. J., Crandall, J. R., Longhitano, D., & Okamoto, M. (2004a). Lateral injury criteria for the 6-year-old pedestrian – Part I: Criteria for the head, neck, thorax, abdomen and pelvis. 2004 SAE World Congress, 2004-01-0323.

Ivarsson, B. J., Crandall, J. R., Longhitano, D., & Okamoto, M. (2004b). Lateral injury criteria for the 6-year-old pedestrian – Part II: Criteria for the upper and lower extremities. 2004 SAE World Congress, 2004-01-1755.

Hu, J., Klinich, K. D., Reed, M. P., Kokkolaras, M., & Rupp, J. D. (2011). (in press), Development and validation of a modified hybrid-III six-year-old dummy model for simulating submarining in motor-vehicle crashes. *Medical Engineering and Physics*, 34(5):541-551. 10.1016/j. medengphy.2011.08.013.

Kallieris, D., Schmidt, G., Barz, J., Mattern, R., & Schulz, F. (1978). Response and Vulnerability of the Human Body at Different Impact Velocities in Simulated Three-Point Belted Cadaver Tests. *Proc. IRCOBI*, pp. 105-209.

Kent, R., Stacey, S., Kindig, M., Forman, J., Woods, W., Rouhana, S. W., Higuchi, K., Tanji, H., St. Lawrence, S.., & Arbogast, K. B. (2006). Biomechanical response of the

pediatric abdomen, part 1: Development of an experimental model and quantification of structural response to dynamic belt loading, *Stapp Car Crash Journal, Vol. 50*, 06S-22.

Kent, R., Salzar, R., Kerrigan, J., Parent, D., Lessley, D., Sochor, M., Luck, J., Loyd, A., Song, Y., Nightingale, R., Bass, C., & Maltese, M. (2009). Pediatric Thoracoabdominal Biomechanics. *Stapp Car Cash Journal. Vol. 53*.

Kent, R., Lamp, J., Salzar, R., Kerrigan, J., Parent, D., Lau, S., Lopez-Valdes, F., Lessley, D., & Sochor, M. (2011). Characterization of the Pediatric Thorax and Abdomen Under Loading Conditions Relevant to Automotive Impacts, Report to Insurance Institute for Highway Safety, University of Virginia, Center for Applied Biomechanics.

King, A. I., Viano, D. C., Mizeres, N., &States, J. D. (1995). Humanitarian Benefits of Cadaver Research on Injury Prevention. *The Journal of Trauma: Injury, Infection and Critical Care, Vol. 38*, No. 4.

Lopez-Valdes, F. J., & Parent, D., (2011a), Madymo model of Hybrid III-6-year-old in high-back booster seat on Ford Taurus rear seat, internal communication.

Lopez-Valdes, F. J., Seacrist, T., Balasubramanian, S., Maltese, M. R., Arbogast, K. B., Tanji, H., Higuchi, K., & Kent, R. (2011b). Comparing the Kinematics of the Head and Spine between Volunteers and PMHS: a Methodology to Estimate the Kinematics of Pediatric Occupants in a Frontal Impact. Proceedings of the 2011 IRCOBI Conference proceedings, Krakow, Poland, .

MADYMO (2011). Model Manual, Release 7.3, TASS BV, The Netherlands.

Maltese, M. R., Castner, T., Niles, D., Nishisaki, A., Balasubramanian, S., Nysaether, J., Sutton, R., Nadkarni, V., & Arbogast, K. B. (2008). Methods for Determining Pediatric Thoracic Force-Deflection Characteristics From Cardiopulmonary Resuscitation. *Stapp Car Crash J 52*: 83-106.

Maltese, M., Arbogast, K., Nadkarni, V., Berg, R., Balasubramanian, S., Seacrist, T., Kent, R., Parent, D., Craig, M., & Ridella, S. (2010). Incorporation of CPR Data into ATD Chest Impact Response Requirements. *Ann Adv Automot Med 54*: 79-88.

National Highway Traffic Safety Administration. (2000). Part 572.120 Subpart N—Six-year-old Child Test Dummy, Beta Version. Washington, DC: Author.

Ouyang, J., Zhao, W., Xu, Y., Chen, W., &Zhong, S. (2006). Thoracic impact testing of pediatric cadaveric subjects,.*The Journal of Trauma, Injury, Infection and Critical Care*.

Parent, D. P. , Crandall, J. R. , Bolton, J. R. , Bass, C. R. , Ouyang, J. and Lau, S. H. (2010). Comparison of Hybrid III child test dummies to pediatric PMHS in blunt thoracic impact response, *Traffic Injury Prevention 11*:4, 399 — 410.

Reed, M. P., Sochor, M. M., Rupp, J. D., Klinich, K. D., & Manary, M. A. (2009). Anthropometric specification of child crash dummy pelves through statistical analysis of skeletal geometry. *Journal of Biomechanics, 42*:1143-1145.

Reed, M. P. (2009). Shoulder Anthropometry Targets for a Modified 6YO Hybrid--III: Preliminary Results. UMTRI document. October 22, 2009.

Seacrist, T., Balasubramanian, S., Garcia-Espana, J. F., Maltese, M. R., Arbogast, K. B., Lopez-Valdes, F. J., Kent, R., Tanji, H., & Higuchi, K. (2010). Kinematic Comparison of Pediatric Human Volunteers and the Hybrid III 6-Year-Old Anthropomorphic Test Device. Proceedings of the AAAM 54th Annual Scientific Conference.

Shaw, G., Parent, D., Purtsezov, S., Lessley, D., Crandall, J., Kent, R., Guillemot, H., Ridella, S., Takhounts, E., & Martin, P. (2009). Impact Response of Restrained PMHS in Frontal Sled Tests: Skeletal Deformation Patterns Under Seat Belt Loading. *Stapp Car Crash Journal. Vol. 53*, pp. 1-48.

Sherwood, C. P., Shaw, C. G., van Rooij, L., Kent, R. W., Crandall, J. R., Orzechowski, K. M., Eichelberger, M. R., & Kallieris, D. (2003). Prediction of Cervical Spine Injury Risk for the 6-Year-Old Child in Frontal Crashes. *Traffic Injury Prevention, 4*:206-213.

8 Signature

Helmond, June 19th 2012 Placeholder

V.G.M. Hendrickx
Head of department

L. van Rooij
Author

9 Appendix A: Abdomen parameter optimization

While the results in Section 4.4.1 are the final optimized results, the optimization algorithm for the abdomen, which was performed prior to the other body regions, resulted in different results that will be discussed below. After the optimization of the abdomen parameters, the thorax parameters were optimized and changed. The changing of thoracic parameters, mainly the shoulder flesh stiffness, influenced the responses of the abdomen belt test setups. Figure 9-1 gives the responses of the optimized Hybrid III 6-year-old dummy model in the abdomen setups before the optimization of the thoracic and neck/spine parameters. These responses show less undesirable fluctuations than the responses after the complete optimization.

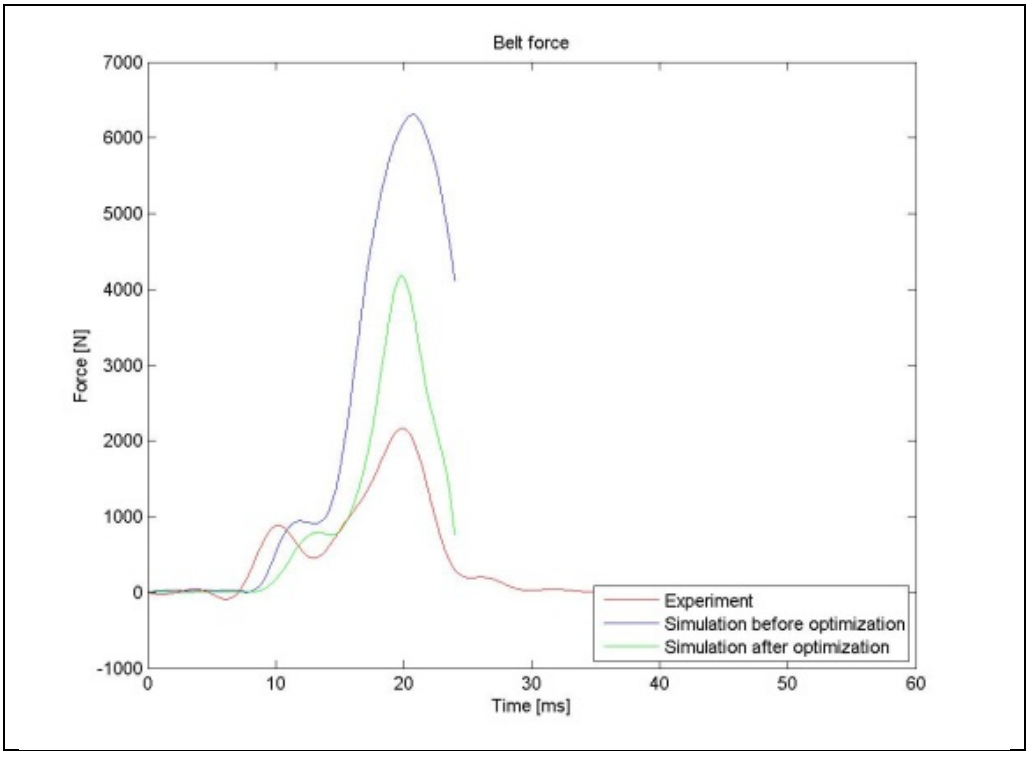

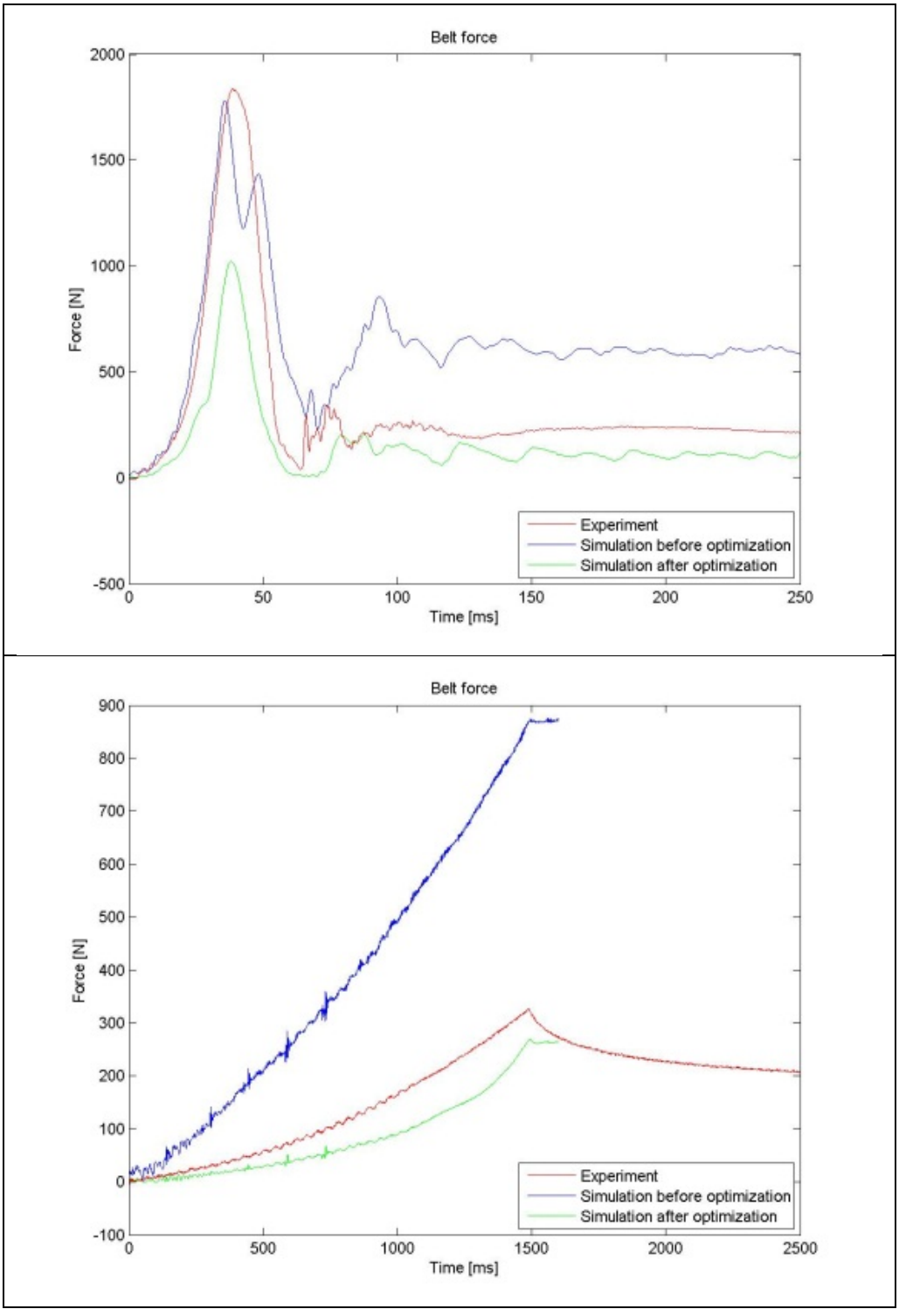

Figure 9-1. Response of the simulations with optimized parameterized ellipsoid Hybrid III 6-year-old model after abdomen optimization (green) and Hybrid III 6-year-old model before optimization (blue) and experimental data (red) of high rate dynamic belt load test PAC1.16 (Kent, 2006) (a), low rate dynamic belt load test PEDVE025 (Kent, 2011) (b) and quasi-static belt load test PEDVE024 (Kent, 2011) (c).

10 Appendix B: Ford Taurus rear bench, booster and 3-point belt setup validation

A simulation setup was developed and validated based on a 2004 model year Ford Taurus rear bench, a Graco Step 3 Turbobooster high-back booster seat in an Autoliv 3-point belt restraint with a standard belt without force limiting and pretensioner (Lopez-Valdes, 2011a). The base model setup, kinematic comparison between Hybrid III 6-year-old hardware dummy and Madymo 6-year-old Hybrid III dummy model and comparison of relevant dummy outputs are presented by Lopez-Valdes (2011a) and repeated here for matters of completeness.

In Figure 10-1, the Madymo model environment of the rear bench, high back booster, 3-point belt system and the Hybrid III 6-year-old dummy are shown.

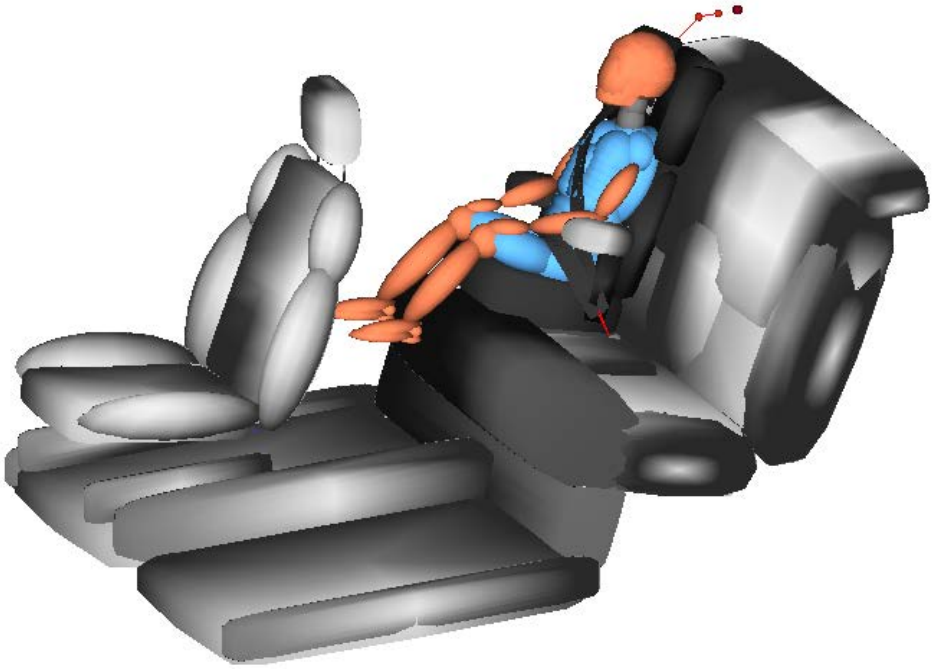

Figure 10-1. Ford Taurus rear bench, high-back booster, 3-point belt and Hybrid III 6-year-old model setup (Lopez-Valdes, 2011a).

Model validation was performed based on hardware sled tests (Forman, 2008) with the described vehicle systems and a Hybrid III 6-year-old dummy (Lopez-Valdes, 2011a). Tests were performed at 29 km/h and 49 km/h crash speeds respectively. Dummy readings chest acceleration, shoulder belt tension and chest deflection for both numerical and hardware dummy at both test speeds are shown in Figure 10-2.

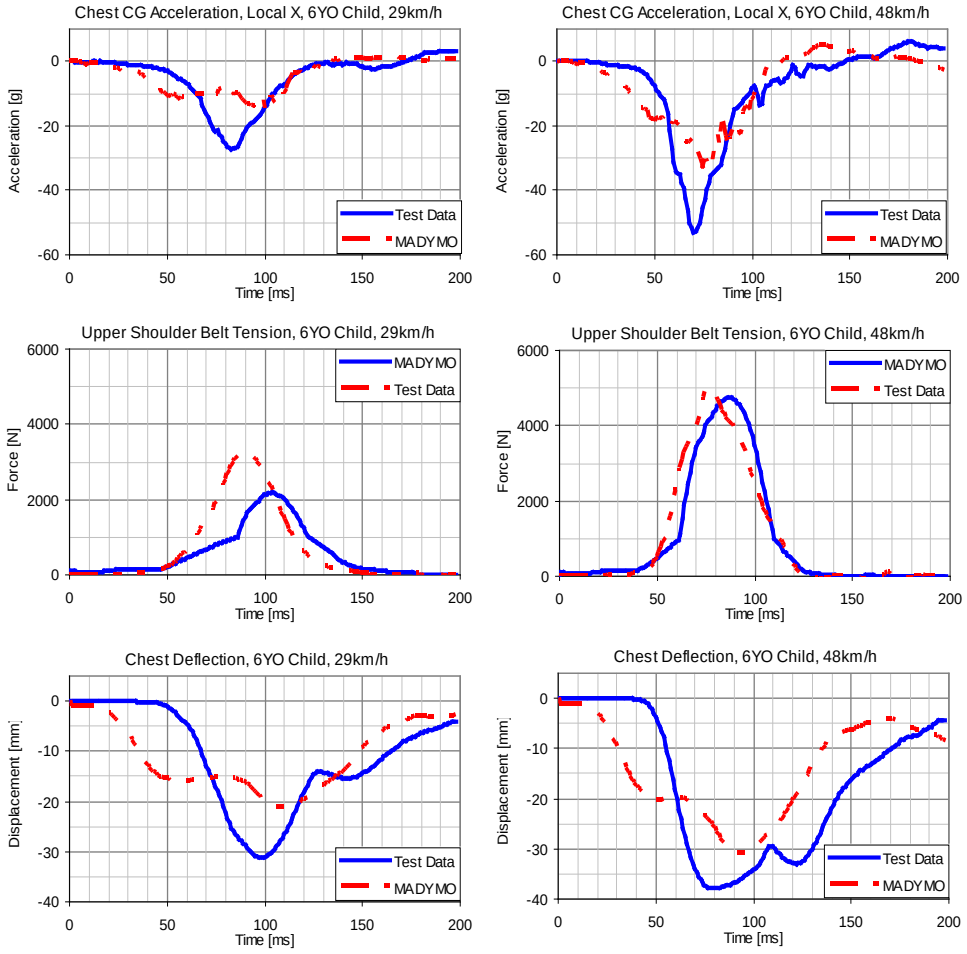

Figure 10-2. Ford Taurus rear bench, high-back booster, 3-point belt and Hybrid III 6-year-old model response (MADYMO) compared to experimental test data (TestData) for 29 km/h crash speed (left) and 48 km/h crash speed respectively (Lopez-Valdes, 2011a).

A comparison of kinematics of the model versus hardware dummy in the test with 48 km/h crash speed is shown in Figure 10-3, adopted from (Lopez-Valdes, 2011a).

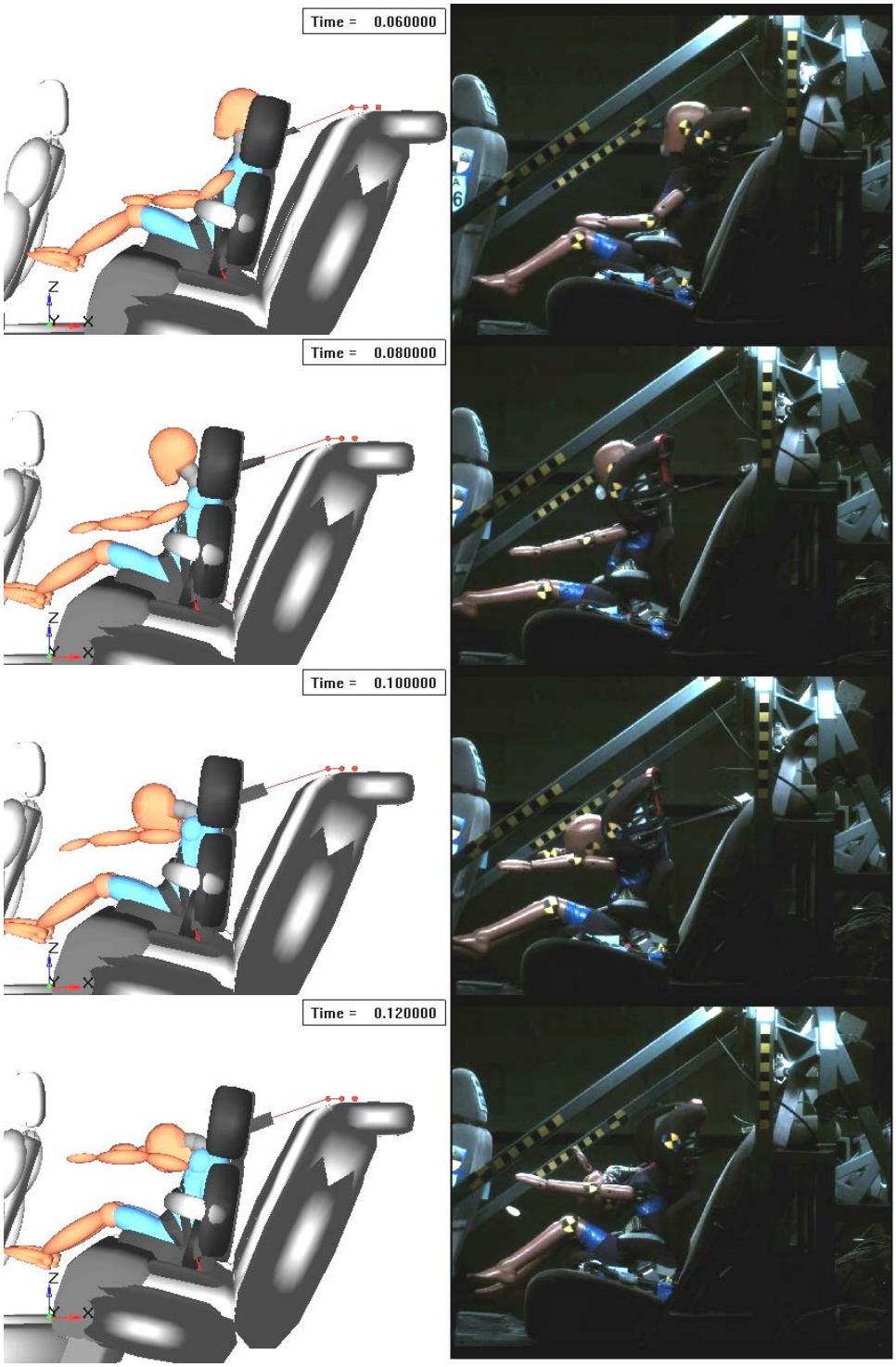

Figure 10-3. Ford Taurus rear bench, high-back booster, 3-point belt and Hybrid III 6-year-old model kinematic response (left) compared to experimental test data (right) (Lopez-Valdes, 2011a).

11 Appendix C: CHOP sled setup validation

11.1 Model setup

A model was created of the sled setup created at the Children's Hospital of Philadelphia CHOP. Seacrist (2010) has presented tests using this setup with a Hybrid III 6-year-old dummy (seen in Figure 11-1 on the left). Since within MADYMO there is the availability of this exact dummy in a validated ellipsoid model version, Seacrist's tests were used to validate the model of the sled setup (seen in Figure 11-1 on the right). Based on CAD data of the setup and coordinates of the various reflecting markers, the model was created. Markers were positioned at the following anatomical locations: head top, opisthocranion, nasion, C4, T1, iliac crest left. All components were assumed rigid and undeformable. The dummy was positioning based on pre-simulations with pure gravitational loading, while controlling for identical marker positions. Not all markers positions could be replicated due to intrinsic differences between the hardware and software dummy or due to inaccuracies in the measurements. Belts with provided parameters were fitted to the dummy. The acceleration pulse was provided and is as used in the volunteer tests, as shown in Figure 3-20.

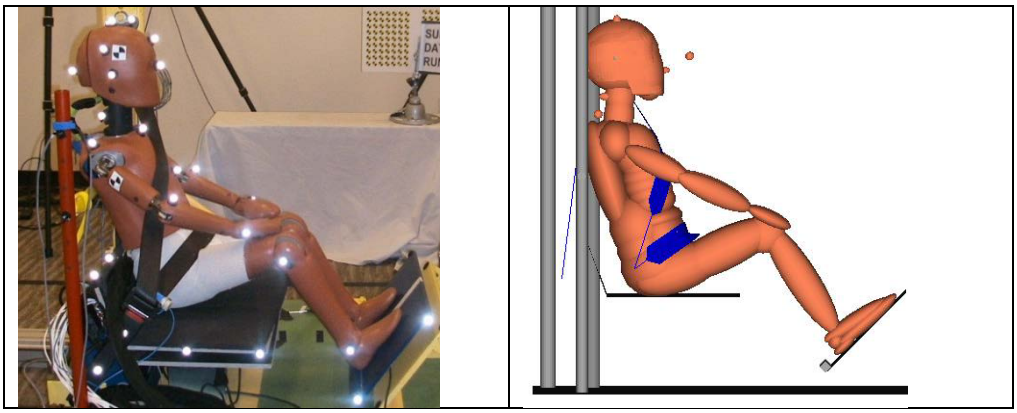

Figure 11-1. CHOP sled test setup with Hybrid III dummy (left) and MADYMO simulation setup for validation with standard Hybrid III model (right).

During the validation process, in order to have the model meet the experimental data as good as possible, parameters that were not known exactly were varied. The parameters that were unknown and/or hard to measure were:

- Friction coefficients; between dummy and seat and between dummy and belt.
- Slack values in the belts; as well in the lap belt and in the shoulder belt

11.2 Results

While belt slack was a tuning parameter, and while belt forces are a good indicator for timing of loading the pelvis as well as the torso, the belt forces resulting from the tuning in the validation are shown in Figure 11-2 and Figure 11-3 for lap and shoulder respectively. The figures show that the onset of belt loading is very well described by the model. Later, the peaks and timing of peaks are fairly well predicted. The model peaks later in the lap belt and earlier in the shoulder belt, when compared to the test.

This may indicate slightly more forward motion in the model for the pelvis and less for the shoulder, resulting in a more tilted torso during impact for the model.

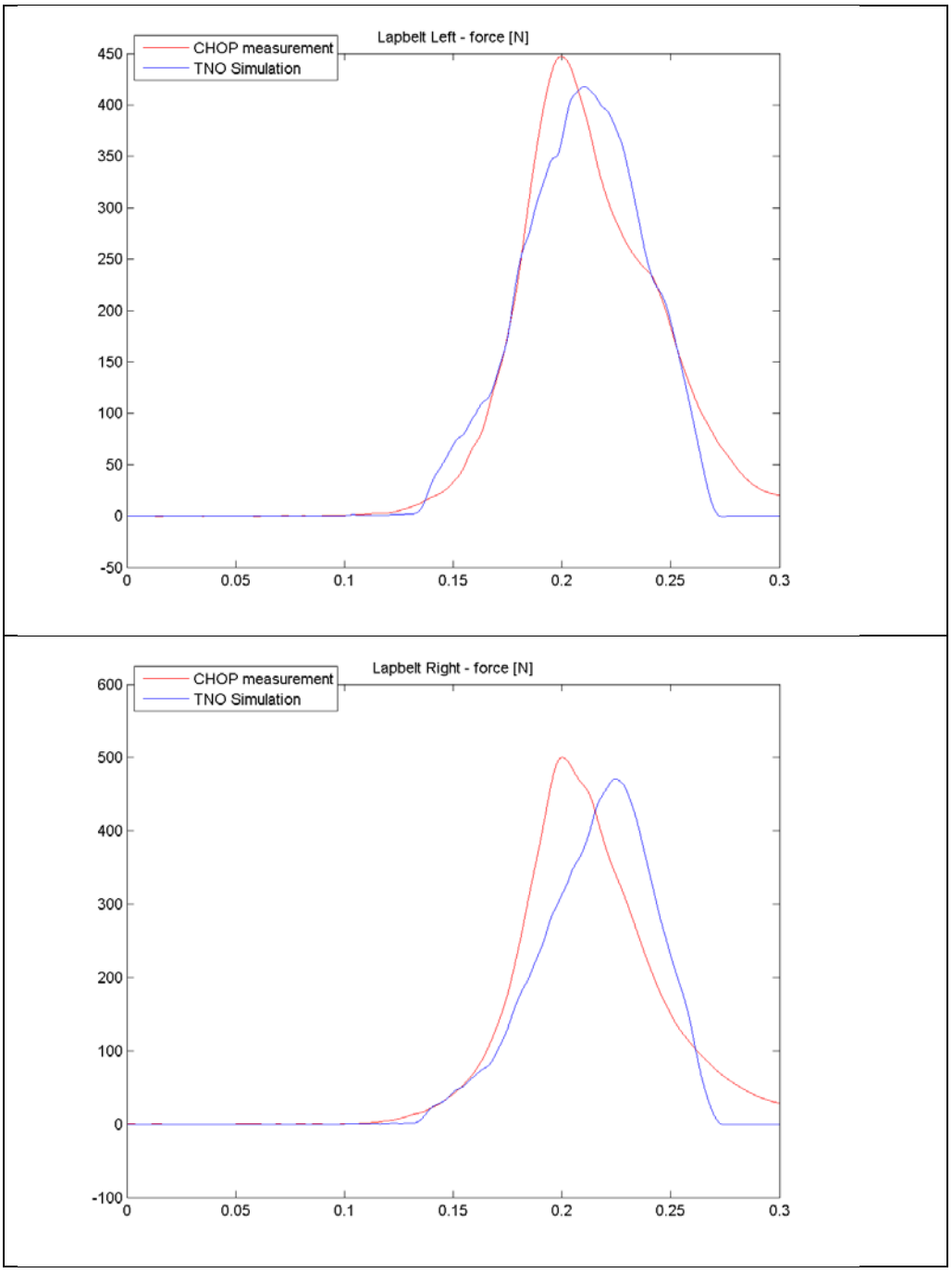

Figure 11-2. Lap belt force validation results of MADYMO model of CHOP hardware sled setup with Hybrid III dummy measured at left (left) and right (right) side of lap belt.

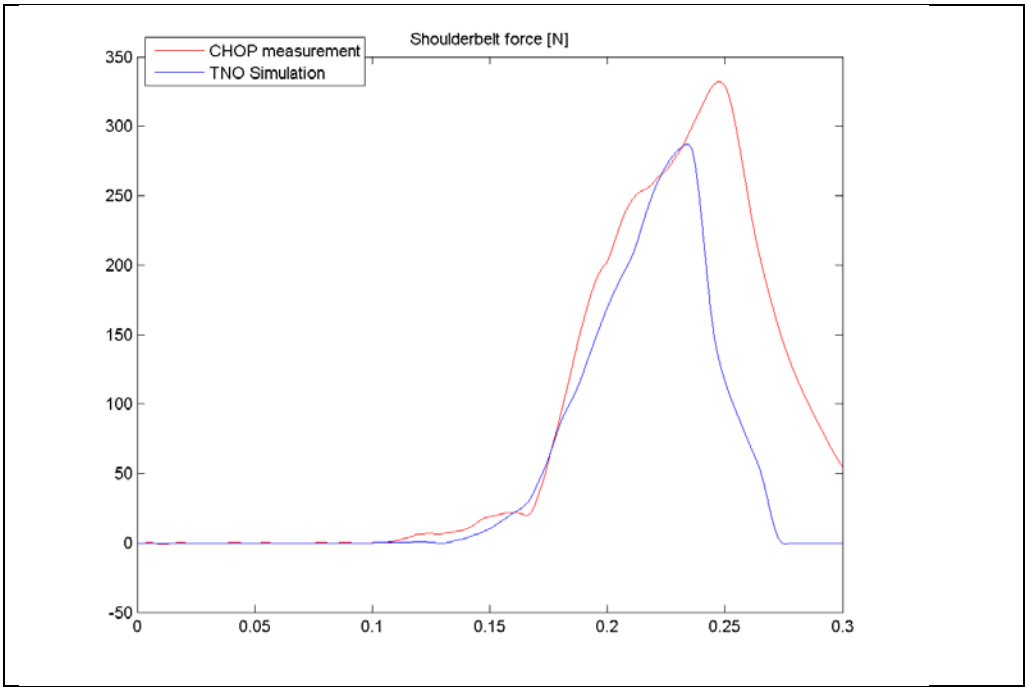

Figure 11-3. Shoulder belt force validation results of MADYMO model of CHOP hardware sled setup with Hybrid III dummy measured below the D-ring.

The kinematics of the dummy resulting from the acceleration pulse and the restraint offered by the 3-point belted and the seat pan are shown in Figure 11-4 for both simulation as well as experiment. Please note that the experimental video-images are not exactly synchronized with the simulation time, due to the absence of time in the videos. The kinematics is similar between simulation and experiment, both characterized by whole body translation first and neck flexion to occur later.

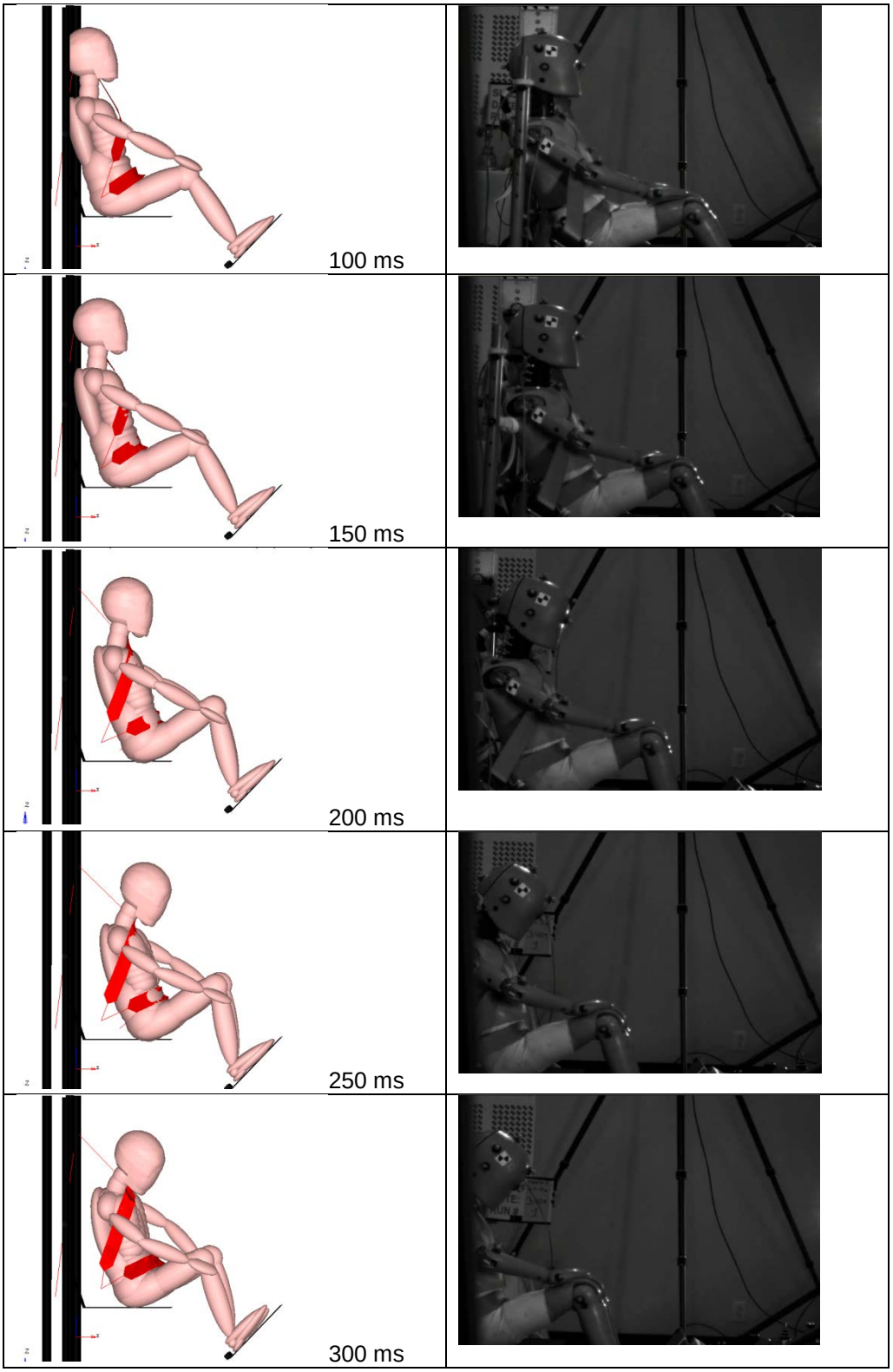

Figure 11-4. Dummy kinematics validation results of MADYMO model of CHOP hardware sled setup with Hybrid III dummy at various time frames. Please note, experimental video images are not exactly synchronized.

Kinematics is better quantified based on trajectory analysis, as is shown in Figure 11-5, Figure 11-6 and Figure 11-7 for head top, T1 and left iliac crest (ICL) trajectories respectively. Trajectories are plotted relative to the seat coordinate system. It is shown that the model replicates the pelvis (ICL) forward (X) motion accurately, at least until 250 ms after start of the test. Nevertheless, both the T1 and head top forward motion are substantially smaller in the model compared to the test. The T1 translates roughly 60 mm less forward in the dummy, while the head top approximately 200 mm less. Some analysis on the trajectories indicates that in the model torso rotation is smaller than in the test, deducing from an approximately 50 mm lower difference between the T1 and the ICL forward motion. The same but amplified holds for the head top relative to T1. The model head top moves around 120 mm less forward relative to T1 when compared to the test. This could be due to the same lower torso rotation; however, due to the extent it also indicates lower amounts of neck flexion to occur.

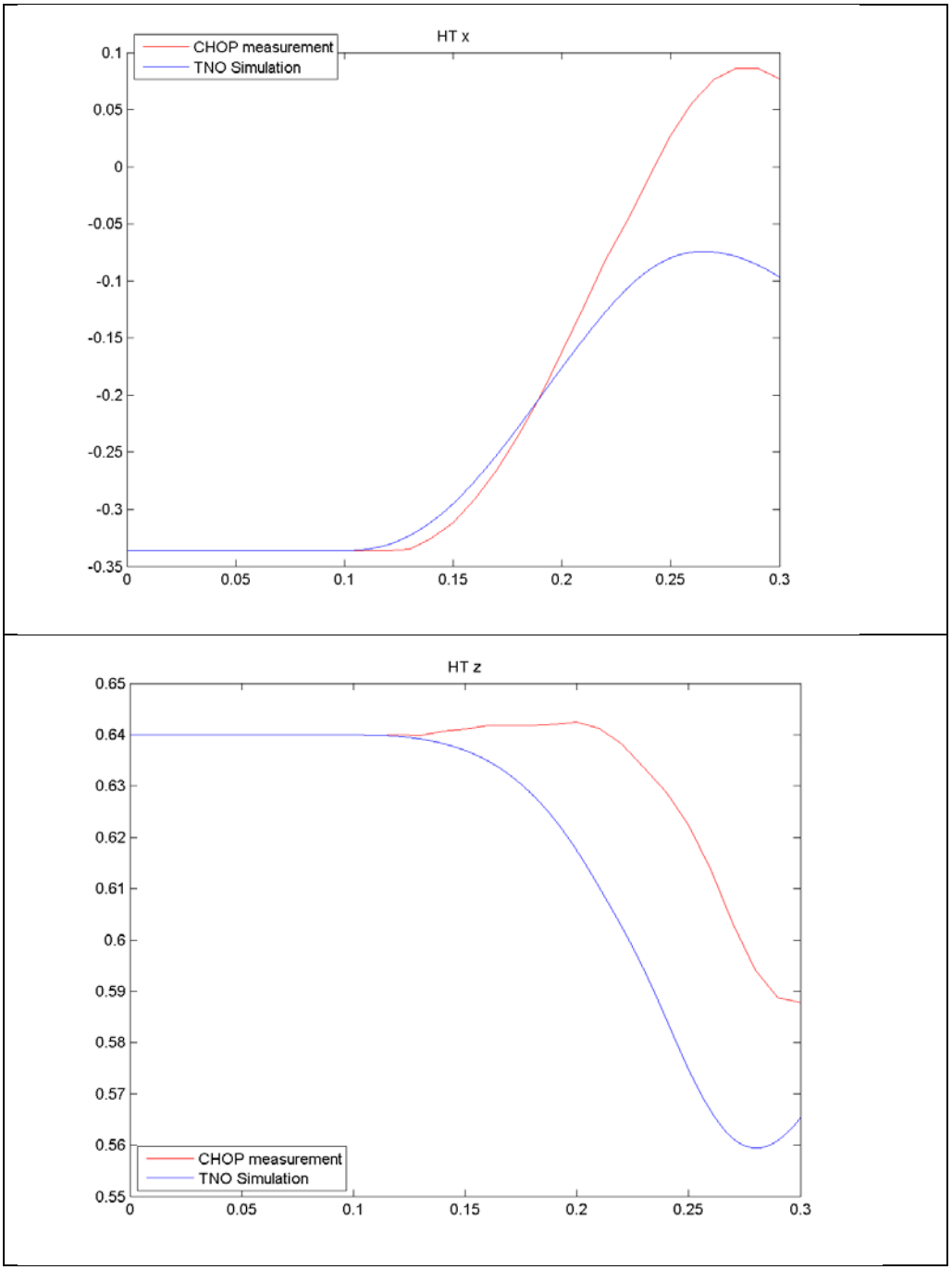

Figure 11-5. Head top trajectory validation results of MADYMO model of CHOP hardware sled setup with Hybrid III dummy in X-direction (left) and Z-direction (right).

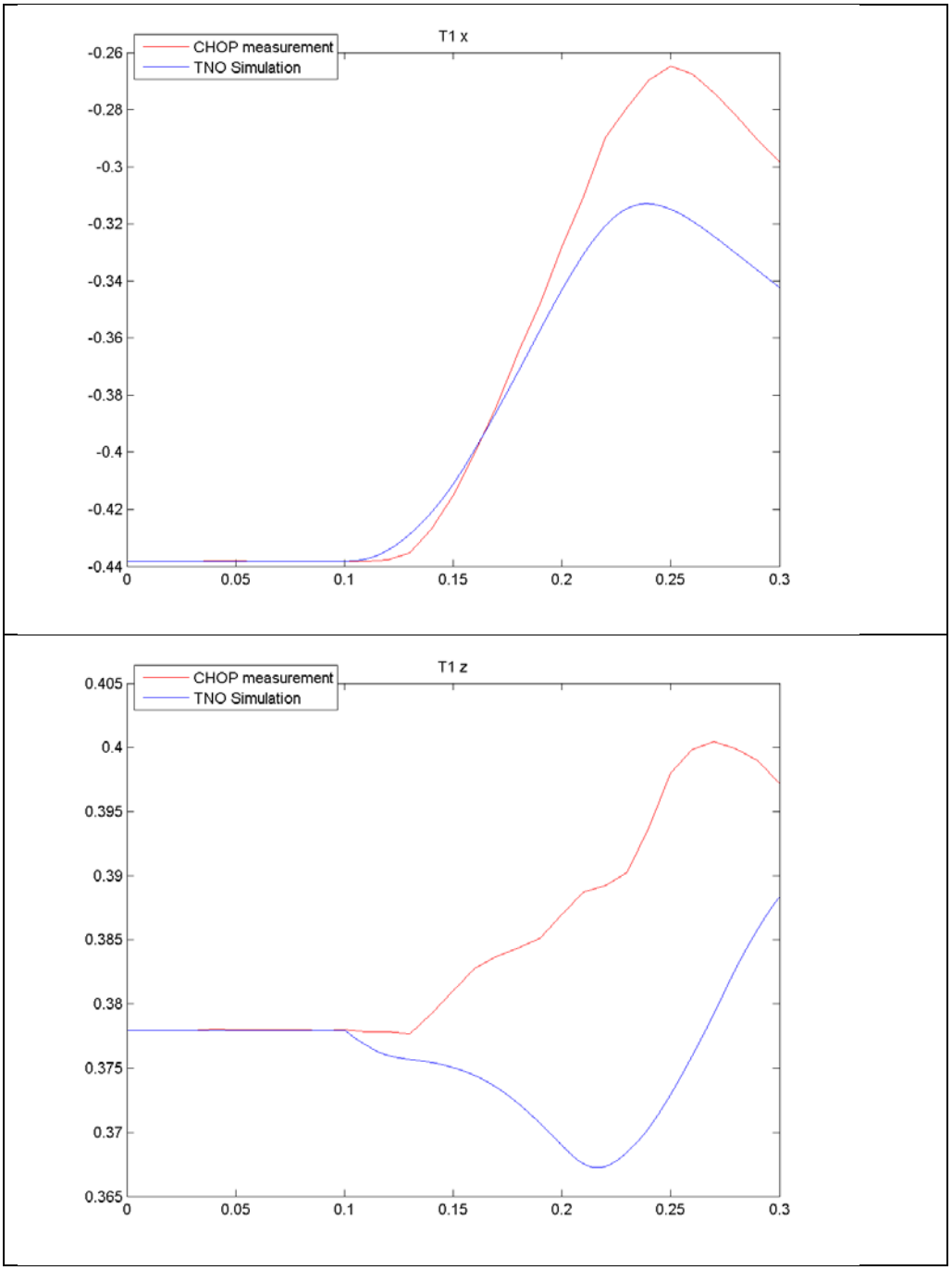

Figure 11-6. Thorax (T1) trajectory validation results of MADYMO model of CHOP hardware sled setup with Hybrid III dummy in X-direction (left) and Z-direction (right).

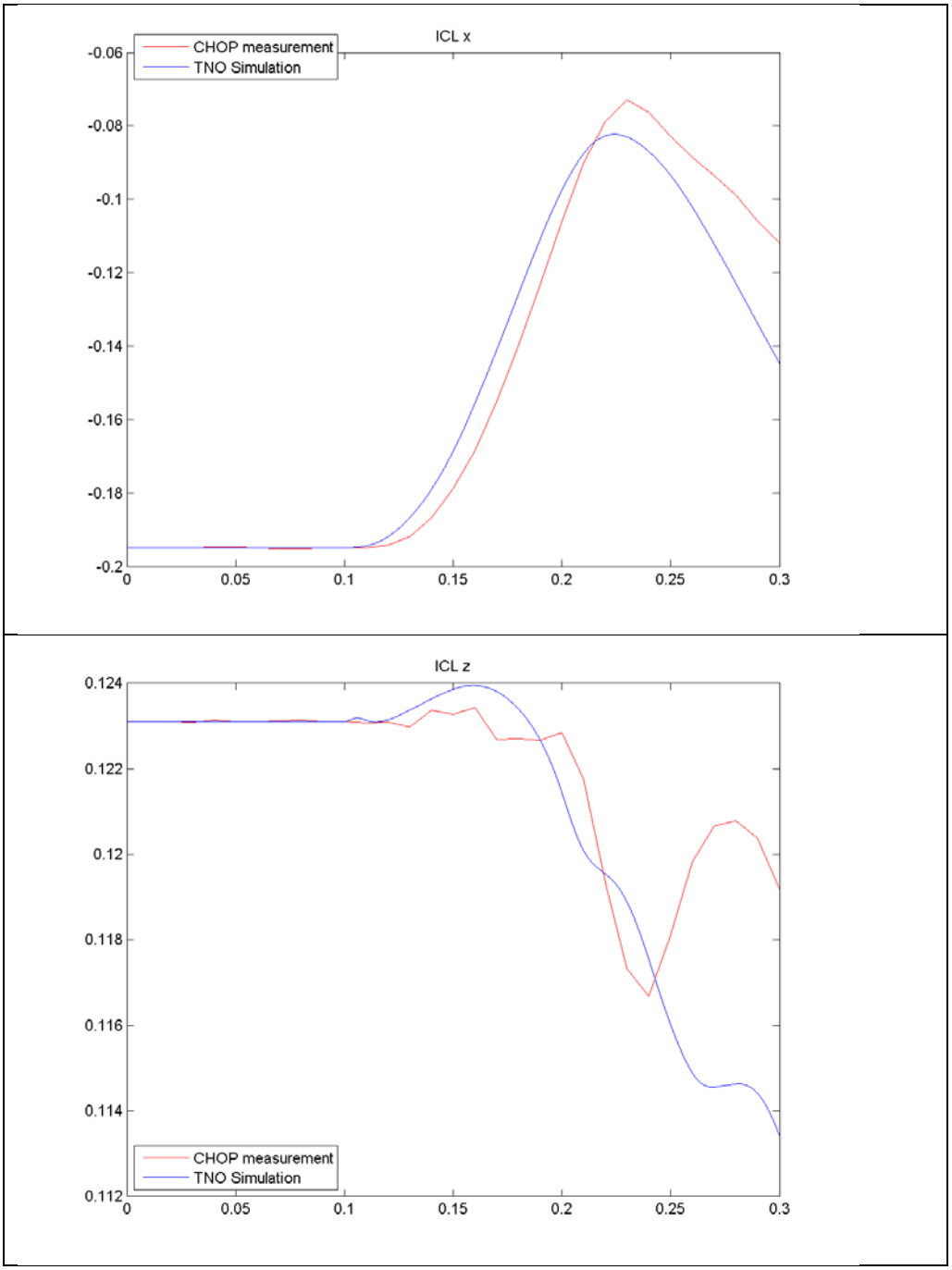

Figure 11-7. Pelvis (iliac crest left / ICL) trajectory validation results of MADYMO model of CHOP hardware sled setup with Hybrid III dummy in X-direction (left) and Z-direction (right).

Based on the kinematics, differences in neck behavior are observed. The loads in the upper neck are plotted in Figure 11-8 and Figure 11-9. While the shear force (Fx) matches well, except for a difference in pre-load, the axial force (Fz) and flexion-extension moment differ between simulation and experiment. In the model, both neck flexion and neck tension are lower than in the experiment. This can be caused by the

earlier discussed difference in torso rotation. Less torso rotation would lead to a lower neck axial force, since in a more upright body, lower forces are experienced in the axial direction as a result of a frontal impact. In addition, lower neck flexion creates even less neck axial force.

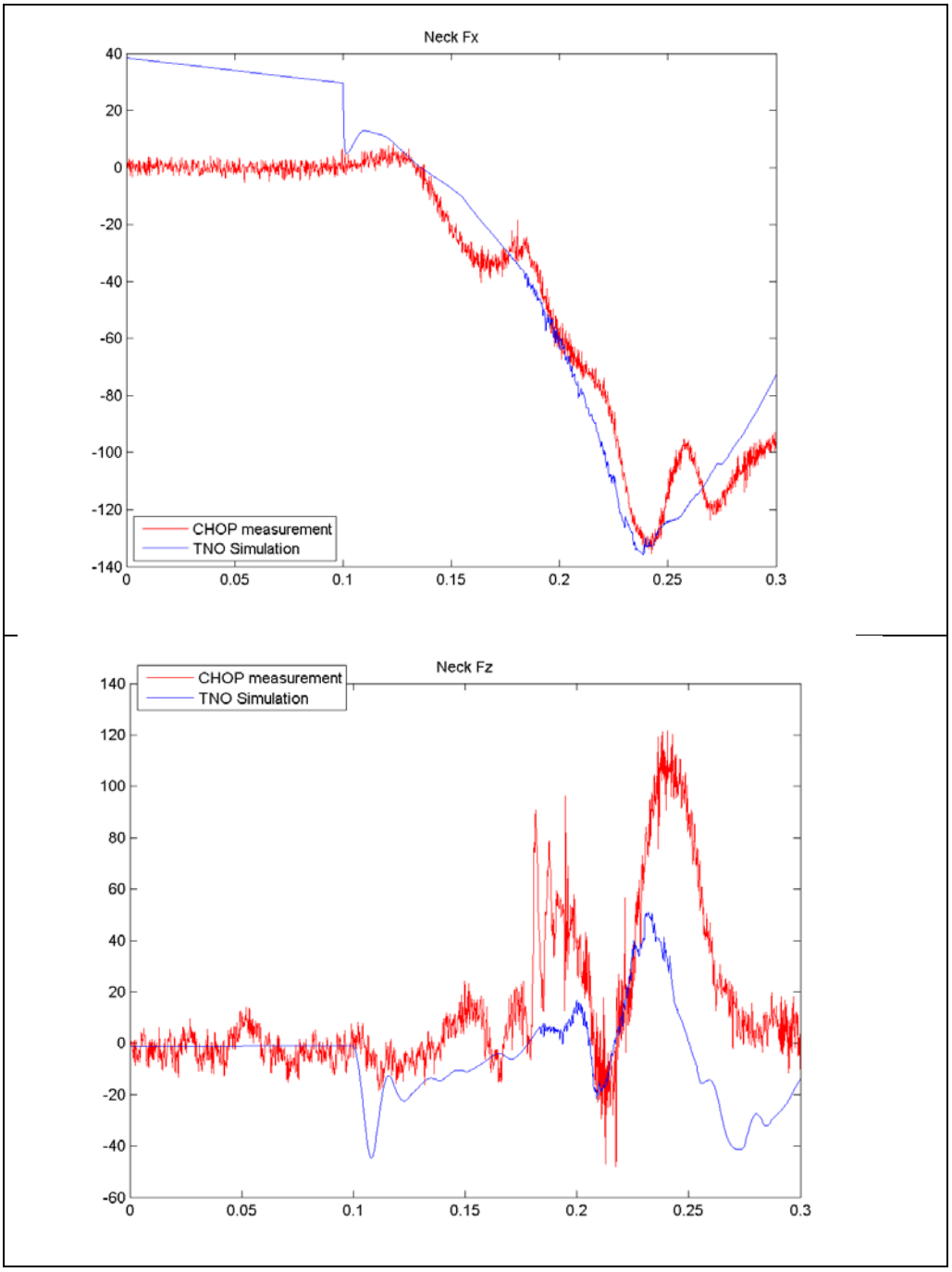

Figure 11-8. Neck force validation results of MADYMO model of CHOP hardware sled setup with Hybrid III dummy in shear X-direction (left) and axial Z-direction (right).

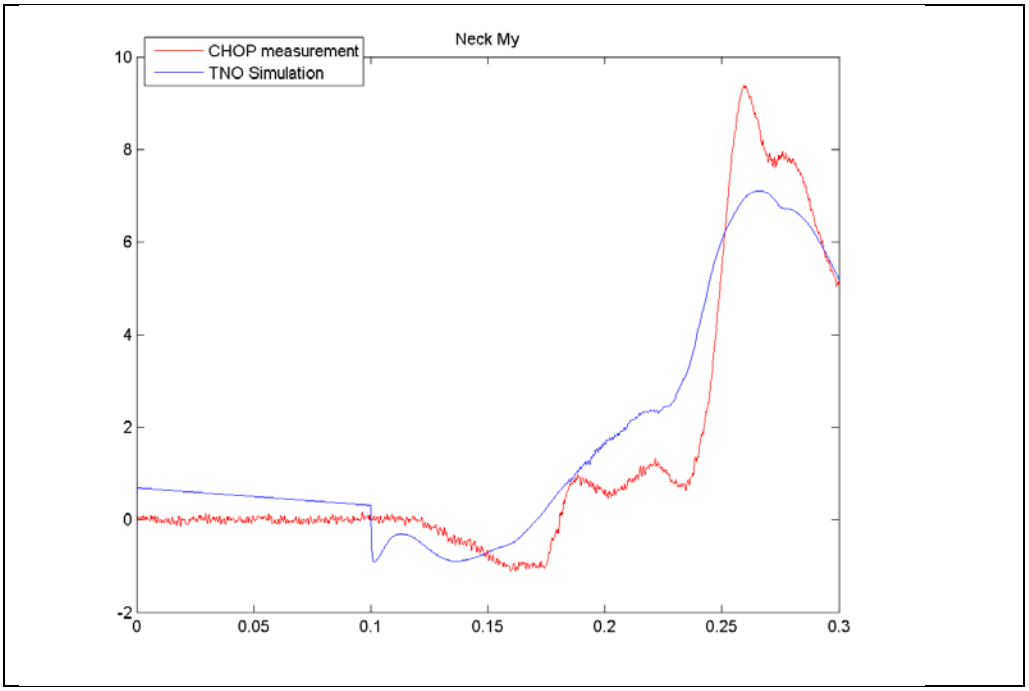

Figure 11-9. Neck moment validation results of MADYMO model of CHOP hardware sled setup with Hybrid III dummy in flexion-extension Y-direction.

The validation results of the model of the CHOP sled environment with a Hybrid III 6-year-old dummy show that the model simulates the dummy behavior with some limitations. While kinematics analysis based on markers is typically less accurate than belt force or dummy load measurement, the higher differences in kinematics based on markers is accepted. Hence, this current setup can be used for further analysis in sensitivity and optimization studies.

DOT HS 811 860
December 2013

U.S. Department
of Transportation
**National Highway
Traffic Safety
Administration**

www.nhtsa.gov

9554-121113-v2